NEW MEXICO DEPARTMENT OF TRANSPORTATION

RESEARCH BUREAU

Innovation in Transportation

Determining Fatigue Endurance Limits of New Mexico Asphalt Mixes for Designing Perpetual Pavements and Implementation of MEPDG to its Full Capacity

Final Report

Prepared by:
University of New Mexico
Department of Civil Engineering
Albuquerque, NM 87131

Prepared for:
New Mexico Department of Transportation
Research Bureau
7500B Pan American Freeway NE
Albuquerque, NM 87109

In Cooperation with:
The US Department of Transportation
Federal Highway Administration

Report NM11MSC-02

NOVEMBER 29, 2013

USDOT FHWA SUMMARY PAGE

1. Report No. NM11MSC-02	2. Recipient's Catalog No.
3. Title and Subtitle Determining Fatigue Endurance Limits of New Mexico Asphalt Mixes for Designing Perpetual Pavements and Implementations of MEPDG to its Full Capacity Part I: Final Report	4. Report Date December 31, 2013
5. Author(s): Rafiqul A. Tarefder and Ghazanfar Barlas	6. Performing Organization Report No. NM11MSC-02
7. Performing Organization Name and Address University of New Mexico Department of Civil Engineering 1 University of New Mexico MSC01 1070 Albuquerque, NM 87131	8. Performing Organization Code 456A 9. Contract/Grant No. 456-325
10. Sponsoring Agency Name and Address Research Bureau New Mexico Department of Transportation 7500B Pan American Freeway PO Box 94690 Albuquerque, NM 87199-4690	11. Type of Report and Period Covered Final Report September 1, 2010 – December 31, 2013 12. Sponsoring Agency Code
13. Supplementary Notes The research project is funded by NMDOT in cooperation with the FHWA	

14. Abstract

It is believed that Hot Mix Asphalt (HMA) mixtures used in long-lasting pavements contain a threshold of strain value below which no fatigue damage occurs. This concept is known as the fatigue endurance limit (FEL). Although previous studies have shown that an endurance limit does exist for HMA mixtures, an established value is yet to be determined, with values varying from 70-400 microstrain (με) based on mixture variability. This study determined the FEL of two HMA mixtures, SP-II (coarse mix) and SP-III (fine mix) using laboratory testing, which are collected from an onsite project on I-25 near Budagher. The SP-II mix with PG 64-22 and the SP-III with PG 70-22 were collected from the field, while SP-II with PG 70-22 and the SP-III mix with PG64-22 were prepared in the laboratory. All the samples were compacted in the laboratory with samples having air voids around 5.5±0.5%. Samples were conditioned and tested using a four-point bending beam apparatus. Due to time limitations, laboratory testing was conducted on selected strain amplitudes and data are used to find the FEL values using a phenomenological approach as well as a fundamental energy based approach, the dissipated energy concept. The FEL values for the SP-II with PG 64-22 and with PG70-22 mixes are 195 and 125 με, respectively. The FEL values for the SP-III with PG 64-22 and with PG 70-22 are estimated to be 185 and 180 με respectively.

15. Key Words Fatigue endurance limits, perpetual pavement, design, performance, hot mix asphalt		16. Distribution Statement Available from NMDOT Research Bureau	
17. Security Classif. (of the Report) None	18. Security Classif. (of this page) None	19. Number of Pages 104	20. Price N/A

THIS PAGE LEFT BLANK INTENTIONALLY

PROJECT NO. NM11MSC-02

DETERMINING FATIGUE ENDURANCE LIMITS OF NEW MEXICO ASPHALT MIXES FOR DESIGNING PERPETUAL PAVEMENTS AND IMPLEMENTATION OF MEPDG TO ITS FULL CAPACITY

FINAL REPORT

A Report on Research Sponsored by:

Research Bureau
New Mexico Department of Transportation
7500B Pan American Freeway NE,
PO Box 94690
Albuquerque, NM 87199-4690
(505)-841-9145
Research.bureau@state.nm.us
http://NMDOTRearch.com

Prepared by:

Rafiqul A. Tarefder and Ghazanfar Barlas

Department of Civil Engineering
University of New Mexico
1 University of New Mexico
MSC01 1070
Albuquerque, NM 87131

PREFACE

This project conducts laboratory fatigue testing of HMA mixtures with the objective of identifying the fatigue endurance limits of two New Mexico asphalt mixtures, using simplified methods such as extrapolation techniques and the dissipated energy ratio approach.

NOTICE

The United States Government and the State of New Mexico do not endorse products or manufacturers. Trade or manufactures' names appear herein solely because they are considered essential to the object of this report. This information is available in alternative accessible formats. To obtain an alternative format, contact the NMDOT Research Bureau, 7500B Pan American Freeway NE, PO Box 94690, Albuquerque, NM 87199-4690, (505) 841-9145.

DISCLAIMER

This report presents the results of research conducted by the authors and does not necessarily reflect the views of the New Mexico Department of Transportation. This report does not constitute a standard or specification.

ACKNOWLEDGEMENTS

The authors would like to express their sincere gratitude and appreciation to Mr. Jeff Mann, Pavement Management and Design Bureau Chief, NMDOT, for being the advocate of this project and for his regular support, sponsorship, and suggestions. The UNM research team appreciates the valuable service and time of the Project Manager Mr. Virgil Valdez for this project.

The UNM research team would like to thank the Project Technical panel for their valuable suggestions during the quarterly meeting. Special thanks go to several Project Panel members namely, Mr. Parveez Anwar, State Asphalt Engineer, NMDOT Materials Bureau, Mr. Stephen J. Hemphill, Construction Engineer, Dist. 4 NMDOT, Mr. Bryce Simons, NMDOT Materials Testing Engineer, Kelly Montoya, Pavement Design Engineer, Mr. James Gallegos, Manager, Asphalt Section, NMDOT Materials Bureau, and Mr. Robert McCoy, previously Pavement Exploration Section Head, now Research Implementation Engineer for their assistance and suggestions for this project.

This project is funded by the New Mexico Department of Transportation (NMDOT) Research Bureau. The authors would like to thank the research Bureau Chief, Mr. Scott McClure for his support, and Administrator, Ms. Dee Billingsley for her fine accounting and reimbursements. The authors would like to thank several members and personnel at UNM for their support. Special thanks to Ms. Rebekah Lucero, UNM Civil Engineering accountant.

TABLE OF CONTENTS

LIST OF TABLES

LIST OF FIGURES

INTRODUCTION

RESEARCH NEED AND SIGNIFICANCE

The predominant use of Hot Mix Asphalt (HMA) in pavement structures within the United States and worldwide has brought about a significant change in the way pavements are built today. Pavement design standards are continuously changing as researchers develop new ways to analyze and predict the behavior of HMA, which significantly improves design reliability for pavement design projects. Now, for the first time, researchers can look to the past as a way to improve flexible pavement design. Records have shown that some asphalt concrete pavements have been performing for 40 years or more without exhibiting any fatigue damage (*1, 2*). It is believed that the HMA mixtures used in these long-lasting pavements contain an endurance limit below which no fatigue damage occurs. This concept is known as the Fatigue Endurance Limit (FEL). Determining the FEL of HMA mixtures is directly related to the design and construction of long-life or perpetual pavements. The inclusion of FELs in current pavement design guides is only now being considered and is still a long way from being implemented on a project-to-project basis. However, the existence of a FEL in HMA is still relatively new and the purported value has yet to be established.

HMA mixtures are designed primarily to resist rutting and fatigue cracking. In saying this HMA mixtures are still vulnerable to fatigue cracking if they are not designed to meet specific traffic loads. Bottom-up fatigue cracking initiates at the base HMA layer of a pavement due to tensile strains induced from repeated traffic loading. If the applied tensile strain is greater than the endurance strain of the HMA material, cracking initiates and propagates toward the surface. Once the cracks are visible from the surface of the pavement, the only solution is complete reconstruction. This problem can be avoided by implementing two different design approaches; (*1*) build a pavement thick enough so that the tensile strains experienced at the base of the pavement are negligible, and (*2*) use a rich-bottom base layer (RBL) that is flexible enough to withstand the tensile strains caused by repeated traffic loading. The first option is a conservative approach and is expensive. The other alternative is much more appealing because a thinner pavement containing a flexible base layer will provide the same performance as the thicker pavement, for less cost. However, the binder rich layer creates a ‘bath-tub’ effect due to its lower permeability and moisture becomes trapped within the asphalt layers above, which can lead to extensive moisture damage to the mixture. The endurance strain of the HMA mixture used in this flexible layer must be known in order to prevent fatigue cracking. In summary, identifying the FEL, if it exists, will improve current design guides for both conventional and perpetual pavements.

Up until now, the fatigue endurance limit of HMA mixtures is determined by conducting laboratory fatigue testing whereby the number of loading cycles to failure is related to applied tensile strain and initial stiffness of material. This is called the phenomenological approach because the relationship is purely empirical and does not explain the fundamentals of fatigue failure. Laboratory fatigue testing of HMA mixtures is generally done either by repeated load flexure or by direct tension tests. From the literature search, the FEL of HMA mixtures may vary from 70-200 microstrain, depending on mixture properties (*3,4*). In the State of New Mexico, the FEL of local HMA mixtures is unknown. Determining the FEL of HMA mixtures can provide

valuable data for current pavement design methods and provide significant economic contribution to the State of New Mexico.

Due to significant design and economic benefits, research in this area is gaining popularity. A nationwide study is currently being done by the National Cooperative Highway Research Project (NCHRP 9-44), with the specific goal of validating the existence of FELs in HMA. In addition to this, the NCHRP intends to incorporate the use of a FEL in current pavement design guidelines. However, there is still a need to establish the same design criteria for state highway agencies. By determining the FEL for local HMA mixtures, improved designs for longer-lasting pavements can be implemented on a site-specific basis.

OBJECTIVE

The primary objectives of this study are to:

- Assess current design, testing, and evaluation methods of FEL, with particular emphasis for HMA mixes as appropriate for New Mexico.
- Collect asphalt mixture components in order to replicate specific mix designs in the laboratory. Compact beam samples to a bulk density of 94.5 ± 0.5% of the maximum specific gravity (*Gmm*).
- Conduct fatigue tests in the laboratory for determining FEL of NMDOT's asphalt mixes.
- Analyze the test results and evaluate the FEL value of mixes. Recommend indices and typical values for HMA mixes in New Mexico.
- Define for the purpose of possible future research which of these indices would be suitable to determine the performance measures of the asphalt mix design that accurately reflect the long term performance, that are sufficiently sensitive to accommodate construction variables and that can be performed with commonly available laboratory equipment.

REPORT ORGANIZATION

This report is comprised of seven sections. Section 1 presents the research needs and objectives. Section 2 provides a literature review on current fatigue design and analysis approaches. In Section 3, experimental work is discussed. In addition, specimen fabrication, the experimental plan and fatigue testing are discussed. Section 4 presents the fatigue test results and analysis. In Section 5, a comparison of different failure criteria for fatigue testing is discussed. Section 6 presents a study on fatigue crack propagation in HMA. In Section 7, conclusions are made from the findings of this research and future research recommendations are presented.

ASSESSMENT OF FATIGUE ENDURANCE LIMITS

CURRENT FATIGUE DESIGN AND ANALYSIS APPROACHES

The FEL is commonly found in metallic materials. However, not all metals have a well-defined FEL, aluminum being a prime example (*5*). Figure 1 presents such a case where Figure 1(a) describes the increasing fatigue life of a material as the stress is decreased. Figure 1(b) shows the fatigue life of another material increasing until a limit is reached where the fatigue life becomes indefinite.

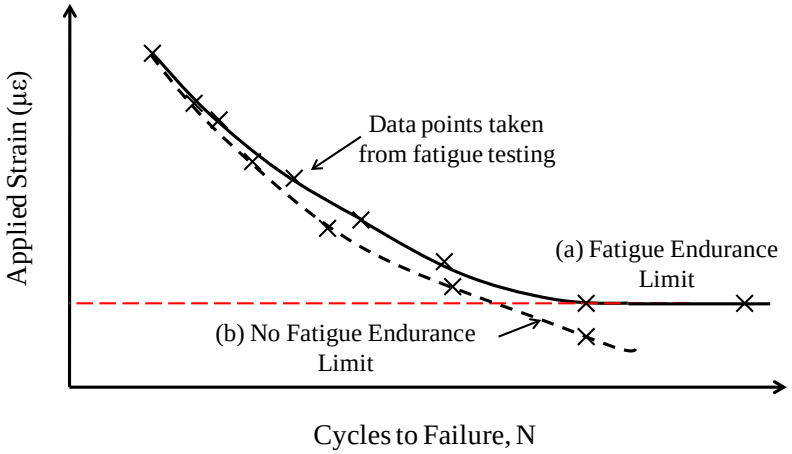

(a) Endurance Limit; (b) No Endurance Limit (Advanced Asphalt Technologies 2008)

FIGURE 1 Typical S-N Diagram for Laboratory Fatigue Tests

There are limited studies on the FEL of HMA mixes. Early work by Carl Monismith at the University of California, Berkeley, suggested that an endurance limit does exist for HMA (*3*). Monismith (3) performed laboratory fatigue testing of local California HMA mixtures using both controlled stress and controlled strain modes of loading. No indication is given from the literature if rest periods are included in the testing or if it is continuous loading. The results suggested that a FEL of 70 με exists for the HMA mixtures. Further research done by the University of Illinois presented HMA endurance limits ranging from 70-100 με taken from 120 different HMA mixes (*6, 7*). However, due to limited research, an established FEL value has not been confirmed.

In summary, there is sufficient evidence to suggest that a FEL does exist for HMA. The following sections present different test methods and analytical models, which are currently being used to prove the existence of a FEL in HMA materials.

LABORATORY FATIGUE TEST METHODS

Traditional mechanistic-empirical approaches for predicting fatigue of HMA mixtures require controlled stress (strain) laboratory testing, usually dictated by a single temperature over a range of applied stress (strain) levels. The number of cycles to failure is then recorded along with the critical stress (strain) level, and this determines the fatigue life of a HMA mixture. Measured fatigue life in the field can also be incorporated to validate this approach.

Four Point Bending Test

Four-point bending is the most commonly used HMA fatigue test. The standards for this bending beam fatigue test (BBFT) are AASHTO T321 (*8*) and ASTM D7460 (*9*). Cyclic loading is applied to an asphalt beam until fracture or failure occurs. Prowell et al. (*10*) applied this test method as part of the NCHRP 9-38 project to validate the existence of a FEL in HMA mixtures (*10*). HMA beam samples are tested (380 mm long by 50 mm thick by 63 mm wide) under constant strain mode using sinusoidal loading at 10 Hz. Testing is conducted using six different strain levels; 800, 400, 200, 100, 70, 50 $\mu\varepsilon$, and the test is terminated once a 50 percent reduction in initial flexural stiffness (E_0*) is reached. The study concluded that a FEL for HMA does exist and can be reasonably extrapolated from 10-12 million cycles using the Weibull function. The major drawback of this study is the time required to run 12 million cycles, which may take as long as 14 days. Another major shortcoming is the absence of rest periods during testing where the beneficial effects of healing are not accounted for. The concept of healing in asphalt concrete is discussed in greater detail in the literature review section.

Uniaxial Tension Test

Direct tension testing has been used by some researchers to determine the FEL of HMA mixtures. Fatigue testing on sample cores (3 in. diameter, 6 in. tall) consisted of haversine load pulses. Fatigue damage required increasing blocks of constant strain (each block = 10,000 cycles), where each block had greater amplitude than the previous one. Steel plates are glued to the ends of the samples with plastic epoxy glue and the specimens are aligned vertically. Testing is conducted until failure. The crosshead displacement is computer-controlled and test results are recorded using a data acquisition system. Linear Variable Differential Transducers (LVDT) are attached to the specimen and a data acquisition system is set up to record the deformation (strain) of the specimen. This test method is favorable among many researchers as it is more simplified than traditional fatigue test methods. This is because direct tension testing does not require the production of HMA beam samples and uses HMA core samples instead. In addition to uniaxial testing, the development of a viscoelastic continuum damage mechanics (VCDM) model enabled FEL identification. The application of VCDM models in determining the FEL is discussed in greater details in the next section.

FATIGUE FAILURE CRITERIA

Flexural Stiffness Reduction

Figure 2 describes the different stages in a typical fatigue test of HMA. The stiffness reduction process is characterized by three phases of degradation. The first phase results from internal heating caused by dissipated energy generation due to the materials viscous properties (*11*). This occurs at the beginning of the test when the beam sample is repeatedly flexed and the sample reaches a new thermal equilibrium ($T + \Delta T_{heat}$). According to Di Benedetto et al. (*11*), this increase in temperature has a significant effect on the stiffness reduction and can be identified as the initial portion of the fatigue curve where the slope is steep. Samples tested at higher strains generate more heat and therefore experience a higher rate of stiffness reduction. As the cyclic loading continues, two major stages are illustrated; formation of micro-cracks which reduce the stiffness by 25%, and crack formation which further reduces the stiffness by 35-40%. Failure of the specimen is expected once these two stages are identified. It must be noted that traditional controlled stress (strain) fatigue tests (failure pronounced at 50% stiffness reduction) do not account for internal heating of a HMA specimen. A correction factor can be applied here to account for the internal heating, but testing within a temperature controlled chamber can reduce the effect of internal heating.

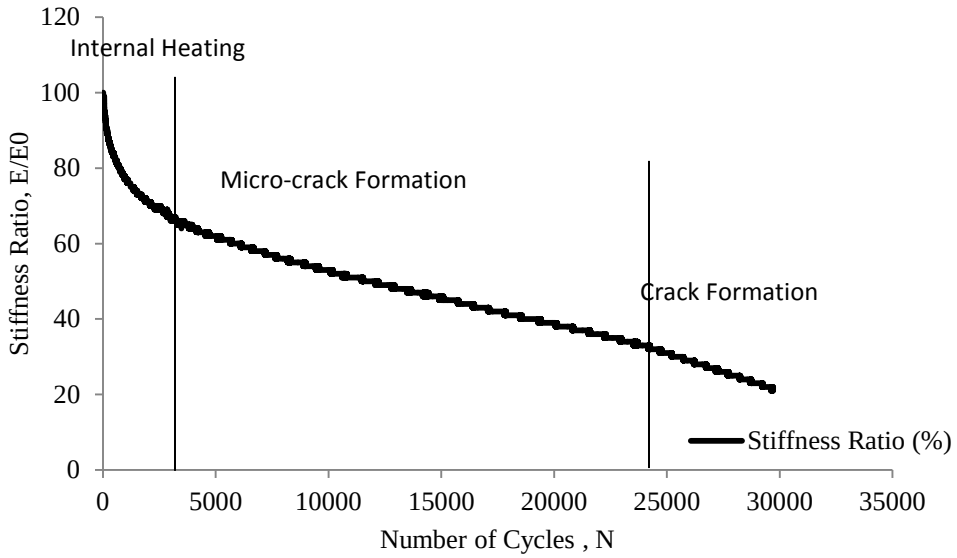

FIGURE 2 Typical Flexural Stiffness Reduction Curve Fatigue Test

Four point beam fatigue testing of HMA materials is usually performed according to AASHTO T 321 Standards (*8*). Asphalt concrete beams undergo damage inducing cyclic loading (displacement control). Using the deflection history, load response history, and geometry of test specimen, the maximum strain and stress in specimen can be calculated using Eq. 1 and Eq. 2 respectively.

$$\varepsilon = \frac{12\,h\,\delta}{3L^2 - 4a^2} \tag{1}$$

$$\sigma = \frac{P\,L}{b\,h^2} \tag{2}$$

where ε = maximum strain, σ = maximum stress, P = load applied by actuator at time t, b = average specimen width and h = average specimen height, δ = deflection at center of beam at time t, a = distance between inside clamps and L = distance between outside clamps. Figure 3 illustrates a schematic of test set-up.

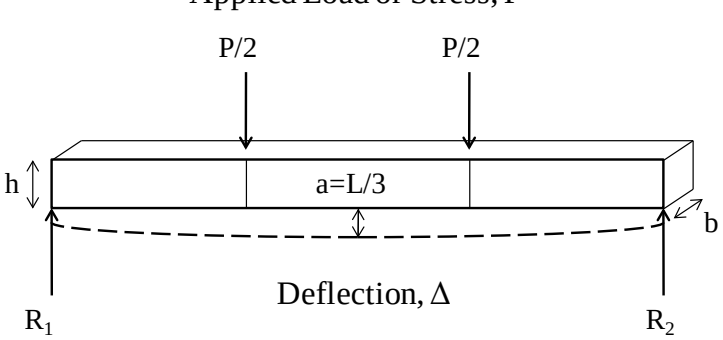

Applied Strain, $\varepsilon = \frac{12*h*\Delta}{3L^2 - 4a^2}$

Measured Stress, $\sigma = \frac{P*L}{b*h^2}$

FIGURE 3 Schematic of Four-Point Beam Fatigue Test

Sample flexural stiffness is then calculated using σ and ε data recorded from each cycle.

$$E = \frac{\sigma_t}{\varepsilon_t} \tag{3}$$

where E = flexural stiffness.

Then, a number of cycles at 50% reduction in stiffness are recorded as failure of beam. Similar process is repeated at other strain levels to obtain relation between applied strain and number of cycles to failure. The same relation is given in Eq. 4. Sometimes, initial stiffness of material is also incorporated into fatigue model as shown in Eq. 5.

$$N_f = k_1 \left(\frac{1}{\varepsilon}\right)^{k_2} \quad (4)$$

$$N_f = k_1 \left(\frac{1}{\varepsilon}\right)^{k_2} \left(\frac{1}{E}\right)^{k_3} \quad (5)$$

Four-point flexural bending of a beam implies that the middle third of the beam is subjected to pure bending. The flexural stiffness in the mid-section is reduced at a higher rate than the outer sections due the presence of higher stresses and strains, where eventually micro-cracking will initiate and propagate. Although the stiffness varies along the length of the beam during fatigue testing, for interpreting measured deflections, it is assumed that there is a constant stiffness throughout the beam. A study by Pronk (*12*) on the stiffness variation of an asphalt beam during four-point fatigue testing showed that errors are induced in the data measurement if the beam stiffness does not reduce at the same rate as that of the mid-section. Pronk (*12*) recommends using strain gauges when performing fatigue tests so as to determine the rate of stiffness reduction in the outer sections and thereby establishing correction factors.

Energy Ratio

Rowe and Bouldin (*13*) introduced the Energy Ratio for modeling fatigue behavior. The Energy Ratio approach is based on a stress-controlled study by Hopman et al. (*14*) which claims to identify the point at which micro-cracking becomes a macro-crack (defined as fatigue failure). The Energy Ratio is obtained by multiplying stiffness by corresponding number of cycle. Laboratory fatigue testing is conducted until flexural stiffness is reduced to at least 20 percent.

The Energy Ratio is cross plotted against number of cycles to find failure location. Such a plot has two distinct regions. In the first region, the stiffness parameter is monotonically increasing where as in the second region stiffness parameter is monotonically decreasing. The reduction in stiffness is linear (*dE*/dn* = slope = constant) in the micro-crack formation phase. As cracks form and begin to propagate, the relative damage (*dE*/dn*) accelerates and resulting product, the energy ratio (*ER*) decreases. The junction of these two regions indicates peak value of stiffness parameter. The peak in the curve indicates the transition point between micro-crack formation and propagation of a macroscopic crack, as shown in Figure 4. The point at which the maximum value of *ER* occurs is defined as the fatigue failure. The peak value can be identified by systematic search or by curve fitting. A systematic search can be made to locate maximum value and then back-calculating number of cycles. The Energy Ratio is defined in Eq. 6:

$$\textit{Energy Ratio (ER)} = \textit{Cycle Number}^* \textit{ Stiffness} \quad (6)$$

where *ER* is the flexural stiffness ratio (%).

Rowe and Bouldin (*13*) point out that beam samples showing 50 percent $|E_0^*|$ reduction may not yet experience crack initiation. The authors recommend that testing be conducted until the modulus has dropped to 20 percent $|E_0^*|$. Another disadvantage with traditional controlled stress (strain) tests is that they do not show the point where micro-crack formations become macro-crack formations (defined as fatigue failure), as highlighted in Figure 4.

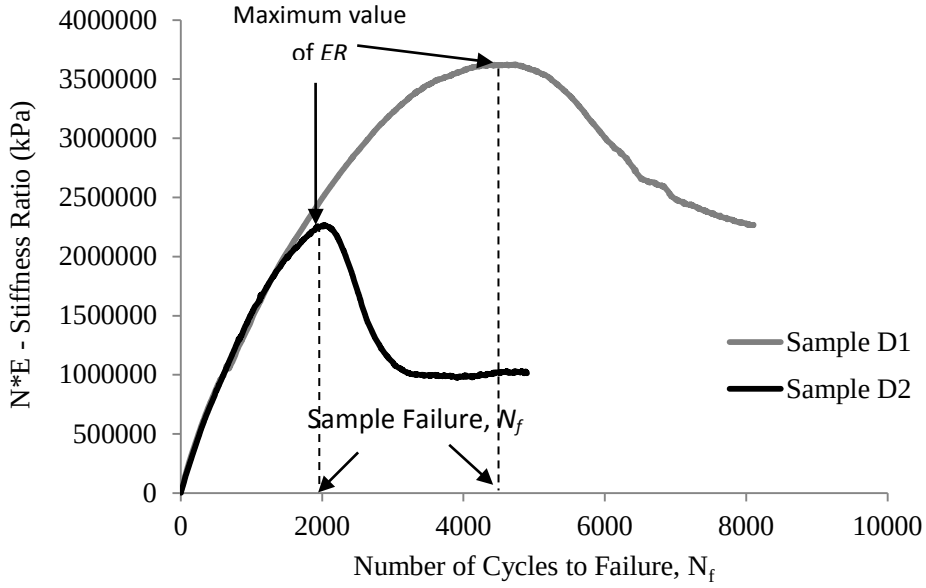

FIGURE 4 Energy Ratio (Rowe) vs. number of cycles to failure

Traditional FEL Criteria

When a beam sample is subjected to 50 million cycles or more, it is considered to have a FEL close to that applied strain level. To better define the exact FEL, further fatigue testing may be required at a slightly higher strain to identify the approximate FEL of the mixture. Target failure by loading cycles is determined by the Highway Capacity Manual (2000) which states that 500 million load cycles is estimated as the maximum possible number of load repetitions expected in a 40 year period. When considering a shift factor of 10, laboratory testing to 50 million cycles would equate to approximately 500 million loading cycles in the field. Based on these analyses, a mix which provided 50 million cycles or more is considered to be below the FEL.

FATIGUE ANALYSIS APPROACHES

The trend of fatigue analysis approaches has changed significantly over the past decade due to the rapid growth in computer technology. Initially, empirical approaches are used to determine fatigue behavior in HMA. However, the introduction of damage mechanics, discrete element analysis, dissipated energy and fracture mechanics along with flexure, direct, and/or indirect tension testing has brought about a shift from empirical-based approaches to mechanistic-based

approaches. This has allowed for a more fundamental understanding of crack initiation, propagation and fracture.

Traditionally, FEL testing is conducted to a maximum of 50 million cycles which may take as long as two months to complete. This amount of time is not practical for routine determination of a FEL. Reducing fatigue testing and introducing a function (Weibull, Power, logarithmic, etc.) to extrapolate the strain level required to reach 50 million cycles is one way to reduce testing time. Furthermore, the use of fatigue analysis approaches reduces extensive testing time required to confirm the existence of FEL. Previous studies show the time-saving benefits of applying fatigue analysis approaches to determining the FEL of HMA mixes (*10, 7, 15, 16*). Fatigue analysis approaches include energy-based techniques as well as viscoelastic damage mechanics models and extrapolation techniques. Each of these approaches is described in the following sections.

RDEC Approach

The Ratio of Dissipated Energy Change (RDEC) approach is perhaps the most refined energy method, which can be used not only to extrapolate fatigue life, but also determine the FEL. The RDEC is defined as the difference in dissipated energy between two loading cycles which contributes to damage. In other words, the area found inside a hysteresis loop (created during cyclic loading and unloading of HMA) is the dissipated energy. The difference in area of each loop indicates the damage produced by dissipated energy.

$$RDEC = \left(\frac{DE_n - DE_{n+x}}{DE_n}\right) \div x \quad (7)$$

where DE_n = total dissipated energy at cycle n, DE_{n+x} = total dissipated energy at cycle $n+x$, and x = the number of cycles between the two data points.

Previous studies by Ghuzlan (*17*) and Carpenter et al. (*16*) described the damage curve using the RDEC versus loading cycles shown in Figure 5. It can be seen that the damage curve is separated into three stages: the initial period (Stage I), the plateau period (Stage II), and the failure period (Stage III). Stage I shows rapidly decreasing dissipated energy ratio which indicates ‘settling’ of the beam sample. The average dissipated energy ratio in Stage II is known as plateau value. The plateau stage is when a constant percentage of dissipated energy produces damage. This behavior continues until an increase in dissipated energy ratio occurs which signifies fatigue failure and unstable crack propagation (Stage III).

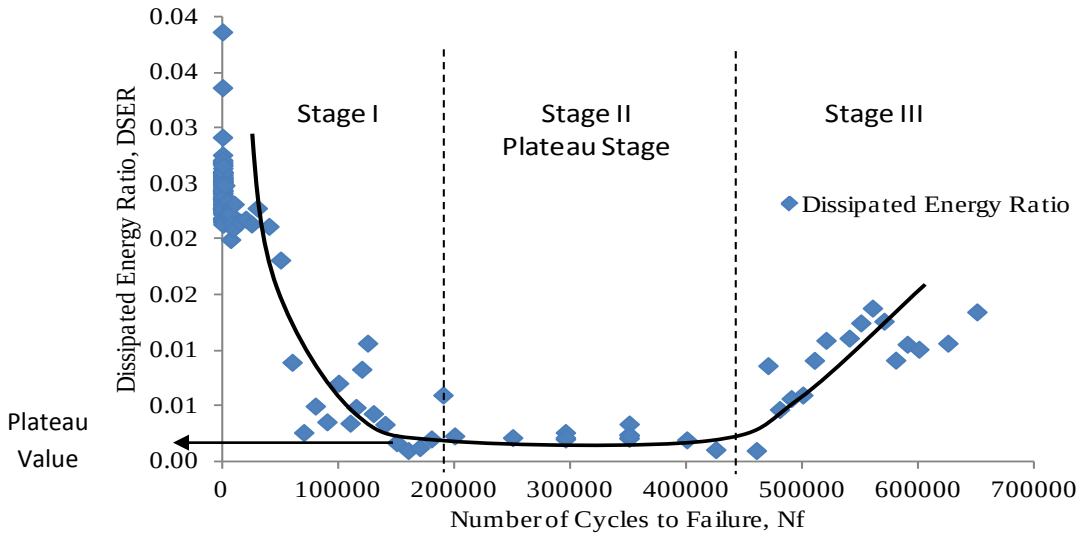

FIGURE 5 Typical Dissipated Energy Ratio Plot Showing Three Stages of Fatigue

From the plateau stage (Stage II), a value can be determined which indicates fatigue failure in a sample. This is called the Plateau Value and is defined as the RDEC value at the number of cycles equal to the failure point (N_{f50}). Failure is defined as a 50 percent reduction in initial stiffness, with the initial stiffness being determined at the 50th loading cycle. Lower PVs correspond to longer fatigue lives (*18*). According to Carpenter and Shen (*7, 15,19*), the *PV-*N_f relationship is not mixture specific and is supposedly independent of temperature, mode of loading, frequency, and healing capacity (rest periods). However, the relationship between the strain amplitude and the PV must be determined for each HMA mixture.

The PV approach can also be used to determine the effects of mixture variables on the fatigue life. A study by Carpenter and Shen (*15*) produced a PV prediction model based on applied strain and material properties. By varying material properties such as binder content, flexural stiffness, nominal maximum size of aggregate gradation, the predicted PV changes, and in turn the predicted fatigue life changes. This unique *PV-*N_f relationship suggests that the PV can be used to predict fatigue life (damage) as well as the effect of mixture variables and load on the fatigue life.

Furthermore, the PV approach can also be used to determine the FEL. A study by Carpenter and Shen (*7*), included fatigue testing of 98 different mixtures, using both modes of loading (stress and strain), and varying rest periods (0-0.4 sec) and frequency (0.5-10 Hz). From the *PV-*N_f relationship, a PV threshold is identified where the fatigue behavior changes considerably between low and normal strain fatigue tests. Below PV of 6.74e-09, HMA mixtures showed extraordinary long fatigue life regardless of applied strain amplitude. Therefore, a strain level which provides a PV of 6.74e-09 or less, indicates FEL behavior.

In this study, a relationship between the PV and the strain amplitude, which is not independent of mixture or temperature, is developed. The PV-strain amplitude relationship is used to predict the strain amplitude that yields a PV of $6.74e^{-09}$ which is the FEL.

$$PV = \alpha(\varepsilon)^{\beta} \tag{8}$$

where ε = strain amplitude, and α and β are regression coefficients (*7, 19*).

Pseudostrain Approach

Some fatigue analysis approaches such as the RDEC approach consider asphalt concrete as an elastic material. However, asphalt concrete is a viscoelastic material and exhibits rate dependent and temperature dependent behavior. Kim (*20*) successfully applied the elastic-viscoelastic correspondence principle for modeling sand-asphalt mixture behavior under multi-level cyclic loading. With the elastic-viscoelastic correspondence principle, the physical strain ε in the elastic theory is replaced with a pseudostrain, ε^R. A pseudostrain is similar to a physical strain, except that it is independent of time or loading history. The pseudostrain accounts for the linear viscoelastic hereditary effects of the material through the convolution integral (Eq. 9) so that damage may be evaluated separately from viscoelastic effects. Without this substitution, identifying damage during cyclic loading is very difficult as there may only be a slight difference in hysteresis loops. The hysteresis loop itself is a direct result of the viscoelastic response of asphalt concrete. However, when applying very low strains, i.e. no damage occurring, the hysteresis loops should lie on top of one another. By applying a pseudostrain, the hysteresis loop collapses and the stress-strain curve should forms a straight line (line of equality). If damage occurs, then the line of equality changes whereby (*i*) a reduction in the slope of the pseudostrain line (secant pseudostiffness) occurs, and/or (*ii*) the pseudostrain line forms a loop.

$$\varepsilon^{R} = \frac{1}{E_R}\int_0^t E(t-t')\frac{\partial \prime \varepsilon}{\partial t \prime}dt' \tag{9}$$

where E(t, t′) = relaxation modulus; and E_R = constant reference modulus (usually taken as unity).

The relaxation modulus describes the linear viscoelastic properties and is determined from dynamic modulus (E*) testing. Data obtained from the E* testing is used to develop a mastercurve and from this, the relaxation modulus is determined.

Kim (*20*) found that the secant pseudostiffness (stress corresponding to maximum pseudostrain divided by maximum pseudostrain in each cycle) value decreases with increasing damage.

Daniel (*21*) and Daniel and Kim (*22*) found that the relationship between the normalized pseudostiffness (*C1*) and the damage parameter (*S1*) is unique for a given asphalt concrete mix (hereafter referred to as damage characteristic curve) under uniaxial mode of loading. The normalized pseudostiffness (*C1*) is obtained by dividing secant pseudostiffness by initial pseudostiffness, while damage parameter (S1) is a function of normalized pseudostiffness, time and material properties and is shown in Eq. 10.

$$S1_i \cong \sum_{i=1}^{N} \left[\frac{I}{2}\left(\varepsilon_{max,i}^{R}\right)^2 (C1_{i-1} - C1_i)\right]^{\frac{\alpha}{1+\alpha}} (t_i - t_{i-1})^{\frac{1}{1+\alpha}} \quad (10)$$

where $\varepsilon^{R}_{max,i}$ = maximum pseudostrain in cycle *i*, $C1_i$ = normalized pseudostiffness in cycle *i*, $S1_i$ = damage parameter in cycle *i*, α = material constant and *t* = time to maximum pseudostrain in cycle *i*.

Due to continuous growth of damage, numerical value of damage parameter continuously increases (with initial value of 0). Further, the normalized pseudostiffness is plotted against the damage parameter to obtain the damage characteristic curve. Swamy (*23*) extended viscoelastic continuum damage mode to flexure mode of loading and found that damage characteristic curve is unique at given temperature under flexure mode of loading. Swamy and Daniel (*24*) found a point of inflection in the damage characteristic curve beyond which the material loses its structural integrity at a faster rate. Also, it is observed that normalized pseudostiffness at this inflection point depends on mixture properties. The failure criterion used by Swamy and Daniel (*24*) is included, where different HMA fatigue failure criteria are analyzed.

The pseudostrain approach can also be used to determine the FEL of HMA. The pseudostrain calculation requires time history of the applied strain. This is achieved using increasing strain amplitude testing where direct tension or uniaxial tension testing is usually performed. Finally, using a cross-plot of stress vs. pseudostrain, damage is identified when there is a reduction in the slope or the appearance of a hysteresis loop. At this point, the FEL can be determined (*19*).

EXTRAPOLATION TECHNIQUES

One of the two main requirements for this analytical approach is to choose the appropriate model for the fatigue analysis. The other main requirement is to determine the minimum number of cycles to use in the model in order to produce an accurate fatigue life estimate. A study done by Prowell et al. (*10*) discusses five different models used with beam fatigue testing of HMA mixtures: exponential model, logarithmic model, single-stage Weibull function, three-stage Weibull function, and the RDEC. HMA mixtures that did not fail within 50 million cycles are extrapolated to the number of cycles corresponding to 50 percent reduction of the stiffness. In addition, each model is evaluated in terms of predicting fatigue failure, using HMA samples that had fatigue lives of 20-50 million cycles. The authors concluded that the best extrapolation method for low-strain fatigue tests is the single-stage Weibull function, which appeared to be the most conservative and also had the least variability.

However, there are some drawbacks to using these models. The AASHTO T321 (*8*) standard does not state whether all of the data (especially the initial data) should be used when solving the constants of the exponential model. The power, logarithmic and RDEC models all overestimate the fatigue life when applied to tests of low cyclic loads (less than 10 million). These models are recommended for estimating fatigue life at strain levels less than or equal to the FEL. A number of initial cycles also need to be eliminated in order to obtain a good fit to the slope at high numbers of cycles. Failure to eliminate some of the initial cycles may result in an overestimation of the fatigue life (*10*).

For this study, the single-stage Weibull function and the RDEC approach are used to extrapolate the fatigue life of HMA samples tested at low and normal strains.

Weibull Single-Stage Function

The single-stage Weibull function has been used before with some success in predicting FEL in HMA. The NCHRP Project 6-46 (*25*) in particular compared several extrapolation techniques in determining the FEL. The NCHRP Project 6-46 concluded that the single-stage Weibull function provided the most reliable results when compared with actual FEL test data. Based on this recommendation, the single-stage Weibull approach is included in this study to predict the fatigue life of low strain tests, and if possible, provide confirmation of the FEL for SP-II and SP-III mixtures. A step-by-step procedure for applying this approach to predicting fatigue life is shown in the NCHRP 6-46 Project report (*25*). The general form of the Weibull function is shown in Eq. 11:

$$R(t) = exp\left[-\left(\frac{t-\delta}{\theta-\delta}\right)^{\gamma}\right] \quad (11)$$

where $R(t)$ = the reliability at time t where t might be time or another life parameter such as loading cycles, γ = the slope, δ = the minimum life, and θ = the characteristic life.

Tsai et al. (*26*) adapted this Eq. 11 where the minimum life, δ, is assumed to be 0. The general form is then simplified into Eq. 12, where the hazard function is equal $1/\gamma$. Since the beam fatigue loading cycles are applied at a constant frequency of 10 Hz, the loading cycles, n, can be substituted for time, t.

$$S(t) = exp\,(-\lambda \times n^{\gamma}) \quad (12)$$

where $S(t)$ = probability of survival until time t, n = number of loading cycles, λ = scale parameter (intercept, b), γ = shape parameter (slope, m).

To characterize fatigue damage, the stiffness ratio (*SR*) is used, which is the stiffness measured at any cycle, divided by the initial stiffness. According to Tsai et al. (*27*), *SR(n)* can be substituted for *S(t)* given the fact that at any one cycle, the sample has a probability of survival past that cycle equal to the stiffness ratio times 100 percent. Eq. 13 allows the scale and shape parameters for laboratory beam fatigue data to be determined by linear regression.

$$ln(-ln(SR)) = ln\,(\lambda) + \gamma \times ln(n) \tag{13}$$

This equation is applied to fatigue test data taken from low strain testing. A plot of the data shows the left-hand side of the equation versus the natural logarithm of the number of cycles, and from this, a straight line regression is produced. Using the slope and intercept parameters as well as a SR of 0.5, Eq. 13 is solved for *n* by Excel solver function. This value of *n* is the extrapolated fatigue life for 50 percent initial stiffness.

Figure 6 presents typical fatigue curves of two HMA samples fitted to the single-stage Weibull function. Both samples are tested at the same strain, and the point where both curves intersect is where both tests initiated. However, from this point on, both curves diverge and follow different paths. The paths are indicative of the rate of fatigue damage occurring in both samples. From this, one can see that sample K_2 has a much steeper slope, which corresponds to a higher rate of fatigue damage, and hence a shorter fatigue life. A linear regression of the curves is shown which can be used to estimate fatigue life using Eq. 13.

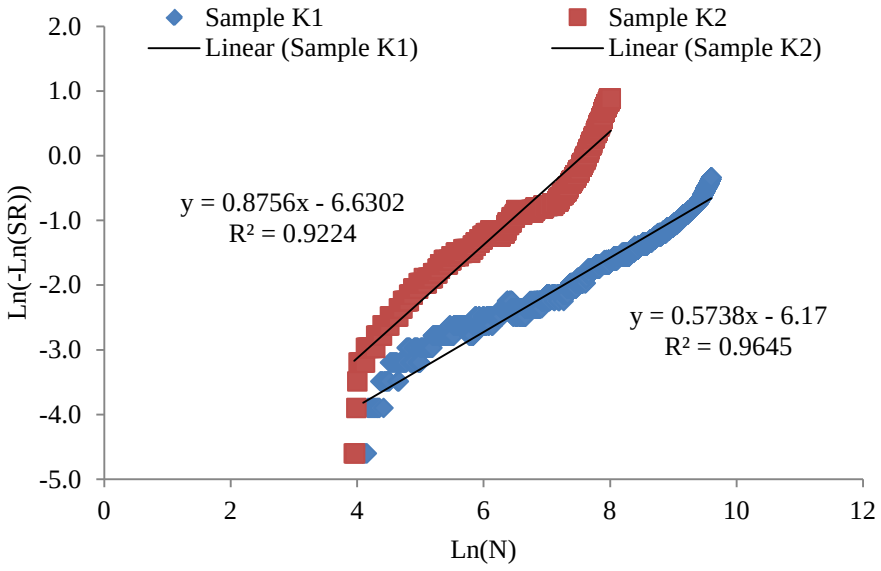

FIGURE 6 Typical Fatigue Curves for SP-II Mixture using Single-Stage Weibull Function

Fatigue Life Extrapolation Using RDEC Approach

For fatigue testing at normal strain amplitudes, the number of cycles to failure, N_{f50}, is plotted versus the dissipated energy (kPa). Figure 7 shows an example of the DE-LC relationship for an SP-II mixture. A best fit equation for the DE-LC data is obtained, using a power law relationship. From the best fit equation, the slope, *f*, of the curve, is noted. As stated earlier, the RDEC is defined as the ratio of dissipated energy change between two loading cycles by the number between the cycles, that is, the average ratio of dissipated energy change per loading cycles, as seen in Eq. 7. However, because of the presence of noise in the raw data, the average RDEC for an arbitrary 100 cycles at cycle '*n*' is calculated using Eq. 14.

$$RDEC_n = \frac{1-\left(1+\frac{100}{n}\right)^f}{100} \tag{14}$$

where *f* = the slope from the regressed DE-LC curve.

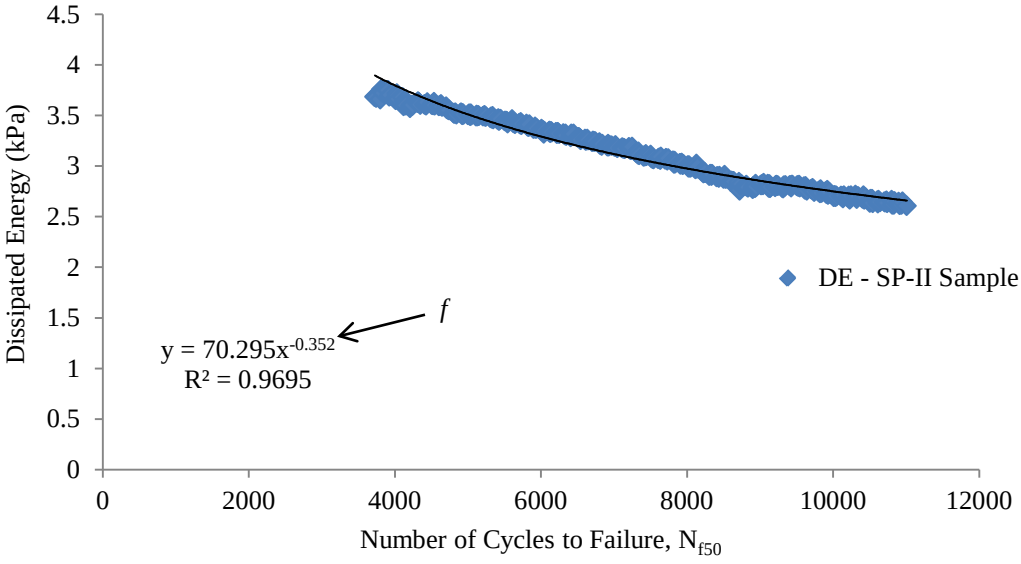

FIGURE 7 Dissipated Energy vs. Number of Cycles to Failure for SP-II Sample

PV calculation from low strain fatigue test data is similar to what is shown above for normal strain testing. The RDEC (Eq. 7) versus loading cycles is plotted using a log-log scale. Eq. 15 is then used with fatigue test data (N_{f50}) from previous fatigue tests performed at normal strain amplitudes. The intersection of these two curves is the estimated fatigue life of the sample tested at low strain. Figure 8 provides an example of a RDEC vs. loading cycle curve for a fatigue test (SP-II-L2) conducted at low strain. Shown on the same plot is a curve displaying the fatigue life of tests conducted at normal strain, which are fitted Eq. 15.

$$PV = 0.4428{N_{f50}}^{-1.1102} \tag{15}$$

The RDEC-LC curve is extended until it crosses the unique PV-N_f curve. The intersection point of these two curves produces the PV (y) and N_{f50} (x). The PV and N_{f50} are then calculated using Eqs. 16 and 17 respectively.

$$PV = \frac{1-\left(1+\frac{100}{N_{f50}}\right)^{f}}{100} \approx -\frac{f}{N_{f50}} \tag{16}$$

$$N_{f50} = \left(\frac{-f}{0.4428}\right)^{-9.0744} \tag{17}$$

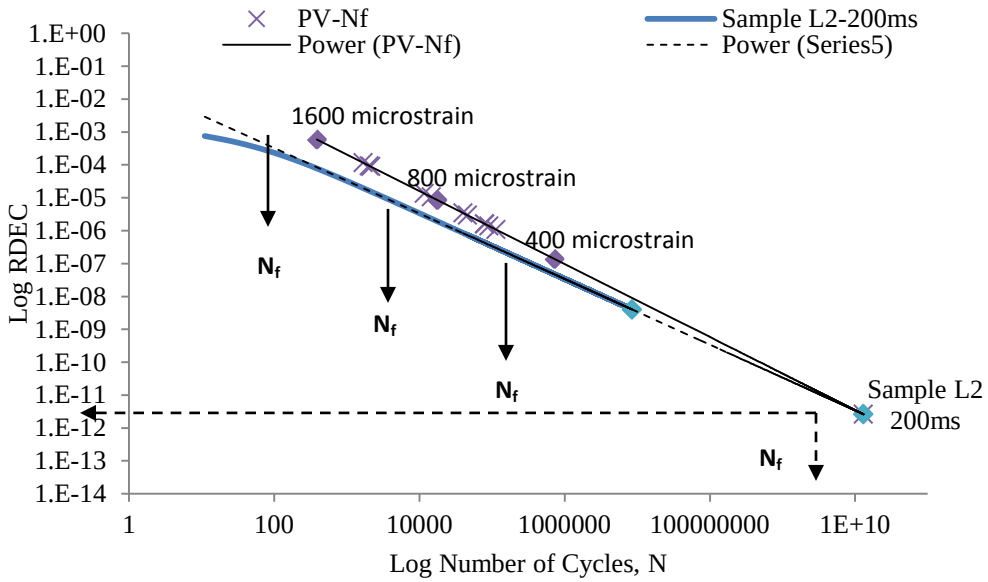

FIGURE 8 Fatigue Life Prediction of SP-II Sample using RDEC Approach

FACTORS AFFECTING THE FEL OF ASPHALT CONCRETE

Effects of Rest Periods

An important concept that has been highlighted recently in pavement design, which directly affects the FEL of HMA, is damage recovery or healing that occurs during rest periods. Current research undertaken by the National Cooperative Highway Research Program considers this concept as their primary objective in designing a perpetual pavement. The aim of the research is to design/build a pavement that ensures that the damage induced by the loading is low enough so that healing occurs. Therefore, there is no accumulation of damage over the life of the pavement (*28*). This design approach differs from traditional perpetual pavement design approaches, which do not consider healing.

Healing is a well-known phenomenon in materials such as polymers, glass and Portland cement (*29, 30, 31, 32, 33*). The healing phenomenon is generally considered as the capability of a material's self-recovery, which occurs between loads when damage is reversed as the asphalt–aggregate interface reattaches, thereby closing microcracks. According to some researchers, it is a continuous physical-chemical reaction that may occur as applied load damage develops, not just between load applications (*15*). According to another study by Freund and Suresh (*34*), when considering a viscoelastic material such as HMA, the actual fatigue behavior can be explained as energy equilibrium between surface energy and the dissipated damage energy. Healing potential is the difference between surface energy and the dissipated damage energy. Little et al. (*35*) showed that surface energy is responsible for microcrack damage rates using Schapery's viscoelastic fracture theory. According to Little et al. (*35*), if surface energy is smaller than the dissipated damage energy, the healing potential is negative; hence the material will increase surface energy through microcracking. This is the process of crack initiation and propagation (damage). If the dissipated damage energy is low, the positive healing potential controls the energy equilibrium whereby a reduction in surface energy will close crack openings through a healing process. The dissipated energy level is determined by external load and internal material properties (*7*).

Another study which helps explain the mechanism of healing in asphalt materials is that of Petersen (*36*), which stated that the association force (secondary bond) is considered the main factor in controlling the physical properties of asphalt. Petersen concludes that the higher the polarity, the stronger the association forces. Lytton (*37*) conducted a similar study, which concluded that the fracture or healing of an asphalt mixture is related to two mechanisms: the surface energy storage and the surface energy release. Therefore, microfracture and healing of HMA are governed by the energy balance per unit of crack area between the dissipated energy released and the energy that is stored on the surface of the crack.

The effects of healing and its contribution to fatigue life of HMA are very much unknown. As yet, there is no current pavement design method that considers the effects of rest periods under real traffic conditions, except for the use of shift factors, which are arbitrary at best. A study done by Carpenter and Shen (*15*) described the effects of healing or rest periods on the fatigue life of HMA and in particular, explains the existence of a FEL in HMA. Data recorded from strain-controlled flexural-fatigue tests on two different mixes (neat and polymer-modified) is analyzed using the RDEC approach (*7*). Figure 9 describes the effect of rest periods on two

HMA mixes. As the rest period increased, the fatigue life also increases for both HMA mixes (*15*). The major disadvantage of this method is the additional time required to incorporate healing. A short rest period of 0.9 second can increase testing time from 3 to 30 hours. A more reasonable rest period of 90 seconds would require 10 to 100 days of continuous testing (*19*).

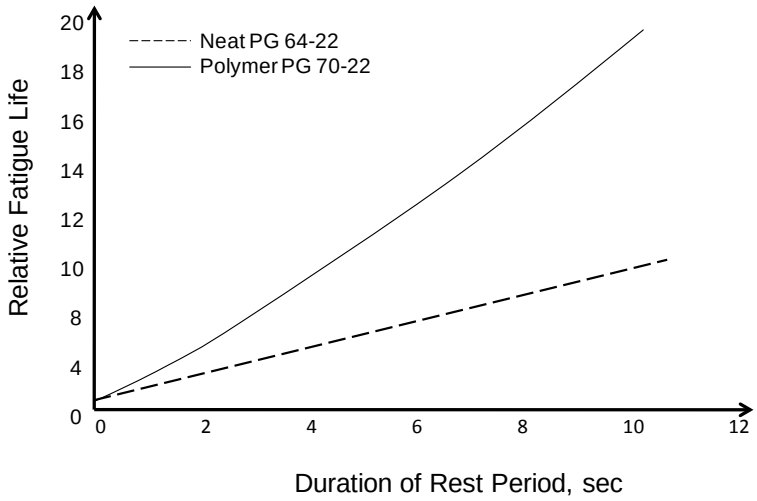

FIGURE 9 Effect of Rest Period on Fatigue Life

(Advanced Asphalt Technologies 2008)

Effect of Applied Strains

There are times during the service life of a perpetual pavement that it will experience strains greater than the design FEL (usually 70 με) that will certainly reduce the fatigue life of the pavement and may even eliminate possible FEL behavior. Some studies have shown that higher applied strains reduce the fatigue life of HMA. In particular, a study by Carpenter and Shen (*15*) applied continuous loading on two different HMA mixes and then compared the fatigue test results of both mixes. The study concluded that higher applied strains yielded higher plateau values, which correspond to a lower fatigue life. This result is expected as higher applied strains are more likely to cause more damage. In addition, healing of the HMA requires more time and if full recovery is not achieved, damage accumulates and the fatigue life shortens.

The theory of reduced fatigue life due to higher applied strain levels is discussed in greater detail by Thompson and Carpenter (*38*) where they investigated the effects of overloading HMA mixtures beyond the FEL. Cyclic loading is carried out to about 50 million cycles at 70 με on a HMA mixture with a fatigue life of 6×10^{11} cycles. At this point the strain level is increased to 500 με and loading is continued for another 6000 cycles. It is also noted that the fatigue life of the undamaged mixture at 500 με is about 20,000 cycles. Following the 6000 cycles, the strain level is reduced to 70 με with the remaining fatigue life expected to be around 2.3×10^{11} cycles, which suggests FEL behavior. Thompson and Carpenter (*38*) concluded that the effects of

overloading do not alter the existence of a FEL. This study also confirms that at higher applied strains, fatigue life is shortened but does not necessarily eliminate the FEL behavior of a perpetual pavement.

Effect of Multiple Temperatures

Environmental effects, especially temperature variations, are considered one of the main contributors to long-life flexible pavement deterioration according to pavement experts in the United Kingdom (*39*). To be of practical use, strain amplitudes on HMA mixes must be applied using a wide range of temperatures. As mentioned previously, applied strains are usually tested in a controlled environment with a temperature of 20 °C. Healing can also be considered but the effect of temperature on healing is very much unknown. Some studies indicate that the healing effect of rest periods increases with increasing temperature (*40*). Research spearheaded by the NCHRP Project 9-19 investigated the effects of using multiple temperatures (along with rest periods) on allowable strains of HMA mixes by applying a time-temperature superposition (*41*). Results showing allowable to applied strain ratios of a specific HMA mix at different temperatures revealed that critical fatigue cracking conditions are more apparent at low-moderate pavement temperatures (10-15 °C). This is expected as fatigue damage is usually reduced at higher temperatures where the HMA mixture softens and the healing rate of damage increases.

Effects of Aging

The effects of aging are very important when characterizing the fatigue life of HMA and the establishing the subsequent FEL. It is well known that as the pavement life ages, the stiffness of the asphalt binder increases and in turn, the dynamic modulus of the HMA increases. In addition, healing of HMA is also affected and one can assume that as the asphalt binder hardens, the healing effect decreases. Only one study has been found from the literature review that comprehensively describes the effects of long-term aging of HMA. Laboratory aging exposure conditions are varied (0, 3, and 6 months) at 60 °C which simulated approximately up to 12 years of aging. Results of strain-controlled laboratory testing showed that binder oxidative aging reduced HMA mixture resistance to cracking and its ability to heal. In addition, all mixtures tested showed an exponentially declining N_f trend due to aging (*42*). The recent pavement design guide developed by AASHTO, the mechanistic-empirical pavement design guide (MEPDG), uses a global aging model to determine aged modulus values of HMA mixes. Further research is needed in this area to determine the effect of aging on HMA healing and consequently the effect of aging on the FEL.

Effects of Binder Content and Mixture Variables

Research on the effect of mix variables on the FEL of HMA have shown a wide range of FEL values depending on binder selection and HMA mix composition. The FEL of HMA mixtures is said to be affected by mixture variables such as air voids, aggregate gradation, asphalt binder content, etc. From the literature search, there are very few studies about the effect of polymer-modified binders on the FEL. Some studies have shown that using certain polymer binders (PG

76-22) in particular HMA mixtures enhances the ability to withstand fatigue cracking. Therefore, the presence of modified binder in HMA materials should improve the FEL of HMA mixtures (*25, 43*). Another study showed mixed results with mixtures containing two different modified binders showing greater fatigue life than mixtures containing one of the unmodified binders. Mixtures containing unmodified binder with lower temperature susceptibility, achieved two to three times the fatigue life of the polymer modified mixtures (*44*).

One particular study utilized the RDEC approach and a fatigue life equation developed by the University of Illinois, to determine the effects of stiffness (flexural), air void content, binder content, and aggregate gradation on the tensile strain experienced in a HMA mixture. Plateau values are determined for HMA mixtures using the RDEC approach. As stated earlier, the PVs are directly related to the fatigue life of a mixture, with lower PVs indicating longer HMA fatigue lives. The relationship between the PV and mixture variables is developed by Carpenter and Shen (*7*) using over 120 mixtures. The equation is shown below:

$$PV = 44.422\varepsilon^{5.140}S^{2.993}VP^{1.850}GP^{-0.4063} \quad (18)$$

Where ε = tensile strain, S = flexural stiffness of HMA from laboratory fatigue test, VP = volumetric parameter,

$$VP = \frac{AV}{AV+V_b} \quad (19)$$

AV = percent air voids, V_b = asphalt content by volume (Roberts et al. 1996),

$$V_b = 100 \times \frac{G_{mb} \times P_{ac}}{G_b} \quad (20)$$

G_{mb} = bulk density of HMA, P_{ac} = percent asphalt content by weight, G_b = bulk specific gravity of binder, GP = aggregate gradation parameter,

$$GP = \frac{P_{NMS} - P_{PCS}}{P_{200}} \quad (21)$$

P_{NMS} = percent aggregate passing nominal max. size sieve, P_{PCS} = percent aggregate passing primary control sieve (PCS = NMS*0.22), and P_{200} = percent aggregate passing #200 sieve. Table 1 presents PCS data for different nominal size mixtures.

TABLE 1 Control Sieves for Various Asphalt Mixes

	Sieve Size					
NMS mm (in.)	37.5 (1.5)	25 (1)	19 (0.75)	12.5 (0.5)	9.5 (0.375)	4.75 (#4)
PCS mm (in.)	9.5 (0.375)	4.75 (#4)	4.75 (#4)	2.36 (#8)	2.36 (#8)	1.18 (#16)

Note: NMS=Nominal Max Sieve Size, PCS=Primary Control Sieve

Once the PV is known, the allowable strain, ε, where no damage accumulates, can be determined using Eq. 22, and this is considered to be the FEL strain of a mixture. Applying a PV of $6.74e^{-09}$, which represents FEL behavior in a HMA mixture (*7*), to Eq. 22, enables a prediction of the FEL using material properties.

$$FEL = 0.0123S^{-0.5832}VP^{-0.3599}GP^{0.0790} \quad (22)$$

The paper concluded that the flexural stiffness, volumetric parameter, percent of air voids, and percent of asphalt content had the most significant impact on the fatigue life of HMA. Early research conducted by Monismith indicated that an increase in HMA stiffness due to a decrease in air voids, and optimum asphalt content produced longer HMA fatigue life (*3*). The mix variable that affected the FEL of HMA the least is the aggregate gradation. Variables included within the aggregate gradation included the gradation parameter, GP, percent passing the nominal maximum size sieve, P_{NMS}, percent passing the primary control sieve, P_{PCS}, and percent passing the #200 sieve, P_{200}. Little or no change is observed due to changes made to these mix variables. Research conducted by Monismith also concludes that aggregate grading also has little effect on fatigue life of HMA (*3*). This conclusion does not seem practical as gradation plays a significant role in the stiffness of HMA mixtures and this in turn may be highly influential on the FEL of HMA (*25*).

Finally, recent studies (*43, 45*) have shown that HMA mixtures containing modified binders have a greater laboratory fatigue life than those that contain unmodified binders. There are very few studies that have explored this area and more research is needed in order to know more about the effect of modified binders on the fatigue life of HMA mixtures.

CORRELATING LABORATORY TESTING TO FIELD PERFORMANCES

Many studies have been conducted to determine the relationship between laboratory fatigue test results and subsequent field performances (*46, 47, 48, 49, 50*). The conclusions of some of these studies indicate that the laboratory fatigue life of HMA specimens do not match the field fatigue life of tested pavements (*49, 50*). One study in particular tried to identify the relationship between laboratory FEL measured strains of pavement test sections (National Center for Asphalt

Technology, NCAT), and the overall performance of these test sections (*51*). Results indicated that no relationship could be found between laboratory testing, measured field strains, and overall pavement performance. Although this paper is not successful in its objective, it does illustrate the difficulty in producing laboratory test results that can be related to field performances.

The other alternative to relating laboratory testing to field performances is the application of shift factors. The application of shift factors to laboratory test results is well documented and from the literature, shift factors vary from 4 to 100 depending on mix design and state agency (*48*, *52*). It appears that from the literature reviewed, the fatigue life of HMA pavements in the field is much greater than the HMA mixes tested in the laboratory. Reasons for this vary from wheel wander in field pavements and fatigue test methods (loading/temperature variations) to the effect of healing/rest periods on the fatigue life of field pavements (*53*). The use of shift factors clearly underlines the difficulty of applying field fatigue conditions to laboratory fatigue test set ups.

FEL IN CURRENT FLEXIBLE PAVEMENT DESIGN

Traditionally, the inclusion of fatigue in flexible pavement design requires the use empirical relationships, which relate the tensile strain to the number of load cycles to failure. An example of this relationship is shown earlier in Eq. (4). This empirical relationship has since been modified based on observed behavior in the field. An example of this can be seen in the Mechanistic Empirical Pavement Design Guide (MEPDG);

$$N_f = K_1(\frac{1}{\varepsilon})^{k_2}[(\frac{1}{E})^{k_3}] \quad (23)$$

where N_f = number of cycles to failure, E is the modulus of the HMA, and K_1, K_2, and K_3 are the regression constants determined from laboratory testing.

MEPDG

The basic inputs for the MEPDG include environmental conditions, materials, and traffic data. The material characterization provides two major inputs; pavement response properties which predict the states of stress, strain and displacement within the pavement due to traffic loading, and distress/transfer functions which relate traffic loading to fatigue cracking, rutting, and other pavement distresses (*42*). The latest version of the MEPDG considers two fatigue factors; (*i*) a HMA fatigue algorithm shown in Eq. 23, and (*ii*) a FEL. The first option determines the tensile strain, ε_t, at the base of the HMA layer due to traffic-induced loading. MEPDG plugs this value into Eq. 23 to determine N_f, which is then used to calculate percent fatigue cracking. The second option compares the calculated ε_t to the predetermined FEL (input value). If the resulting ε_t is below the FEL, fatigue cracking will be negligible (zero). Thompson and Carpenter (*54*) did a study where they applied a FEL input value and then compared the results with the predicted fatigue cracking (no FEL input) using the HMA fatigue algorithm. Results indicated that the FEL input has very little effect on the estimated HMA fatigue cracking.

Illi-Pave

Illi-Pave is a stress-dependent elastic layer program (ELP) developed at the University of Illinois (*55*). Tensile strains at the base of HMA pavements can be calculated using the following fatigue algorithm developed at the University of Illinois;

$$Log\ \varepsilon_{HMA} = 5.746 - 1.549\ LogT_{HMA} - 0.774\ Log\ E_{HMA} - 0.097\ LogE_{Ri} \quad (24)$$

where ε_{HMA} = HMA flexural strain (micro-strain) for a 9-kip wheel load, T_{HMA} = HMA thickness (inches), E_{HMA} = HMA modulus (ksi), and E_{Ri} = subgrade modulus (ksi).

No traffic input is required. Through iterations, the pavement thickness required to achieve a specific FEL can be determined. Illi-Pave is a program that can determine a pavement thickness that ensures HMA strains are less than or equal to the FEL.

PerRoad

Another ELP model widely used is the PerRoad program, which is developed at Auburn University, Alabama (*56*). The HMA fatigue algorithm is identical to Eq. 4 shown earlier. Fatigue results are presented as the percent of HMA strain less than the FEL, which should be close to 100 percent if a perpetual pavement is required. Basic inputs to PerRoad are similar to those used in the MEPDG and both programs can accommodate FEL as design input. The major drawback of these two programs is that predicted HMA strains are not provided as outputs. Thompson and Carpenter (*54*) emphasized this point in their study on the suitability of these three programs in designing perpetual pavements using the FEL. They also stated that the simplicity of the Illi-Pave procedure is an attractive feature compared to the comprehensive nature of the other two programs. The take-home message of this paper is that all three programs are more than capable of providing perpetual pavement designs.

THIS PAGE LEFT BLANK INTENTIONALLY

SAMPLE COLLECTION, PREPARATION, AND FEL TESTING

Mix Selection

Two HMA mixtures: SP-II and SP-III mixtures, which are typically used in major highways and primary routes in the State of New Mexico are used in this study. The SP-II mixture is considered a rut-resistant HMA mixture, predominantly used in intermediate AC layers of a pavement structure. This type of HMA mixture is selected for fatigue analysis on the assumption that although considered a rut-resistant mixture, it may perform poorly in fatigue or other forms of cracking. The SP-III mixture is considered a finer Superpave HMA mixture than SP-II mixture, and is designed with a PG 70-22 binder. SP-III mixture is considered a fatigue resistant HMA mixture usually used in the intermediate and base AC layers of a pavement structure.

Mix Collection

HMA mixtures and aggregate materials are obtained from on-site construction projects and from source batch plants on I-25 near Budagher. Sampling methods in accordance with AASHTO T-168 (*57*) standards and T-2 (aggregates) procedures are followed. In total, about 40-50 bags containing 18-20 kg of HMA mixtures are collected from the project site and about 25-30 bags of similar weight containing HMA granular materials are also collected from the source batch plant. HMA mixtures are sampled using paper bags (double-bagged) where a smaller sample size is more efficient for the heating/compaction process. Samples of PG 64-22 binder and PG 70-22 binder grades are also collected from the source batch plant.

Laboratory testing is performed to determine the physical properties of the HMA mixtures subsequently used for this project. Laboratory testing includes the bulk specific gravity test (G_{mb}), the theoretical maximum specific gravity test (G_{mm}), as well as binder content and aggregate gradation testing.

Mixture Gradation

Aggregate gradation chart of SP-II and SP-III mixtures is shown in Figure 10. Maximum density lines for maximum aggregate sizes of 1 in. and 1.5 in. are plotted in Figure 10, corresponding to maximum aggregate sizes of respective SP-III and SP-II mixtures. Mixes that plot above the maximum density line are generally fine mixes while mixes that plot below the maximum density line are generally coarse mixes. Both SP-II and SP-III mixtures plot below their respective maximum density lines. Therefore, SP-II and SP-III are coarse mixes. Table 2 shows aggregate gradations of three SP-II mixture samples that are tested using AASHTO T30-08 (*58*) standards. Also shown in Table 2 are the upper and lower limits of the SP-II aggregate gradation. Results show that all three sample gradations fall within these limits. Table 3 shows similar results for aggregate gradations of the SP-III mixture, with sample gradations falling within the specified limits.

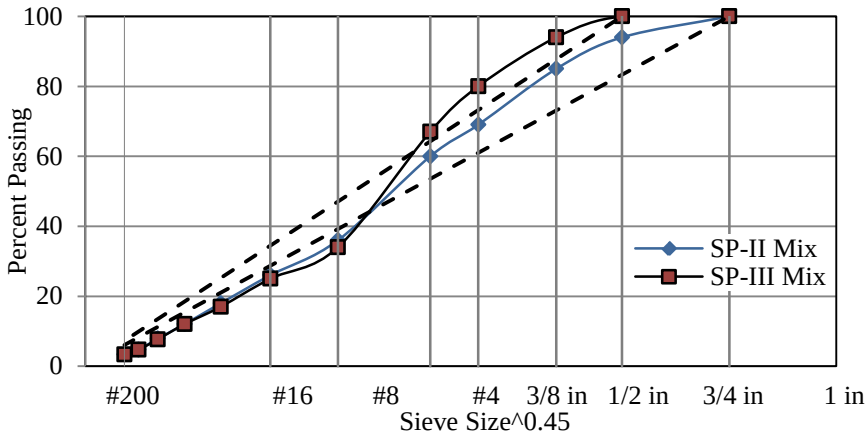

FIGURE 10 Aggregate Gradation for Superpave SP-II and SP-III Mixtures

TABLE 2 Aggregate Gradation for SP-II Mixture

SIEVE SIZE		NMDOT Specification SP-II		PERCENT Passing		
	(mm)	Lower Limit (%)	Upper Limit (%)	Sample A	Sample B	Sample C
2.0″	50.8	100	100	100.00	100.00	100.00
1.5″	38.1	100	100	100.00	100.00	100.00
1.0″	25.4	90	100	97.32	92.18	100.00
3/4″	19	-	90	83.67	87.75	87.98
1/2″	12.7	-	-	58.46	66.70	64.64
3/8″	9.51	-	-	50.27	56.92	54.50
#4	4.76	-	-	33.40	35.82	34.02
#8	2.38	19	45	20.43	21.94	20.81
#16	1.19	-	-	13.75	14.49	13.75
#30	0.595	-	-	9.26	9.59	9.16
#50	0.297	-	-	5.95	5.87	5.66
#100	0.149	-	-	3.36	3.03	2.91
#200	0.075	1	7	1.90	1.40	1.35

TABLE 3 Aggregate Gradation for SP-III Mixture

SIEVE SIZE		NMDOT Specification SP-III		PERCENT Passing		
	(mm)	Lower Limit (%)	Upper Limit (%)	Sample A	Sample B	Sample C
2.0″	50.8	100	100	100.00	100.00	100.00
1.5″	38.1	100	100	100.00	100.00	100.00
1.0″	25.4	100	100	100.00	100.00	100.00
3/4″	19	90	100	95.83	93.58	93.65
1/2″	12.7	-	90	72.11	81.56	70.42
3/8″	9.51	-	-	61.95	62.25	60.78
#4	4.76	-	-	34.78	34.08	34.70
#8	2.38	23	49	25.15	25.52	25.59
#16	1.19	-	-	18.21	18.28	19.05
#30	0.595	-	-	7.90	9.55	8.73
#50	0.297	-	-	5.82	6.01	5.53
#100	0.149	-	-	4.44	4.34	4.15
#200	0.075	2	8	3.03	3.75	3.75

Mixture PG Grade

Among the performance grade (PG) binders typically used in New Mexico, the selected binders for this study are PG 64-22 and PG 70-22. Unlike PG 64-22, PG 70-22 is a modified binder with a polymer that improves its high-temperature properties in terms of the shear and viscosity properties. The design asphalt content for SP-II and SP-III mixtures is 4.4% and 4.6% respectively (NMDOT Specifications 2007). Laboratory testing to determine the binder content of SP-II and SP-III mixtures is performed according to AASHTO T 308 (*59*) standards with the results presented in Table 4. Once again, three samples of each HMA mixture are tested and an average percentage of binder content is presented. Results show that the SP-II and SP-III mixtures contain 4.3% and 4.5% respectively.

TABLE 4 Asphalt Binder Content for NMDOT SP-II and SP-III Mixtures

Asphalt Binder Content	Sample A	Sample B	Sample C	Average
SP-II	4.13	4.76	4.26	4.38
SP-III	4.29	4.63	4.52	4.48

FEL Sample Preparation

In the early stages of sample preparation, there are some major concerns in achieving target density of HMA beam specimens, which are highlighted and discussed below. The dimensions of the HMA beam samples used in FEL laboratory testing are approximately 380 mm x 65 mm x 50 mm (15 in. x 2.5 in. x 2 in.). Samples are compacted to dimensions slightly greater than those shown above using an asphalt beam compactor (due to mold size). In terms of heating and transferring the HMA mixtures, AASHTO T312 (*60*) standards are followed. HMA mixtures are heated to 150 °C for no more than one hour and are then compacted using a GCTS beam compactor, shown in Figure 11. HMA beam samples are compacted using a sinusoidal loading of 80 kN at a frequency of 1 Hz until they reached the specified density (2 in. height). Sample density is determined following AASHTO T 269 (*61*) standards. There are currently no AASHTO standards for HMA beam compaction so a lot of time is spent adjusting compaction methods in order to achieve the target density. However, the target density of 94.5±0.5% is not achieved with the percentage air voids varying from 9 to 12 %.

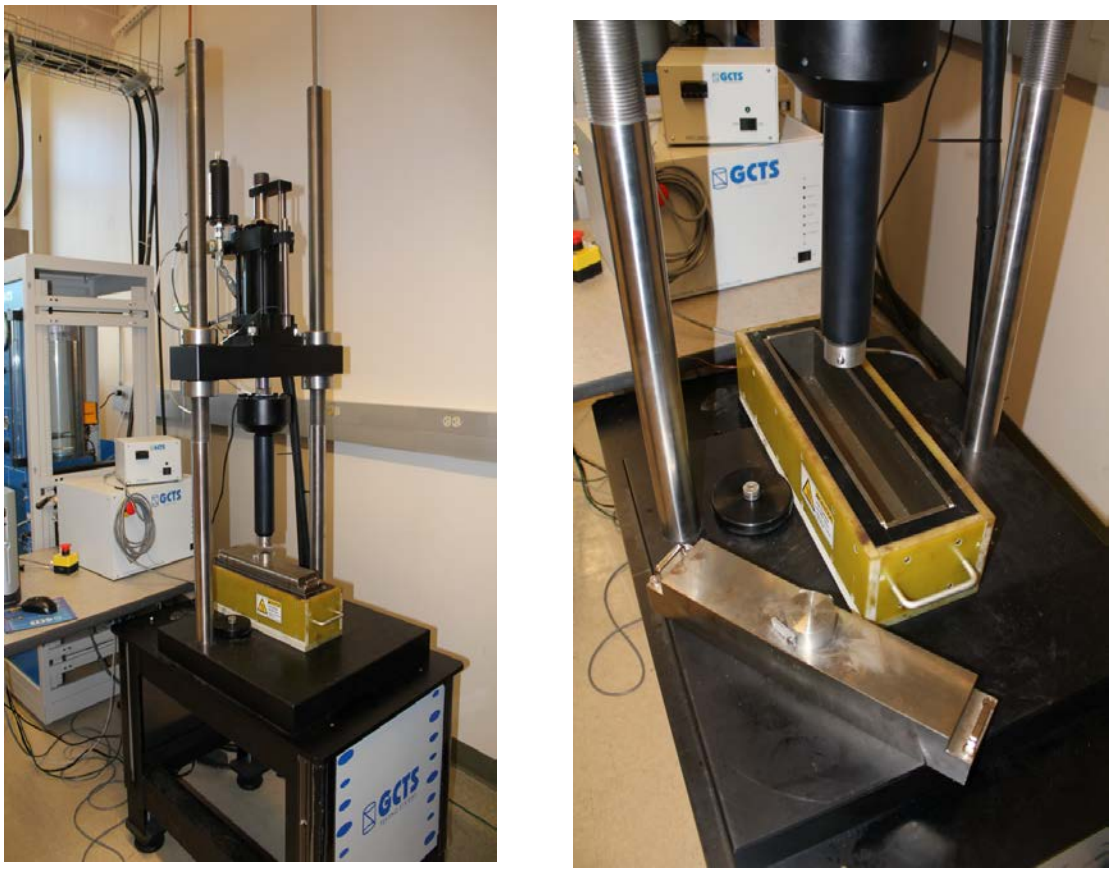

FIGURE 11 Loading Frame and Sample Mold for Beam Compaction

The problem of high air voids in specimens lay with the compaction method, which is inadequate. Reasons for this may be due to absence of kneading action during the compaction process, which provides a better compaction without fracturing the aggregate. These issues are resolved with the acquisition of a new linear kneading compactor. Once installed, the target density of 94.5±0.5% for both SP-II and SP-III mixtures is achievable. The compaction method is very similar to what is used in the field. Figure 12 shows the linear compactor used by the UNM research team. The compactor is very impressive in terms of size and is made primarily of stainless steel and 1045 steel for rugged functionality. The compactor is driven by a hydraulic unit located next to the compactor, which is also shown in Figure 12.

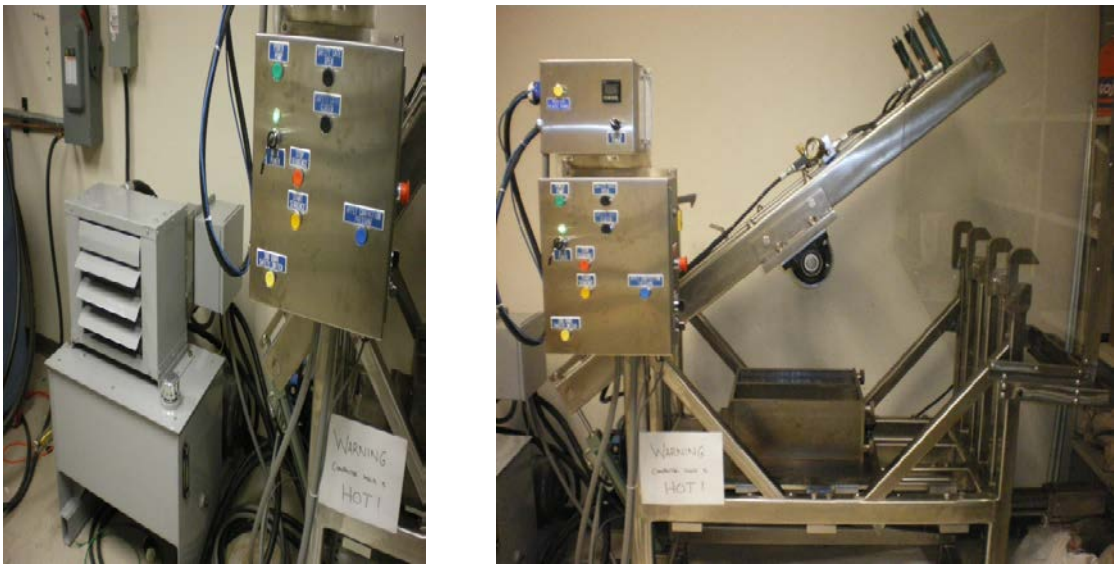

FIGURE 12 PMW Linear Kneading Asphalt Compactor

The compactor is capable of fabricating two test specimens (18 in. x 6 in. x 3 in.) in less than five minutes. Figure 13 shows freshly compacted HMA mixtures within the heated molds and those that have been previously compacted.

FIGURE 13 HMA Beam Samples Compacted by Linear Kneading Compactor

HMA Sample Cutting

Once cooled, the compacted HMA specimens are then cut into two beams (15 in. x 2.5 in. x 2.0 in.) using a GCTS stone-cutting saw, as shown in Figure 14. The stone-cutting saw originally did not come with a clamp that is suitable for cutting beam specimens. The UNM research team enlisted the help of David Woods who is a prototype machinist from the Department of Mechanical Engineering, UNM. With his help, a new clamp assembly was designed to enable safe and precise cutting of the compacted beams.

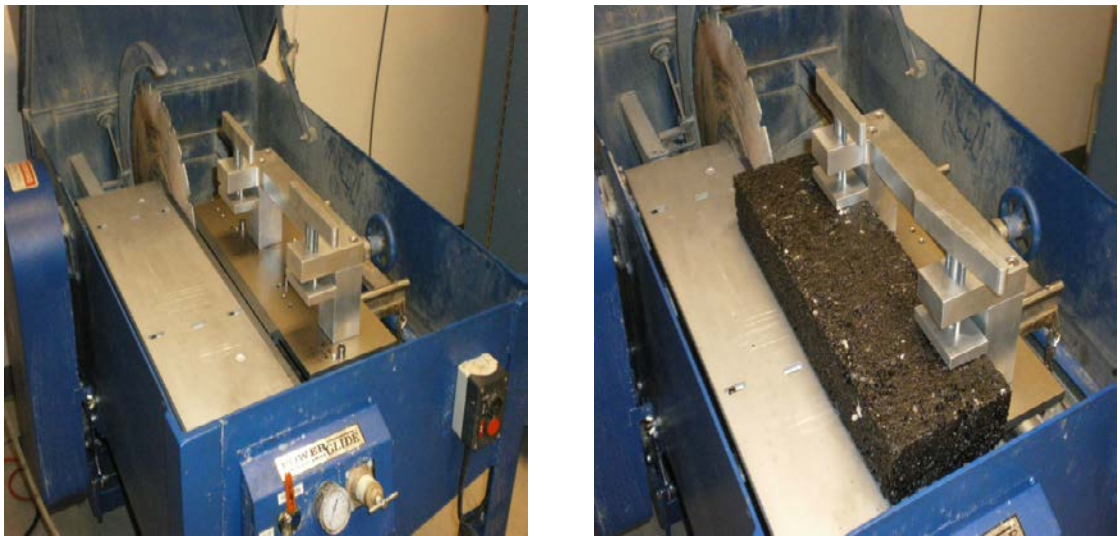

FIGURE 14 Stone Cutting Saw with Modified Clamp

Specimen Volumetric Properties

The theoretical maximum specific gravity (G_{mm}) of the loose HMA mixtures is determined by using the AASHTO T 209 (*62*) standards and the results are shown in Table 5. The G_{mm} at design AC for SP-II and SP-III mixtures is typically 2.439 and 2.430 respectively (NMDOT Specifications 2007). Three samples of each HMA mixture are tested. Table 5 shows that the average G_{mm} for SP-II and SP-III mixtures is 2.401 and 2.420 respectively.

TABLE 5 Theoretical Maximum Specific Gravity of SP-II and SP-III Mixtures

Max. Theoretical Sp. Gravity (G_{mm})	Sample A	Sample B	Sample C	Average
SP-II	2.416	2.386	2.401	2.401
SP-III	2.414	2.415	2.432	2.420

Bulk specific gravity (G_{mb}) testing is performed on HMA beam samples according to AASHTO T 269 (*61*) standards. NMDOT specifications for HMA percent air voids (AV) call for the G_{mb} to be between 5 to 6%.

Sample Conditioning

Prior to laboratory fatigue testing, the HMA beam samples are conditioned to simulate short-term aging in the field. Short-term aging of the HMA mixtures is considered during the compaction process whereby loose HMA mixtures are exposed to 163 °C for one hour prior to compaction. Once cooled, the beam samples are cut to the dimensions specified earlier. Each sample is then conditioned to test temperature, 20 °C, using an environmental test chamber for 2 hours. Figure 15 presents the environmental chamber where sample conditioning is conducted.

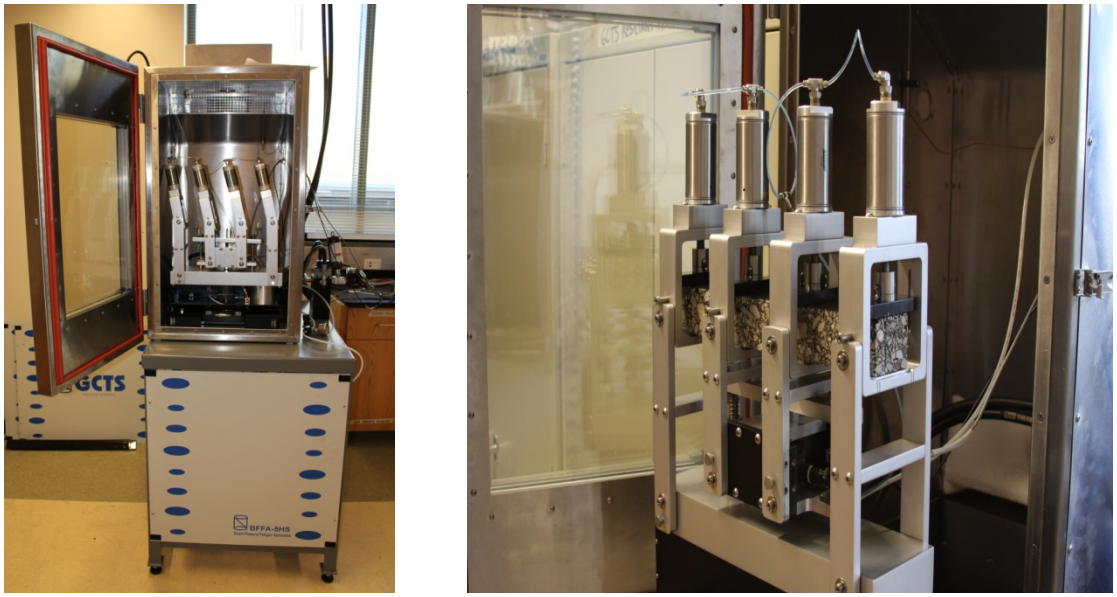

FIGURE 15 Environmental Chamber and Beam Fatigue Apparatus

Four Point Bending Beam Fatigue Test

This study applies the traditional approach to fatigue analysis of asphalt concrete in accordance with the AASHTO T 321-07 (*8*) Standards. This approach consists of relating stress (strain) to the number of load repetitions to failure and is described using Wohler Curves. In addition to this, the energy approach is utilized, which defines fatigue life as a function of dissipated energy change with each loading cycle. This is called the Plateau Value approach, as described earlier.

Cyclic loading using continuous controlled strain is applied to an asphalt concrete beam sample until it fails, where both the critical strain and the number of cycles to failure data is recorded. Figure 16 presents the beam fatigue apparatus. Loading is done using a sinusoidal waveform at a

frequency of 10 Hz at a fixed temperature of 20 °C. Two replicate samples are tested at each strain level. Cyclic loading of the beam sample induces tension in the bottom section where microcracking and subsequent macrocracking will propagate to the top of the beam. This behavior, in essence, simulates field fatigue cracking due to traffic loading. Fatigue testing is conducted at stain levels varying from 400–1200 με, from which a ε-N relationship is developed.

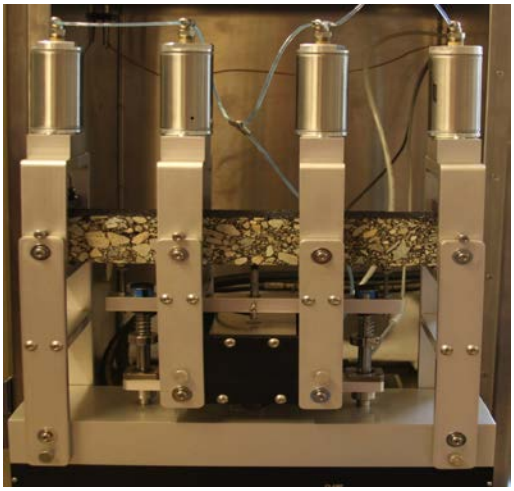

FIGURE 16 Beam Fatigue Apparatus

Although much has been said about the benefits of including rest periods in fatigue testing, this study did not consider this option due to the additional time required. Rather, testing is performed at 10 Hz which simulates traffic speed of 60 mph, similar to what is expected on New Mexico's highways. The time recorded to run each test varied from two hours (high strain) to one month (low strain).

Selected Mode of Cyclic Loading

Controlled strain mode of loading is selected for this study because it best represents the type of loading experienced by thin pavement layers (2-3 inches). Thin asphalt pavement layers are not the main load-carrying components and the strain in the asphalt layer is governed by the underlying layers, and is not affected by the reduction in asphalt stiffness. Therefore, this creates a constant strain mode of loading. The SHRP A003-A project, evaluated various laboratory fatigue test methods of asphalt concrete, and stated that unless thick pavements sections are being considered (4-8 inches), controlled strain mode should be used for all fatigue testing (*53, 4).* For thicker pavements, the asphalt layer is the main load-carrying component and as the asphalt material stiffness reduces, the changes in stress are not significant, which leads to a constant stress mode of loading.

In addition, field fatigue cracking is usually determined by calculating expected strains at the base of the pavement, which means the performance of thick pavements can be determined by

constant strains test (*4, 25*). Finally, perpetual pavements usually contain a thin HMA layer which is placed at the bottom of the section designed especially to resist fatigue cracking.

Data Acquisition and Analysis

Laboratory fatigue testing is controlled using GCTS software and fatigue test data is recorded using a GCTS data acquisition system. From this system, test results featuring the stiffness reduction, dissipated energy, Energy Ratio, and applied strain plots are generated.

FATIGUE TEST RESULTS AND ANALYSIS

General

In this section, laboratory fatigue test results of four HMA mixtures are presented and analyzed. These test results are presented in terms of applied strain amplitude, initial flexural stiffness (psi), percent air voids, and the number of cycles to failure. As stated earlier, fatigue failure is presented using two stiffness-based approaches; number of cycles to attain 50% reduction in stiffness (N_{f50}), and number of cycles at peak Energy Ratio ($N_{f(ER)}$). The Energy Ratio curve is obtained by multiplying stiffness ratio by corresponding cycle number. Laboratory fatigue testing is performed at normal strain amplitudes (600-1200 με) and at low strain amplitudes (200-400 με). Although this study discusses 'normal and low strain' in terms of applied amplitude, these terms are actually referring to the levels of fatigue damage. Low strain usually refers to low damage accumulation whereas normal strain refers to high damage accumulation. In this case, low strain usually ranges from 200-400 με. However, there are some fatigue test results in this study that show high fatigue damage at 400 με.

If the stiffness reduces by 50% as the number of cycles increases, the sample is considered failed. Samples, which did not fail during testing, are analyzed using extrapolation techniques to determine their fatigue life. The extrapolation techniques used for this analysis are the single-stage Weibull function, and the RDEC approach. Previous studies have recommended these techniques in providing good results for extrapolating fatigue life data from low strain fatigue testing (*10*).

Two analytical models are used to estimate the FEL: the Plateau Value approach and the phenomenological approach. The estimated FEL values produced from these two models are compared to those estimated by stiffness-based fatigue failure criteria: traditional N_{f50} and Energy Ratio (ER) criteria. In addition, the effect of binder's PG on the estimated FEL of the four HMA mixtures is also investigated.

Test Matrix

Table 6 presents a test matrix describing laboratory fatigue test parameters for this study. Two different mixture types are tested; SP-II and SP-III mixtures, and these mix types are prepared in the laboratory as well as collected from the field. Field SP-II mixture is designed with PG 64-22 binder, while laboratory SP-II mixture is designed with PG 70-22. For the SP-III mixture, the field design contains PG 70-22. However, the laboratory SP-III mixture contains PG 64-22 binder. The applied strain amplitude varies from 400 to 1200 με while the percent air voids varies from 5 to 6%.

TABLE 6 Test Matrix for Laboratory Fatigue Testing of SP-II and SP-III Mixtures

HMA Mix Type	PG Binder	Applied Strain (με)	% Air Voids
SP-II	64-22, 70-22	400, 800, 1000, 1200	5-6
SP-III	64-22, 70-22	400, 800, 1000, 1200	5-6

Laboratory Fatigue Test Results

Table 7 presents laboratory fatigue test results for field-collected HMA mixtures. An alternative Beam ID is shown which represents the mix-type (SP-II or SP-III), the source of the material (F=field, or L=laboratory), replicate sample notation (S_1, S_2, S_3 etc.), and the percent air voids. Samples that did not meet the percent air voids target criteria are not considered for further FEL analysis. The PG binder grade used for each mix type is also shown, along with the initial stiffness. The fatigue failure criteria listed in Table 7 includes traditional N_{f50} and ER criteria. Figure 17 presents stiffness-based failure curves of an SP-II sample, SP-II-N1. The left and right axis describes the stiffness ratio and ER behavior with increasing cycles respectively. SP-II-N1 is tested at 1000 με where failure is recorded at 1,085 cycles and at 1,249 cycles, according to N_{f50} and $N_{f(ER)}$ failure criteria, which is highlighted in Figure 17.

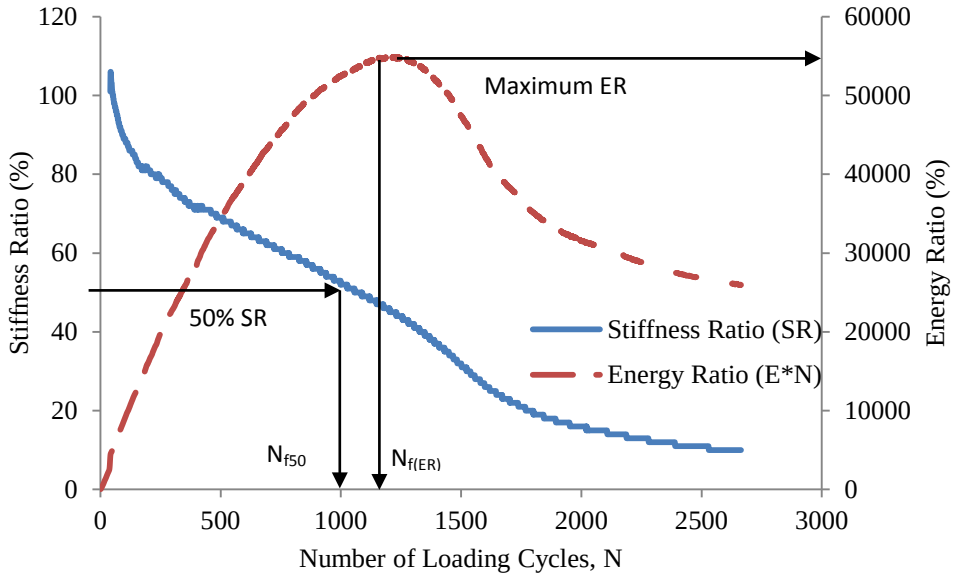

FIGURE 17 Variation of Stiffness Ratio and Energy Ratio with Number of Loading Cycles of SP-II-N1 Sample

TABLE 7 Laboratory Fatigue Test Results for Field SP-II and SP-III Mixtures

Alternative Beam ID	Beam ID	Strain ε_t ($\mu\varepsilon$)	PG Binder	Stiffness E_0 (psi)	% Air Voids	Failure Criteria		Avg. Cycles to Failure	
						N_{f50}	$N_{f(ER)}$	N_{f50}	$N_{f(ER)}$
SP-II MIXTURE									
SPII-F-400-S1-5.2%	N2	400	64-22	646,000	5.2	79,008	69,069	355,377	469,631
SPII-F-400-S2-5.4%	A1	400	64-22	880,310	5.4	263,411	239,818		
SPII-F-400-S3-5.9%	M2	400	64-22	666,158	5.9	723,711	1,100,007		
SPII-F-800-S1-5.1%	I2	800	64-22	471,000	5.1	11,700	10,910	11,100	45,662
SPII-F-800-S2-5.8%	L1	800	64-22	655,716	5.8	10,500	80,412		
SPII-F-1000-S1-4.8%	N1	1000	64-22	853,302	4.8	1,085	1249	2,795	5,795
SPII-F-1000-S2-5.7%	O2	1000	64-22	531,200	5.7	4,504	10,341		
SPII-F-1200-S3-3.5%	K1	1000	64-22	908,661	3.5	1,684	1,547	8,155	7,288
SPII-F-1200-S4-3.0%	K2	1000	64-22	850,501	3.0	14,625	13,029		
SPII-F-1200-S1-4.7%	E1	1200	64-22	680,645	4.7	1,879	4651	1,108	2,599
SPII-F-1200-S2-4.9%	J2	1200	64-22	711,640	4.9	337	547		
SP-III MIXTURE									
SPIII-F-150-S1-6.1%	X14	150	70-22	652,814	6.1	31,024,079	NA	31,024,079	NA
SPIII-F-200-S2-5.4%	X15	200	70-22	654,120	5.4	1,101,500	NA	1,101,500	NA
SPIII-F-250-S1-5.1%	X13	250	70-22	614,814	5.1	760,501			
SPIII-F-250-S2-4.9%	X7	250	70-22	1,050,217	4.9	120,519	NA	440,510	NA
SPIII-F-274-S1-4.8%	X10	274	70-22	1,069,653	4.8	149,398	NA	149,398	NA
SPIII-F-274-S2-4.8%	X3	274	70-22	1,318,537	4.8	6,500,00	NA	6,500,000	NA
SPIII-F-274-S1-4.9%	X4	274	70-22	1,450,377	4.9	6,300,000	NA	6,300,000	NA
SPIII-F-274-S2-6.6%	Q1	274	70-22	655,376	6.6	460,518	NA	460,518	NA
SPIII-F-274-S1-5.7%	X1	274	70-22	718,397	5.7	5.0E+07	NA	5.0E+07	NA
SPIII-F-308-S2-4.8%	Z1	308	70-22	645,254	4.8	11,000,000	NA	11,000,00	NA

Alternative Beam ID	Beam ID	Strain ε_t ($\mu\varepsilon$)	PG Binder	Stiffness E_0 (psi)	% Air Voids	Failure Criteria		Avg. Cycles to Failure	
						N_{f50}	$N_{f(ER)}$	N_{f50}	$N_{f(ER)}$
SP-III MIXTURE									
SPIII-F-400-S1-5.6%	X11	400	70-22	450,487	5.6	2,981,762	NA	1,554,381	NA
SPIII-F-400-S2-5.8%	X12	400	70-22	374,777	5.8	133,000	NA		NA
SPIII-F-600-S1-4.9%	C2	600	70-22	557,499	4.9	770,008	748,820	770,008	748,820
SPIII-F-800-S1-4.7%	J1	800	70-22	455,466	4.7	38001	52,926	54,457	67,970
SPIII-F-800-S2-5.9%	M2	800	70-22	415,678	5.9	42,001	46,826		
SPIII-F-800-S3-5.0%	F2	800	70-22	402,190	5	114,001	148,576		
SPIII-F-1000-S1-4.8%	B2	1000	70-22	433,644	4.8	29,801	35,276	25,201	30,276
SPIII-F-1000-S2-4.8%	P1	1000	70-22	582,762	4.8	20,601	25,276		
SPIII-F-1200-S1-5.0%	P2	1200	70-22	485,731	5	6,476	7,551	8,026	22,149
SPIII-F-1200-S2-5.8%	Q2	1200	70-22	451,938	5.8	9,576	34,551		
SPIII-F-1200-S3-2.8%	D1	1200	70-22	355,000	2.8	2050	4408	2,095	3,223

Table 8 presents laboratory fatigue test results for two HMA mixtures which are prepared in the laboratory. As stated earlier, the only difference between the field and laboratory mixes (SP-II or SP-III) is the binder grade. The respective aggregate gradation and binder content remain the same for both SP-II and SP-III mixes. Similar to the field mixture fatigue results, the fatigue life of the laboratory HMA mixtures is presented using N_{f50} and $N_{f(ER)}$ failure criteria.

TABLE 8 Fatigue Test Results of Laboratory Prepared SP-II and SP-III Mixtures

Alternative Beam ID	Beam ID	Applied ε_t (με)	PG Binder	Stiffness E_0 (psi)	% Air Voids	Failure Criteria		Avg. Cycles to Failure	
						N_{f50}	$N_{f(ER)}$	N_{f50}	$N_{f(ER)}$
SP-II MIXTURE									
SPII-L-400-S1-4.3%	1A	400	70-22	732,504	4.3	71,618	56,907	237,877	544,477
SPII-L-400-S2-4.5%	1B	400	70-22	680,476	4.5	122,008	875,620		
SPII-L-400-S3-5.1%	5B	400	70-22	834,120	5.1	520,004	700,904		
SPII-L-800-S1-4.7%	2A	800	70-22	579,362	4.7	19,494	18,303	15,827	20,715
SPII-L-800-S2-4.5%	2B	800	70-22	476,521	4.5	12,160	23,127		
SPII-L-1000-S1-5.1%	7A	1000	70-22	675,111	5.1	2,363	3,657	2,240	3,195
SPII-L-1000-S2-4.8%	7B	1000	70-22	707,020	4.8	2,117	2,733		
SPII-L-1200-S1-5.0%	8A	1200	70-22	774,222	5.0	718	787	629	661
SPII-L-1200-S2-5.0%	8B	1200	70-22	697,054	5.0	539	535		
SP-III MIXTURE									
SPII-L-400-S1-4.8%	6A	400	64-22	1,040,810	4.8	146,711	131,514	387,008	442,215
SPII-L-400-S2-5.1%	6B	400	64-22	995,268	5.1	627,304	752,915		
SPII-L-800-S1-5.0%	9A	800	64-22	676,177	5.0	2,300	2,869	7,576	6,581
SPIII-L-800-S2-6.3%	9B	800	64-22	709,450	6.3	2,422	3,243		
SPIII-L-800-S3-6.0%	10B	800	64-22	661,054	6.0	18,006	13,631		
SPIII-L-1000-S1-5.0%	8A	1000	64-22	581,865	5.0	7,200	22,685	6,569	17,666
SPIII-L-1000-S2-6.3%	8B	1000	64-22	522,036	6.3	5,937	12,647		
SPIII-L-1200-S1-6.2%	4B	1200	64-22	610,473	6.2	4,205	3,642	2,558	2,451
SPIII-L-1200-S2-6.5%	10A	1200	64-22	592,931	6.5	910	1,260		

Analysis of Laboratory Data

Individual fatigue life results (N_{f50} and $N_{f(ER)}$) show considerable variation. For example, SP-II sample N2 has a much lower fatigue life than its replicate, sample A1, and the same can be said again for SP-II samples A1 and M2, even though all three are tested under the same conditions and load. One would attribute to testing three samples can take care of this issue. Figure 18 illustrates the varying stiffness reduction rates for these SP-II samples. This may be attributed to the effect of percent air voids, as it can be seen that the fatigue life of these three samples increases as the percent air voids increases. However, this theory does not hold true when looking at the fatigue life data of SP-III samples J1, M2, and F2 (three replicates). These replicate SP-III samples are each tested at 800 με yet their associated fatigue life did not follow the same trend as shown earlier for the SP-II samples. SP-III-M2 had the highest percent air voids of the replicate samples, yet showed a similar fatigue life to SP-III-J1, and much lower fatigue life than SP-III-F2. Due to the complex nature of fatigue crack initiation and propagation, replicate samples of similar air voids did not show similar behavior due to density gradient that exists in samples. The average fatigue life of replicate samples decreases as the strain amplitude increases, with the exception of SP-II samples, K1 and K2, which did not meet the target air voids criteria. Finally, there is no apparent trend from Table 7 that indicates high initial stiffness has an effect on the associated fatigue life. SP-II sample stiffness varied from 470 to 900 ksi and SP-III sample stiffness varied from 300 to 600 ksi.

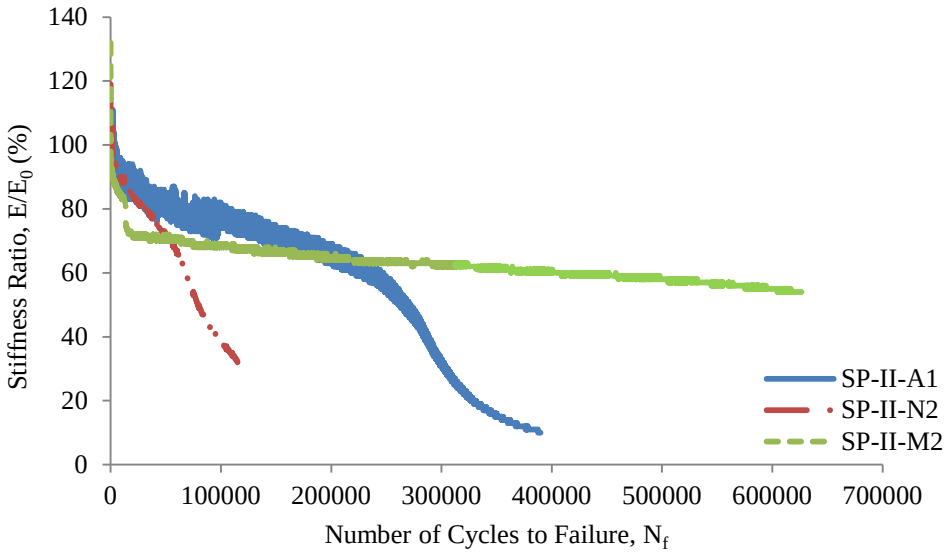

FIGURE 18 Stiffness Ratio Reduction Curves of Replicate SP-II Samples

In terms of laboratory fatigue life data, Table 8 shows a similar trend to what is observed in field HMA mixtures. The majority of the results show replicate samples with lower percent air voids have lower fatigue life. That being said, SP-III samples SP-III-4B and SP-III-10A show the opposite behavior, albeit with percent air voids that are slightly higher the target criteria. SP-II sample stiffness varied from 480 to 830 ksi and for the SP-III samples, initial stiffness varied from 520 to 1000 ksi. Once again, no apparent trend could be seen which suggests that variation in stiffness affects the fatigue life of replicate samples.

Figures 19 and 20 compare the average fatigue life of field-collected mixtures with laboratory prepared mixtures tested at varying strain amplitudes (N_{f50} results only). It can be seen here that the SP-II samples show similar results, as shown in Figure 19. For the SP-III mixture, Figure 20 shows that the fatigue life of the laboratory prepared samples is slightly lower than that shown for the field samples. Mixture variables for laboratory prepared SP-III specimens are identical to those shown in field collected SP-III materials except for the PG binder grade. Laboratory prepared mixtures contained neat PG 64-22 binder, whereas field mixtures used modified PG 70-22. Therefore, the difference in observed fatigue lives may be attributed to change in PG binder.

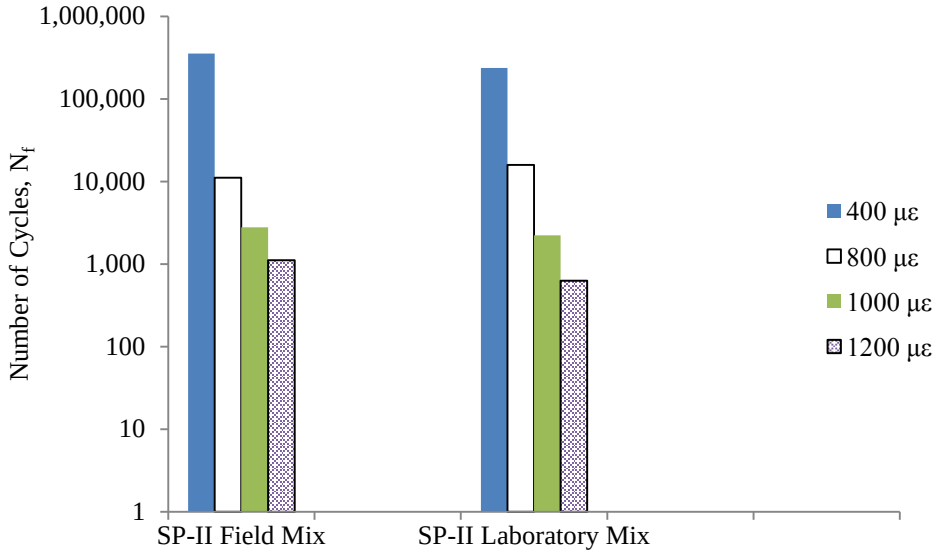

FIGURE 19 Comparison of Fatigue Life between Field and Laboratory SP-II Mixtures

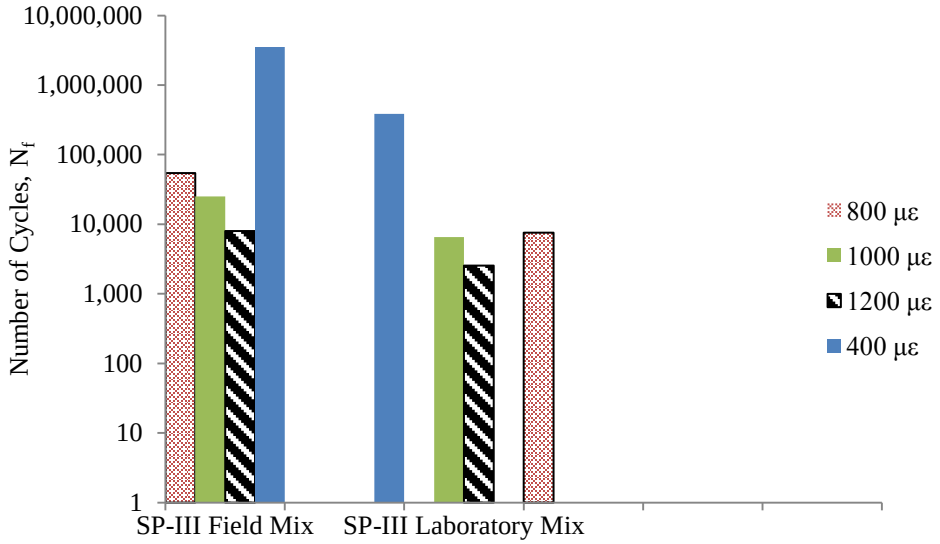

FIGURE 20 Comparison of Fatigue Life between Field and Laboratory SP-III Mixtures

Extrapolation of Fatigue Life

Low strain fatigue testing (70 – 500 με) may often lead to an unreasonable number of loading cycles without ever achieving failure. In order to confirm the existence of the endurance limit, fatigue test data from low strain testing needs to be extrapolated to predict a failure point. Table 9 shows extrapolated fatigue failure for failed samples as well as those which have not failed. SP-II and SP-III mixtures both contained samples which did not fail; SP-II-L2 and SP-III-B1. For the SP-II sample (SP-II-L2), approximately 8.5 million cycles are run yet the initial stiffness only reduced by 30%. Therefore, the fatigue life is extrapolated using the single-stage Weibull function and the RDEC approach, and the estimated fatigue life is 81.5 million cycles and 102.5 million respectively. Figure 21 presents the fatigue curve of SP-II-L2 fitted to the single-stage Weibull function.

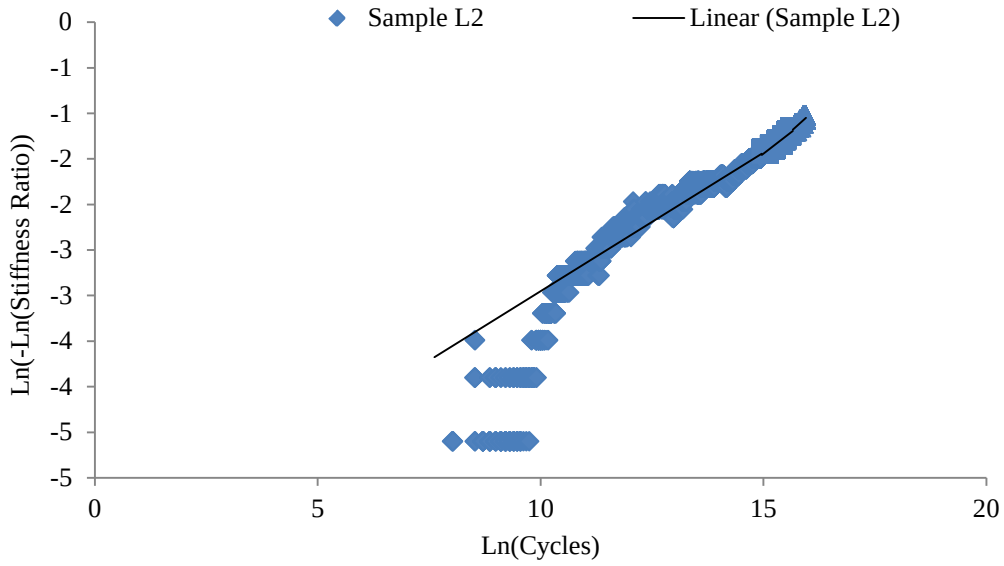

FIGURE 21 Fatigue Curve for SP-II Sample (L2) using Weibull Function

TABLE 9 Extrapolated Fatigue Test Results for Field SP-II and SP-III Mixtures

Alternative Beam ID	Beam ID	Applied ε_t (με)	Initial E_0 (psi)	% Air Voids	Cycles Tested	Extrapolated Cycles to N_{f50}		Failure Criteria	
						RDEC	Weibull	N_{f50}	$N_{f(ER)}$
SP-II MIXTURE									
*SPII-F-200-S1-5.4%	L2	200	954,638	5.4	8,479,090	102,493,275	81,486,025	91,989,650[1]	NA
SPII-F-400-S1-5.2%	N2	400	646,000	5.2	79,008	77,779	86,600	79,008	69,069
SPII-F-400-S2-5.4%	A1	400	880,310	5.4	389,811	222,502	220,900	263,411	239,818
SPII-F-400-S3-5.9%	M2	400	666,158	5.9	723,711	877,612	1,335,000	723,711	1,100,007
SPII-F-800-S1-5.1%	I2	800	471,000	5.1	11,700	11,510	11,940	11,700	10,910
SPII-F-800-S2-5.8%	L1	800	655,716	5.8	90,000	25,097	20,650	10,500	80,412
SPII-F-1000-S1-4.8%	N1	1000	853,302	4.8	2,665	1,486	860	1,085	1,249
SPII-F-1000-S2-5.7%	O2	1000	531,200	5.7	17,256	4,797	4,642	4,504	10,341
SPII-F-1200-S1-3.5%	K1	1000	908,661	3.5	13,148	1,788	2,073	1,684	1,547
SPII-F-1200-S2-3.0%	K2	1000	850,501	3.0	18,046	871	407	14,625	13,029
SPII-F-1200-S3-4.7%	E1	1200	680,645	4.7	6,553	1,964	625	1,879	4,651
SPII-F-1200-S4-4.9%	J2	1200	711,640	4.9	1,542	13,697	24,690	337	547
SP-III MIXTURE									
*SPIII-F-400-S1-4.9%	B1	400	537,945	4.9	3,539,851	4.8E+19	1.5E+09	2.4E+19[1]	NA
SPIII-F-600-S1-4.9%	C2	600	557,499	4.9	833,560	89,727	1,110,000	770,008	748,820
SPIII-F-800-S1-4.8%	J1	800	455,466	4.8	106,276	39,303	24,130	38001	52,926
SPIII-F-800-S2-5.9%	M2	800	415,678	5.9	79,176	23,569	29,900	42,001	46,826
SPIII-F-800-S3-5.0%	F2	800	402,190	5.0	150,000	129,567	71,250	114,001	148,576
SPIII-F-1000-S1-4.8%	B2	1000	433,644	4.8	50,701	32,335	21,250	29,801	35,276
SPIII-F-1000-S2-4.8%	P1	1000	582,762	4.8	40,901	20,832	13,110	20,601	25,276
SPIII-F-1200-S1-5.0%	P2	1200	485,731	5.0	12,326	6,962	5,187	6,476	7,551
SPIII-F-1200-S2-5.8%	Q2	1200	451,938	5.8	52,526	9,704	9,230	9,576	36,746
SPIII-F-1200-S3-2.8%	D1	1200	355,000	2.8	13,949	2,159	2,115	2050	4408
SPIII-F-1200-S4-2.8%	D2	1200	300,000	3.0	4,898	1,963	1,928	2140	2038

SP-III sample and SP-III-B1 yielded a 20% reduction in stiffness after 3.5 million cycles. The fatigue life is extrapolated using the single-stage Weibull function and the RDCE approach, showing an estimated fatigue life of 1.46x10^09 cycles and 4.81x10^19 cycles respectively. Although there is no failed fatigue test data to confirm these fatigue lives, the estimated values are extremely high. In order to determine whether these two extrapolation techniques provide reasonable predictions, fatigue life of failed samples is also predicted. Figure 22 compares predicted fatigue life of SP-II samples with the fatigue life recorded from laboratory testing using both extrapolation techniques. It can be seen here that there is good consistency between the predicted and laboratory tested fatigue life, especially for the tradition N_{f50} criterion. For the SP-III samples, Figure 23 also shows good consistency, more so for the single-stage Weibull function, whereas the RDEC approach seems to overestimate the fatigue life.

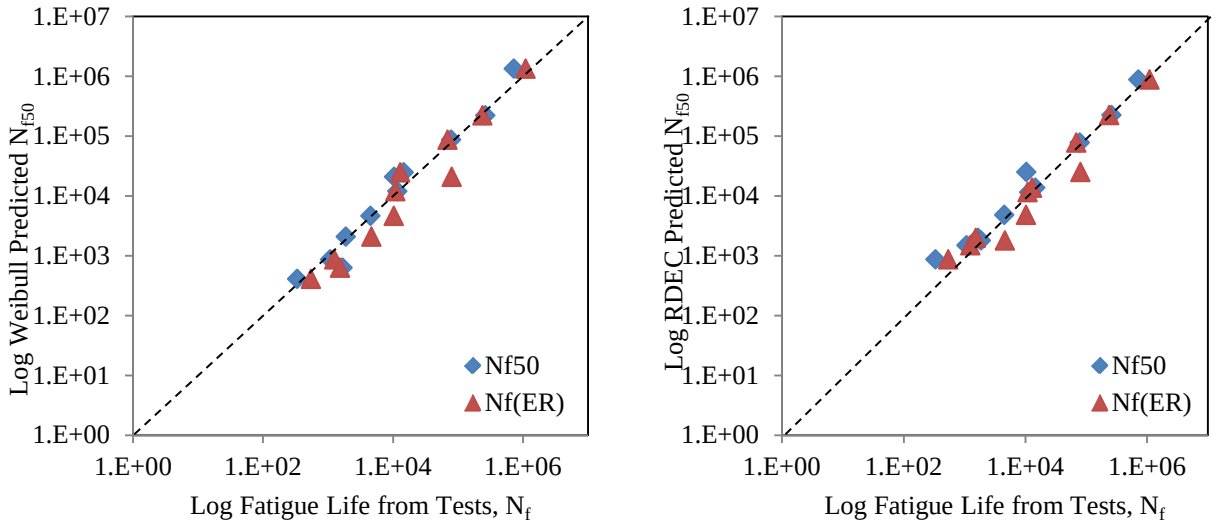

(a) Single-Stage Weibull Function (b) RDEC Approach

FIGURE 22 Comparison of Extrapolated and Tested Fatigue Life Results of Field SP-II Mixtures

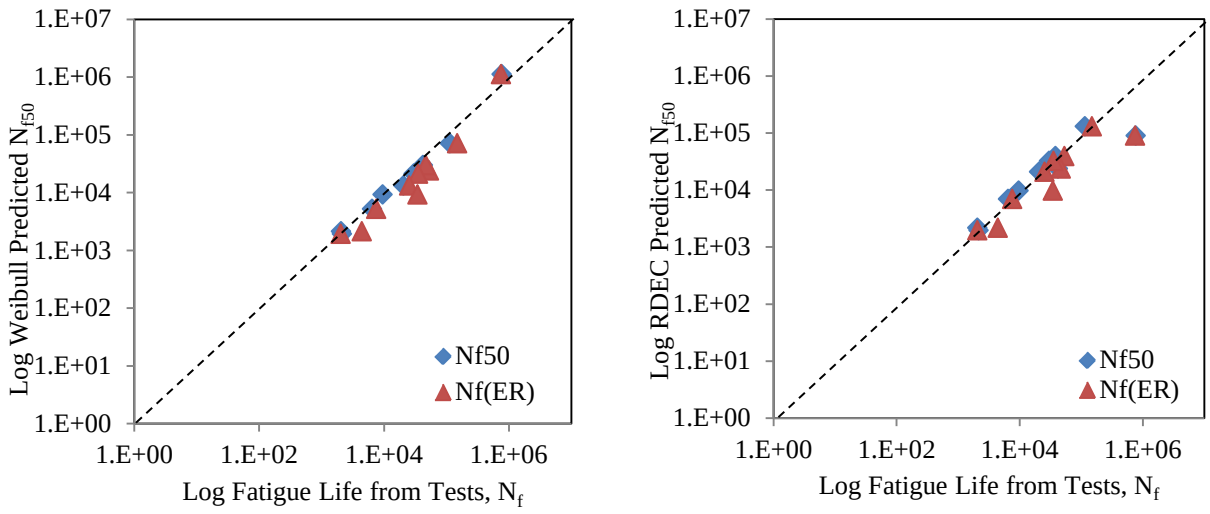

(a) Single-Stage Weibull Function

(b) RDEC Approach

FIGURE 23 Comparison of Extrapolated and Tested Fatigue Results of Field SP-III Mixtures

The Effect of Applied Strain on Fatigue Life

The applied strain amplitude plays a vital role in the fatigue life of asphalt concrete. Figures 24 and 25 show flexural stiffness vs. initial number of loading cycles for both SP-II and SP-III mixtures tested under increasing strain levels. Figure 24 shows that even though SP-II samples SP-II-M2 and SP-II-L1 have the same initial stiffness, the fatigue damage rate is much different due to the difference in strain amplitude with sample SP-II-L1 showing a greater reduction in stiffness. The same can be said for SP-III mixtures as shown in Figure 25. SP-III-E2 has a much higher rate of fatigue damage in the initial cycles, than SP-III-F2. However, as the loading cycles continue the rate of fatigue damage rate reduces where the fatigue curves of both SP-III-E2 and SP-III-F2 show similar stiffness reduction rates. Sample SP-III-E2 is close to failure as it approaching 50% of its initial stiffness, whereas sample SP-III-F2 will not fail for another 100,000 cycles.

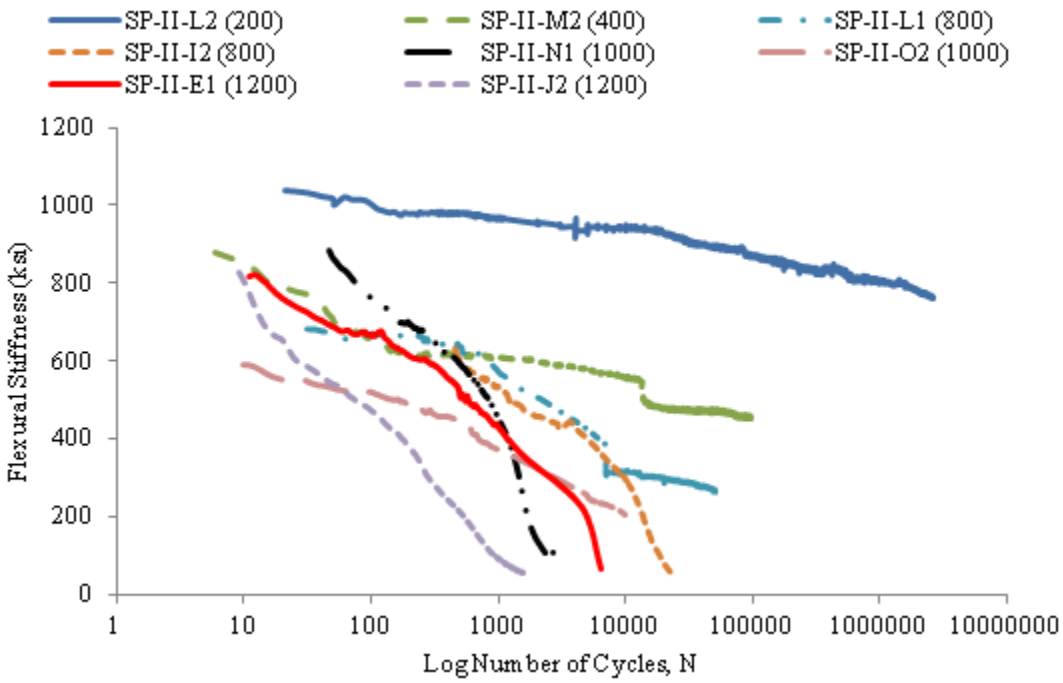

FIGURE 24 Flexural Stiffness vs. Loading Cycles for Field SP-II Mixtures

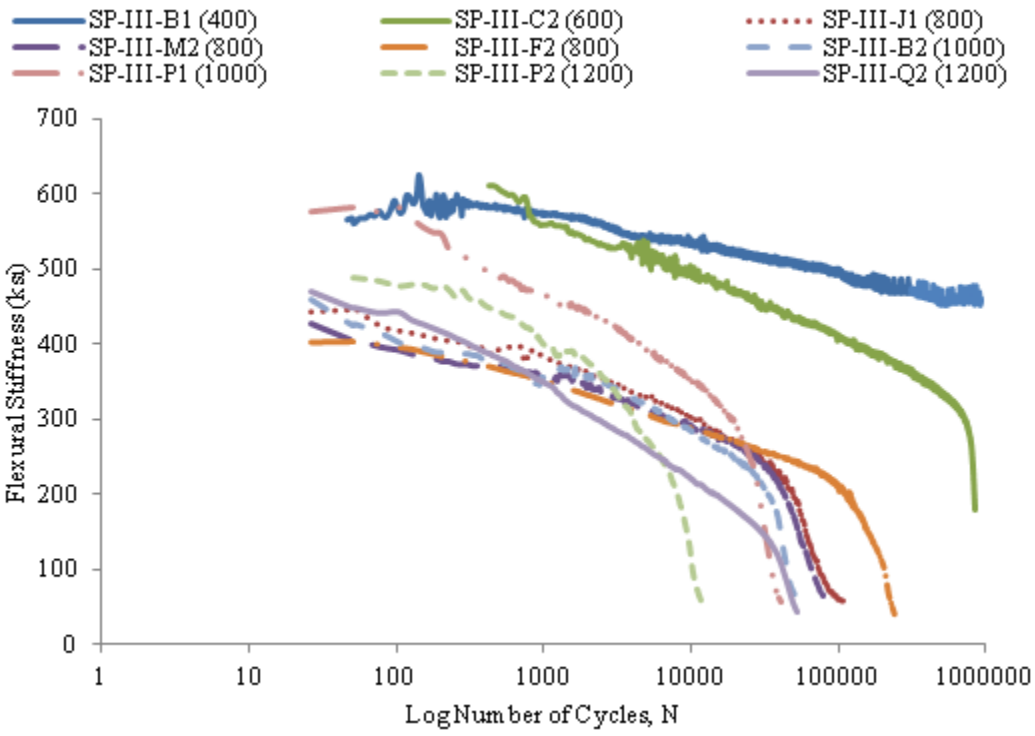

FIGURE 25 Flexural Stiffness vs. Loading Cycles for Field SP-III Mixtures

Figures 26 and 27 also show strain amplitude vs. the fatigue life curves (ε-N_f) of SP-II mixture. As the tensile strain is reduced, the number of cycles to failure increased, exhibiting an asymptotic curve. This behavior is indicative of FEL, which suggests that below a specific strain level, a material can experience infinite loading cycles without accumulating damage. Figure 26 features log-log plots of ε-N_f curves fitted to both failure criteria using the power series, where both curves exhibit similar fatigue behavior of SP-II mixtures. The traditional approach (N_{f50}) showing a slightly better fit than that of Rowe's stiffness ratio approach. The same can be said of Figure 28, where the fatigue curves of the SP-III mixture are almost identical. It must be noted that even though the two different failure criteria provided similar results, the ER approach showed samples failing long after they had exceeded the 50% stiffness reduction. Figure 29 illustrates the asymptotic behavior of the SP-III mix fatigue curve as the applied strain reduces.

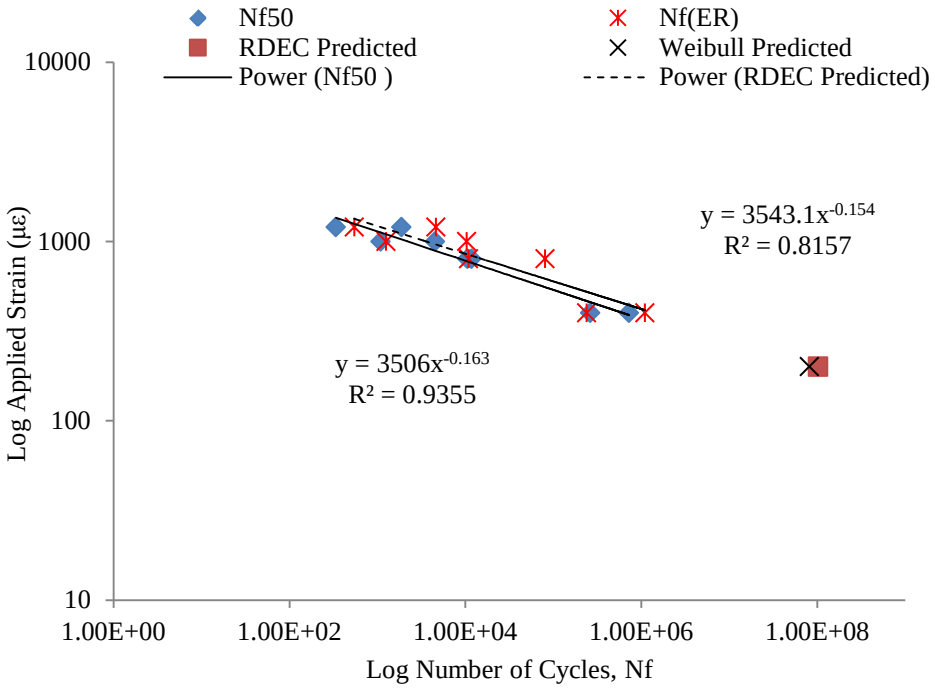

FIGURE 26 Log-log ε-N_f Curve for Field SP-II Mixtures

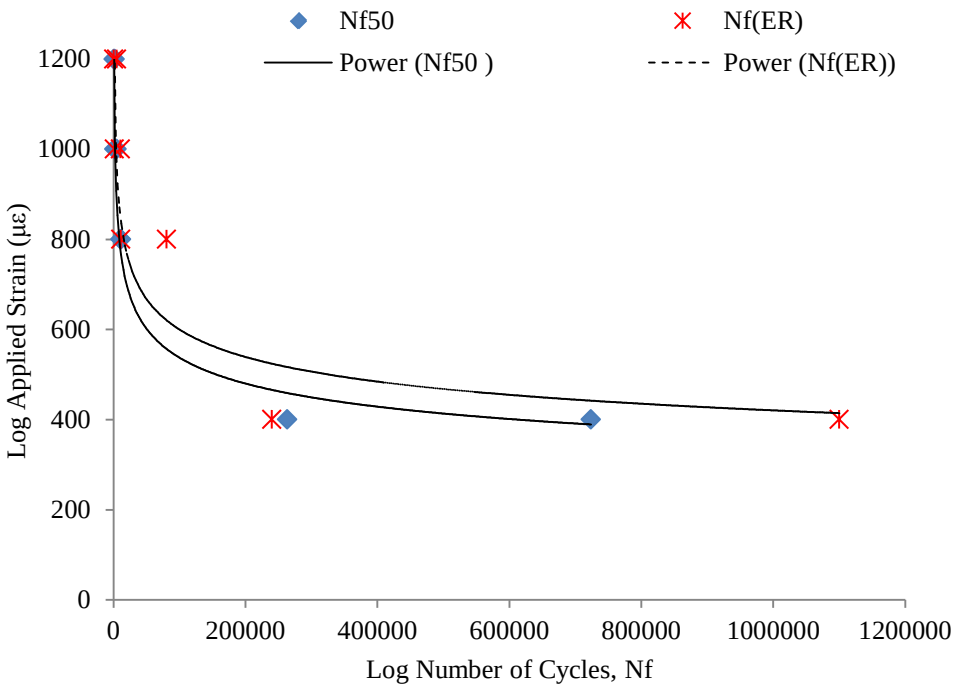

FIGURE 27 ε-N_f Curve for Field SP-II Mixtures

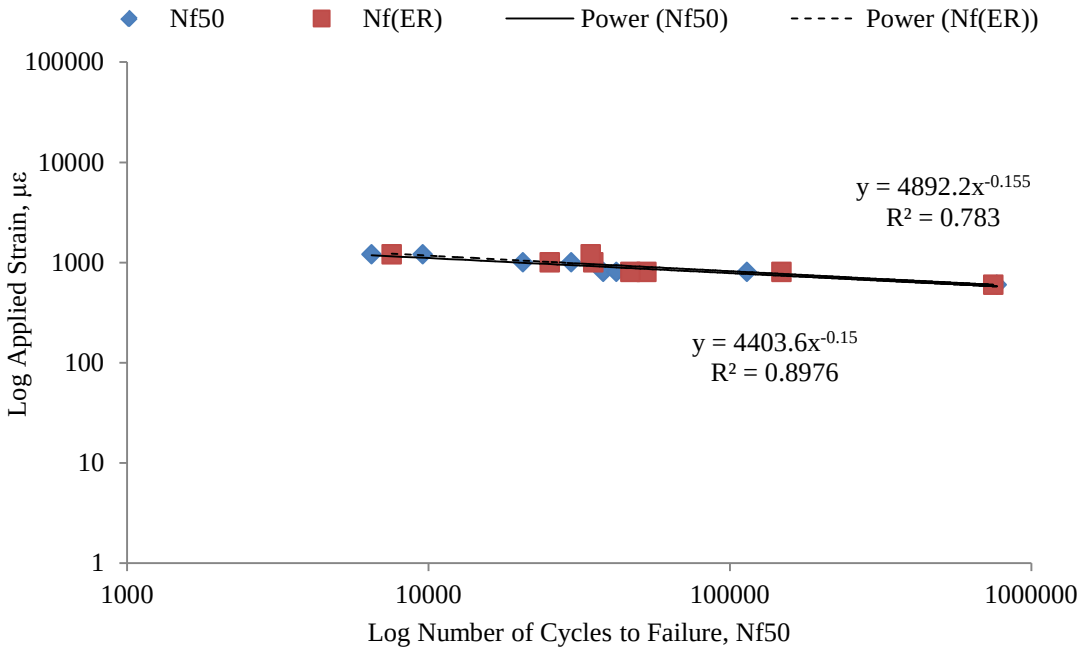

FIGURE 28 Log-log ε-N_f Curve for Field SP-III Mixtures

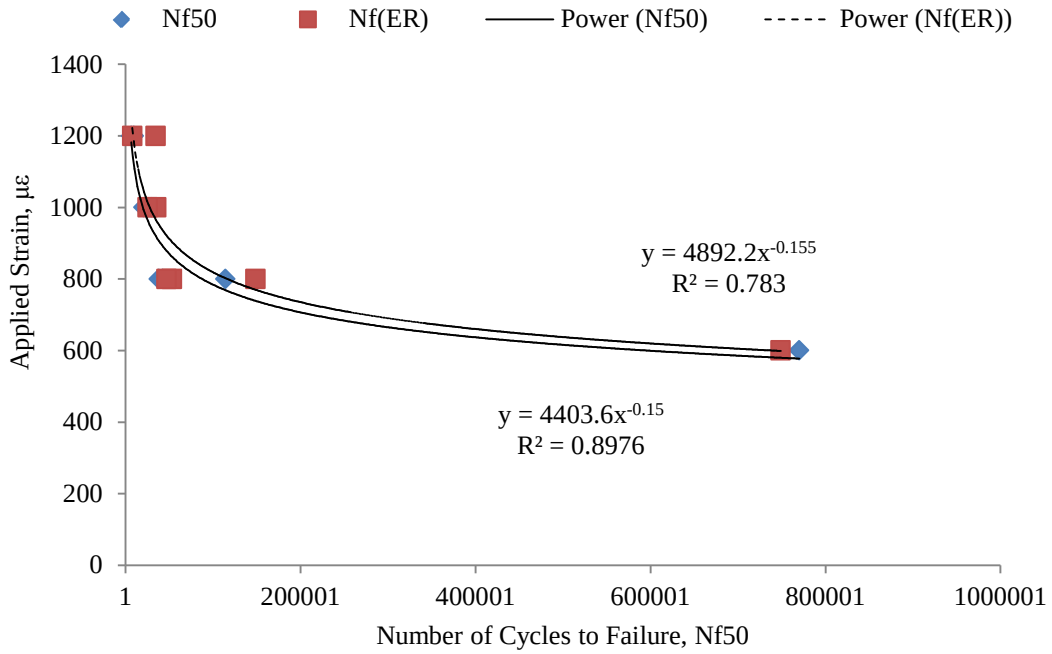

FIGURE 29 ε-N_f Curve for Field SP-III Mixtures

Fatigue Endurance Limit Prediction

The fatigue endurance limit of SP-II and SP-III mixtures is determined using two different approaches: (*i*) the strain amplitude-fatigue life (ε-N) approach, and (*ii*) the RDEC approach. The ε-N approach is considered the traditional approach to determining the FEL which is equivalent to 50 million cycles. The RDEC approach applies the unique PV-N_f relationship where the strain amplitude which yields a PV equivalent to a fatigue life of 50 million cycles is deemed the FEL.

FEL Prediction Using the ε-Nf Method

Plots (log-log) of applied strain levels versus the number cycles to failure (ε-N_f) of field SP-II and SP-III mixtures are shown in Figure 26 and Figure 28. Research has shown that the log-log transformation of the data from tests conducted at normal strain levels (above the endurance limit) produce a straight line (*25*). A fatigue life of 50 million cycles is used to predict the micro-strain level which is equivalent to the fatigue endurance limit. Using Eq. 25, the FEL is determined.

$$FEL = \alpha(N)^{\beta} \tag{25}$$

where α and β are regression coefficients, and N = 50 million cycles.

Using the ε-N_f models, the strain which is equivalent to a fatigue life of 50 million cycles is determined. For the field SP-II mixtures, a FEL of 195 με is predicted using N_{f50} criterion and 231 με using ER failure criterion. These FEL values are reasonable considering that fatigue testing of SP-II-L2 sample at 200 με provided an extremely high number of cycles which required extrapolation to determine failure. Furthermore, the FEL values shown for the SP-II mixture in this study are similar to what has been shown for HMA mixtures in previous studies (*25*).

In terms of the field SP-III mixtures, a FEL of 180 με is predicted using traditional N_{f50} criterion, and 311 με using the ER criterion. Due to the mixture variables, such as the use of a modified binder and higher binder content, the FEL can be significantly different from different mixtures. Some studies have shown that the presence of a modified binder in HMA mixtures may improve fatigue resistance (*43*).

FEL Prediction Using the RDEC

In this study, the Ratio of Dissipated Energy Approach (RDEC) approach is used to predict the FEL of HMA mixtures by determining the relationship between the Plateau Value (PV) and the strain amplitude, which is not independent of mixture or temperature. The PV-strain amplitude relationship allowed for the prediction of the strain amplitude that yields a PV of 6.74×10^{-09} i.e. $N_f = 1.1 \times 10^7$ loading cycles, which is the FEL.

$$PV = \alpha(\varepsilon)^{\beta} \tag{26}$$

where ε = strain amplitude, and α and β are regression coefficients (*7*, *52*).

Figure 30 presents the ε-PV curves for field SP-II and SP-III mixtures. It can be seen here that the mixture with the lower PV corresponding to induced damage for the same strain level has a longer fatigue life; which is the SP-III mixture. The slopes of both curves are very close to each other, which means that the change in percentage of dissipated energy contributing to damage is similar for both mixtures. Using the ε-PV model, the estimated FEL for the field SP-II mixture is 216 με (*ER*) and 242 με (N_{f50}). The FEL of the field SP-III mixture is estimated to be 291 με (*ER*) and 334 με (N_{f50}).

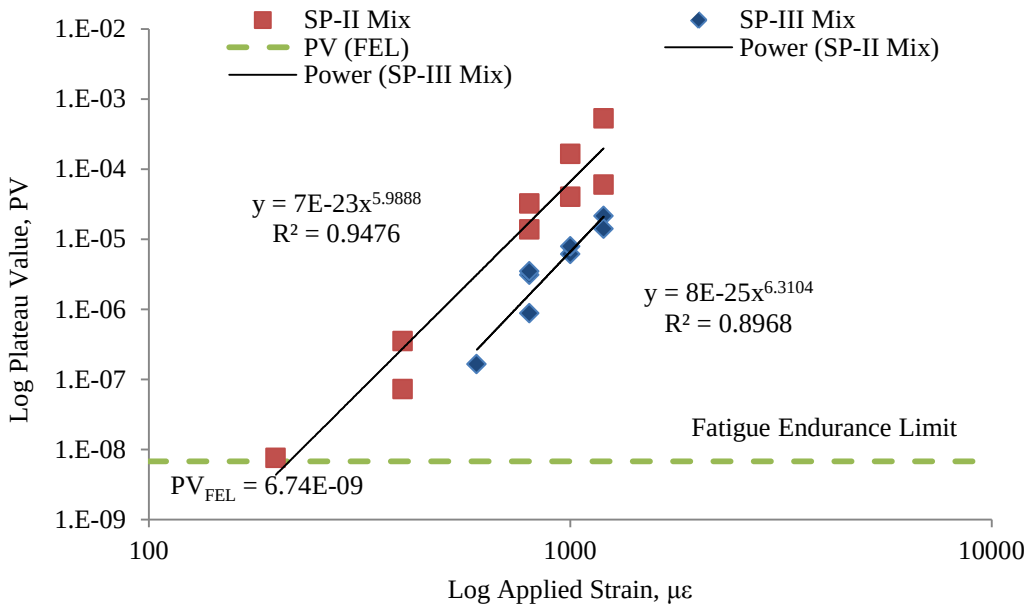

FIGURE 30 Plateau Value vs. Strain Amplitude for Field SP-II and SP-III Mixtures

Figure 31 presents the PV-N_f relationship for field SP-II and SP-III mixtures and is fitted to a power model (solid line). The dotted line represents Carpenter and Shen's (*7*) relationship which is fitted to the fatigue test data recorded from this study, using Eq. 27, shown below.

$$PV = 0.4428\ (N_f)^{-1.1102} \tag{27}$$

It can be seen here that both relationships are almost identical and follow a similar trend. The PV corresponding to the FEL of 6.74x10^-09 is also plotted on Figure 30.

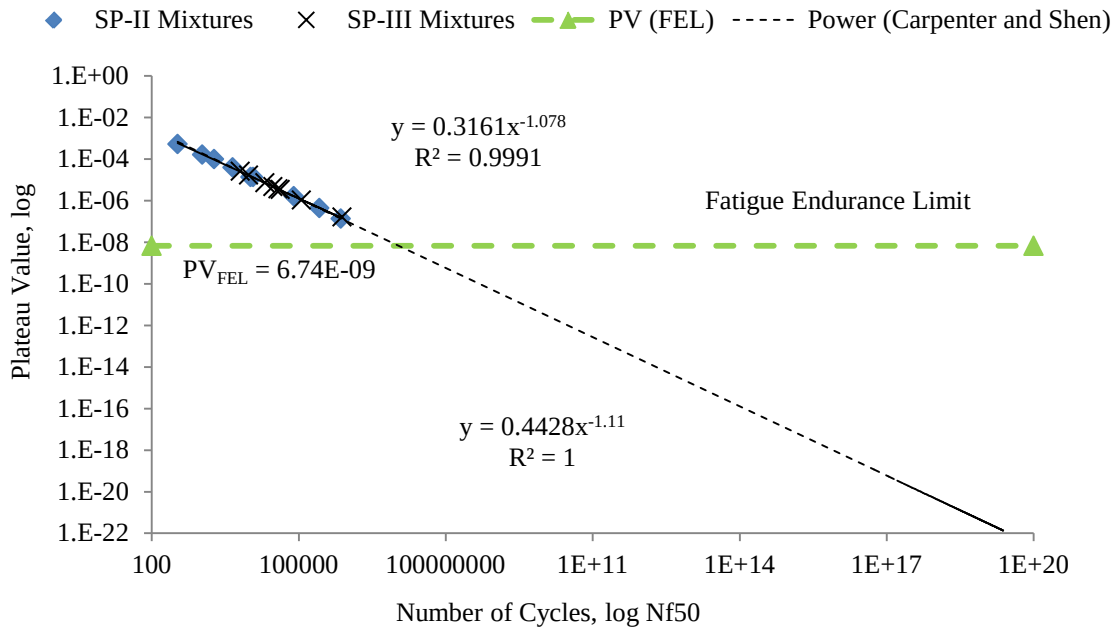

FIGURE 31 Plateau Value vs. Cycles to Failure for Field SP-II and SP-III Mixtures

PV Prediction Model

The PV prediction model uses material properties such as the flexural stiffness (S), Volumetric Parameter (VP), and the Gradation Parameter (GP) are used to predict the PV. Eq. 28 presents the PV model;

$$PV = 44.422\varepsilon^{5.140}S^{2.993}VP^{1.850}GP^{-0.4063} \quad (28)$$

Where S = flexural stiffness, VP = Volumetric Parameter;

$$VP = \frac{AV}{AV+V_b} \quad (29)$$

where AV = percent air voids, V_b = asphalt content by volume (Roberts et al. 1996),

$$V_b = 100 \times \frac{G_{mb} \times P_{ac}}{G_b} \quad (30)$$

G_{mb} = bulk density of HMA, P_{ac} = percent asphalt content by weight, G_b = bulk specific gravity of binder (1.019 for PG 64-22, and 1.020 for PG 70-22), GP = Gradation Parameter,

$$GP = \frac{P_{NMS}-P_{PCS}}{P_{200}} \quad (31)$$

P_{NMS} = percent aggregate passing nominal maximum size sieve, (NMS is defined as one sieve size greater than the first sieve to retain more than 10 percent of the material), P_{PCS} = percent aggregate passing primary control sieve (PCS = NMS*0.22), and P_{200} = percent aggregate passing #200 sieve.

Table 10 shows predicted PV values for field SP-II and SP-III mixtures respectively. PV values based on the predictive model (Eq. 28) are compared with those measured from tests and Figure 32 shows good consistency, with data points loosely following the line of equality but with some scattering. Therefore, it can be said that the PV model is an alternative method to predict the PV of HMA mixtures using only material properties and load/response parameters.

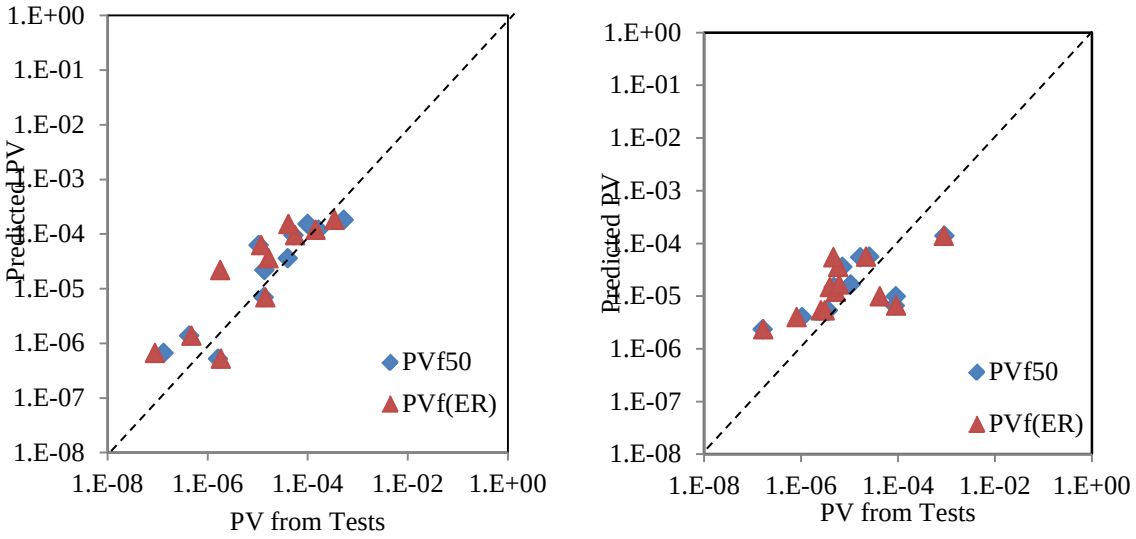

FIGURE 32 Comparison between PV from Model with PV from Test Results for Field Mixtures

Using this PV predictive model, the FEL is estimated using material properties such as the flexural stiffness (S), Volumetric Parameter (VP), and the Gradation Parameter (GP).

$$FEL = 0.0123S^{-0.5832}VP^{-0.3599}GP^{0.0790} \quad (32)$$

The estimated FEL from the PV model is then compared with FEL predictions provided from the two previous models described in this study, the ε-N_f approach and the ε-PV approach.

Using Eq. 32, FEL values of 160 με and 207 με are predicted for field SP-II and SP-III mixtures respectively. Table 12 compares FEL values for SP-II and SP-II mixtures predicted using the ε-N_f and ε-PV approaches, as well as those predicted using the material properties (Eq. 31). It can be seen here that the FEL values estimated using the PV model, is conservative when compared with the other two approaches (ε-N_f and ε-PV), which is not a bad thing in terms of design consideration.

TABLE 10 Plateau Value Results for Field SP-II and SP-III Mixtures

Beam ID	Applied ε_t (με)	Initial E_0 (psi)	% Air Voids	VP	Failure Criteria		Plateau Values		Predicted
					N_{f50}	$N_{f(ER)}$	PV_{f50}	$PV_{f(ER)}$	PV
SP-II MIXTURE									
N2	400	646,000	5.2	0.3305	79,008	69,069	8.3E-06	9.5E-06	5.2E-07
A1	400	880,310	5.4	0.3390	263,411	239,818	3.5E-07	3.8E-07	1.4E-06
M2	400	666,158	5.9	0.3591	723,711	1,100,007	7.2E-08	4.8E-08	6.6E-07
I2	800	471,000	5.1	0.3263	11,700	10,910	3.2E-05	3.4E-05	6.9E-06
L1	800	655,716	5.8	0.3551	10,500	80,412	1.4E-05	1.8E-06	2.2E-05
N1	1000	853,302	4.8	0.3131	1,085	1249	1.7E-04	1.4E-04	1.2E-04
O2	1000	531,200	5.7	0.3512	4,504	10,341	4.0E-05	1.7E-05	3.6E-05
E1	1200	680,645	4.7	0.3086	1,879	4,651	6.0E-05	2.5E-05	1.5E-04
J2	1200	711,640	4.9	0.3175	337	547	5.3E-04	3.5E-04	1.8E-04
K1	1200	908,661	3.5	0.2494	1,684	1,547	5.2E-05	5.7E-05	9.5E-05
K2	1200	850,501	3.0	0.2217	14,625	13,029	2.0E-05	2.2E-05	6.2E-05
SP-III MIXTURE									
B1	400	537,945	4.9	0.3090	NA	NA	NA	NA	2.60E-07
C2	600	557,499	4.9	0.3090	770,008	748,820	1.6E-07	1.7E-07	2.3E-06
J1	800	455,466	4.8	0.3002	38001	52,926	3.1E-06	2.2E-06	5.3E-06
M2	800	415,678	5.9	0.3500	42,001	46,826	3.5E-06	3.1E-06	5.3E-06
F2	800	402,190	5.0	0.3133	114,001	148,576	8.8E-07	6.7E-07	3.9E-06
B2	1000	433,644	4.8	0.3046	29,801	35,276	6.1E-06	5.2E-06	1.5E-05
P1	1000	582,762	4.8	0.3046	20,601	25,276	7.8E-06	6.4E-06	3.6E-05
P2	1200	485,731	5.0	0.3133	6,476	7,551	2.1E-05	1.8E-05	5.6E-05
Q2	1200	451,938	5.8	0.3461	9,576	36,746	1.4E-05	3.7E-06	5.4E-05

Note: VP = Volumetric Parameter, NA = no data available, [1]Less than 6.74E-9 proposed by Carpenter and Shen (2005) as indicative of long fatigue life.

TABLE 11 Plateau Values Results for Laboratory SP-II and SP-III Mixtures

Beam ID	Applied ε_t ($\mu\varepsilon$)	Initial E_0 (psi)	% Air Voids	VP	Failure Criteria		Plateau Values		Predicted
					N_{f50}	$N_{f(ER)}$	PV_{f50}	$PV_{f(ER)}$	PV
SP-II MIXTURE									
1A	400	732,504	4.3	0.2914	71,618	56,907	1.2E-06	1.5E-06	6.0E-07
1B	400	680,476	4.5	0.3008	122,008	875,620	8.3E-07	1.2E-07	5.1E-07
2A	800	579,362	4.7	0.3101	19,494	18,303	9.4E-06	1.0E-05	1.2E-05
2B	800	476,521	4.5	0.3008	12,160	23,127	1.6E-05	8.4E-06	6.2E-06
7A	1000	675,111	5.1	0.3278	2,363	3,657	9.1E-05	5.9E-05	6.4E-05
7B	1000	707,020	4.8	0.3146	2,117	2,733	1.6E-04	1.3E-04	6.9E-05
8A	1200	774,222	5.0	0.3235	718	787	4.2E-04	3.8E-04	2.4E-04
8B	1200	697,054	5.0	0.3235	539	535	3.4E-04	3.4E-04	1.8E-04
SP-III MIXTURE									
6A	400	1,040,810	4.8	0.3044	146,711	131,514	6.0E-07	6.7E-07	1.8E-06
6B	400	995,268	5.1	0.3174	627,304	752,915	1.8E-07	1.5E-07	1.7E-06
9A	800	676,177	5.0	0.3131	2,300	2,869	1.2E-04	9.6E-05	1.9E-05
9B	800	709,450	6.3	0.3648	2,422	3,243	1.1E-04	8.3E-05	2.9E-05
10B	800	661,054	6.0	0.3536	18,006	13,631	8.5E-06	1.1E-05	2.2E-05
8A	1000	581,865	5.0	0.3131	7,200	22,685	2.5E-05	7.8E-06	3.7E-05
8B	1000	522,036	6.3	0.3648	5,937	12,647	4.6E-05	2.2E-05	3.6E-05
4B	1200	610,473	6.2	0.3609	4,205	3,642	1.0E-04	1.2E-04	1.4E-04
10A	1200	592,931	6.5	0.3721	910	1,260	1.1E-04	7.9E-05	1.4E-04

Note: VP = Volumetric Parameter

TABLE 12 Predicted FEL Values for SP-II and SP-III Mixes

HMA Mix Type	Strain-Nf	Strain-PV	PV Model
SP-II (field)	195	216	160
SP-II (lab)	125	166	168
SP-III (lab)	185	182	160
SP-III (field)	180	334	207

The Effect of Polymer-Modified Binder on the FEL of HMA Mixtures

As shown in the literature search, there are very few studies about the effect of polymer-modified binders on the FEL. This study performed fatigue testing on four HMA mixture types with two different binder grades, PG 64-22 and PG 70-22. Figures 33 and 34 present ε-N_f curves describing the fatigue behavior of laboratory SP-II mixture. A fatigue life of 50 million cycles is used to predict the strain level which is equivalent to the FEL. From the relationships shown in Figure 33, and using Eq. 25, the FEL of the laboratory SP-II mixture is estimated to be 150 με and 191 με, using traditional N_{f50} criterion and ER failure criterion respectively. Figure 34 presents ε-N_f curves of the SP-II mixture without using log-log scale where the estimated FEL using ER criterion is clearly higher than the FEL using the N_{f50} criterion. Figures 35 and 36 describe the ε-N_f curve of the SP-III mixtures from which, the FEL is estimated to be 185 με (N_{f50}) and 202 με ($N_{f(ER)}$).

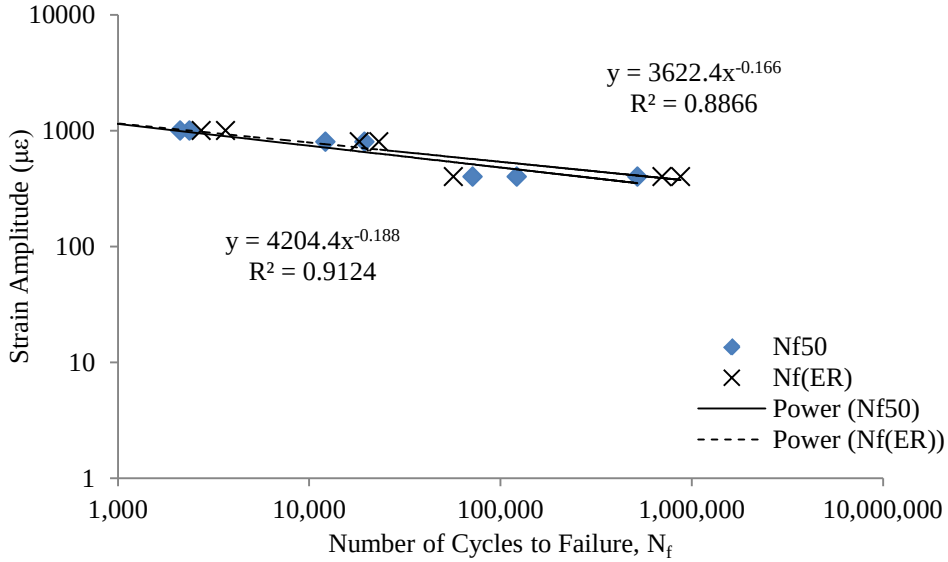

FIGURE 33 Log-log ε-N_f Curves for Laboratory SP-II Mixtures

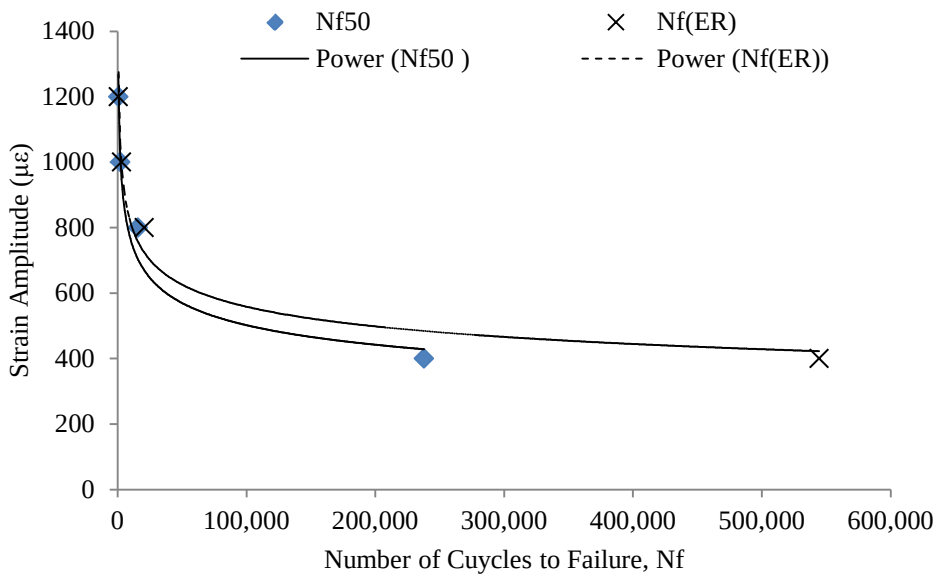

FIGURE 34 ε-N_f Curves for Laboratory SP-II Mixtures

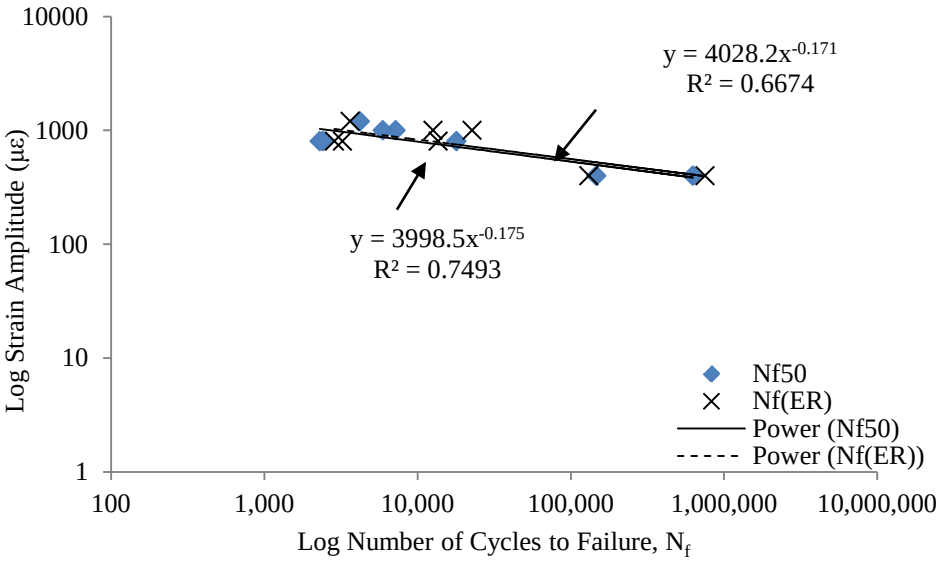

FIGURE 35 Log-log ε-N_f Curve for Laboratory SP-III Mixtures

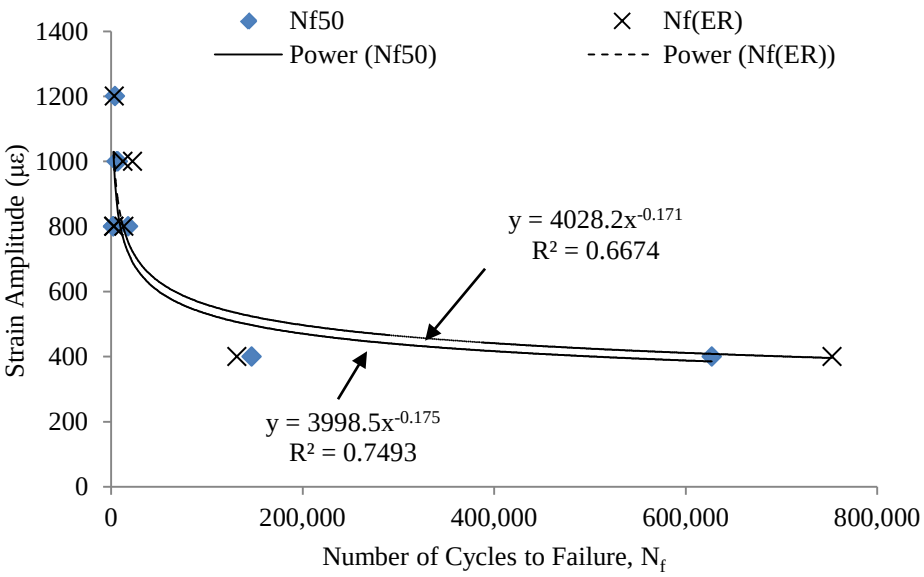

FIGURE 36 ε-N_f Curve for Laboratory SP-III Mixtures

From the above results, the addition of a modified binder, PG 70-22, to the SP-II mixture, reduced the estimated FEL by 27%. For the SP-III mixture, the use of the neat PG 64-22 binder saw a reduction in the estimated FEL by 30%.

Figure 37 presents ε-PV curves describing the fatigue behavior of both laboratory prepared mix types. Once again, the PV of 6.74e-09 is used to estimate the strain level which indicates FEL behavior. Using Eq. 26, the FEL of the laboratory SP-II mixture is estimated to be 166 με (N_{f50}) and 213 με ($N_{f(ER)}$). For the laboratory SP-III mixture, the FEL is estimated to be 182 με (N_{f50}) and 170 με ($N_{f(ER)}$). The results show a similar trend to what is found earlier, using the ε-N_f model. The addition of modified binder, PG 70-22, reduced the estimated FEL of the laboratory SP-II mixture by 18%. The FEL of the SP-III mixture containing neat PG 64-22 is almost half (44%) the estimated FEL of the field mixture.

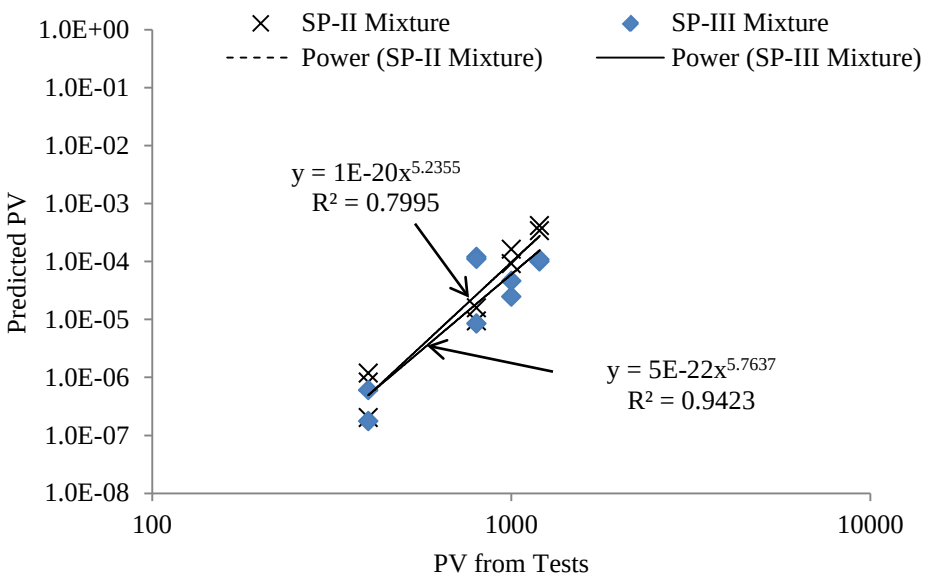

FIGURE 37 ε-PV Curves for Laboratory SP-II and SP-III Mixtures from Laboratory Fatigue Testing

Laboratory vs. Field Mixture Fatigue Performance

This section summarizes the fatigue performance of laboratory mixtures and that of field mixtures. The predicted FEL values for all four mix types are shown in Table 12. It can be seen here that the FEL of laboratory mixtures is much lower than that of the field mixes when looking at the ε-N_f and ε-PV results. However, the PV prediction model shows an increased FEL for the laboratory SP-II mixture, suggesting that the higher PG binder grade improves the estimated FEL. Figure 38 compares the fatigue life of both laboratory and field mixtures. Figure 38(a) shows data points loosely following the line of unity which indicates similar fatigue life for the SP-II mixture. However, Figure 38(b) shows more scatter whereby the fatigue life of the field SP-III mixture seems to be greater than that of the laboratory mixture.

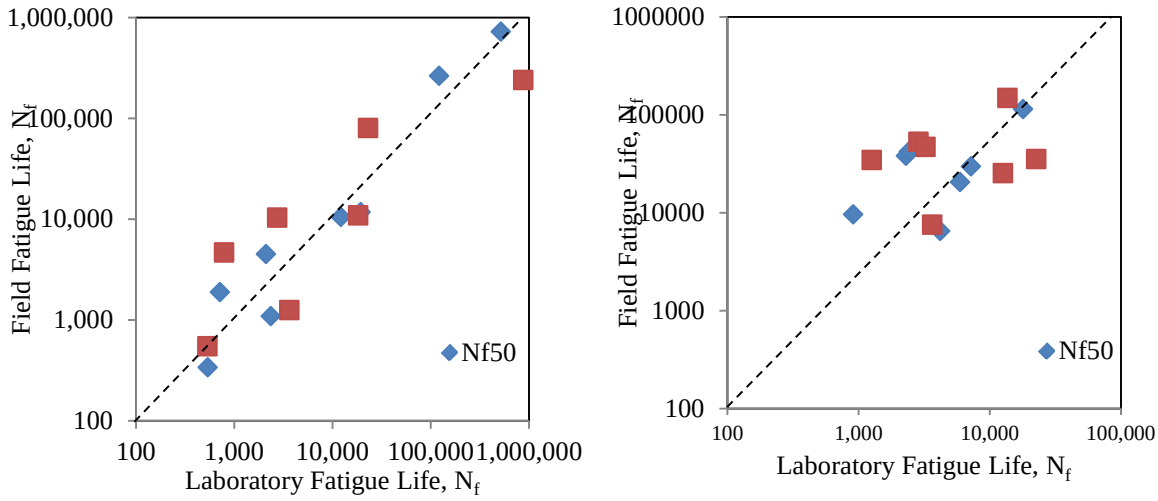

(a) SP-II Mixture

(b) SP-III Mixture

FIGURE 38 Comparison of Fatigue Life for Laboratory and Field Mixtures

Another way to analyze fatigue life of these mixtures is to compare their PV data. As stated in the literature, the PV represents fatigue life and lower PV indicates longer fatigue life. Figure 39 presents PV data for both laboratory and field SP-II and SP-III mixtures. A similar trend to what is shown earlier is also seen here with Figure 39(a) showing good consistency, indicating similar fatigue life for laboratory and field mixtures. Figure 39(b) confirms the earlier observation that the fatigue life of the field SP-III mixture is much longer than that of the laboratory mixture with lower PV data indicating greater fatigue life.

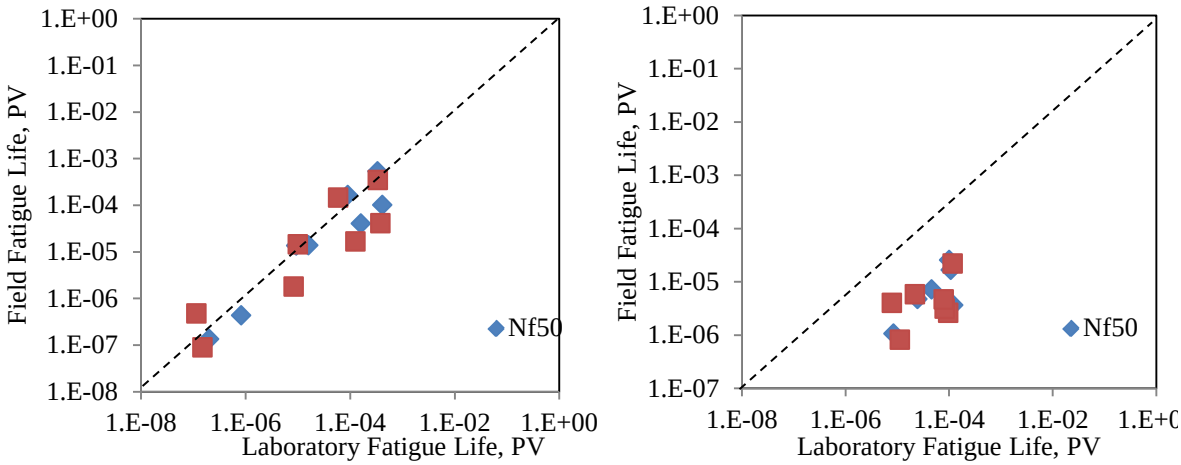

FIGURE 39 Comparison of Plateau Values for Laboratory and Field Mixtures

Statistical Analysis

To determine whether two fatigue curves using the traditional (N_{f50}) and Energy Ratio (ER) approaches, from different mixtures are statistically the same, the F-Test is introduced. The hypothesis, H_o, states that the two failure curves are the same, and H_a states that two curves are different. H_o is rejected if the p-value is less than α = 0.05. The p-value is the level of significance, which is defined as the probability of obtaining a value of the test statistic that is more likely to reject H_o than the actual observed value of the test statistic. This probability is computed assuming that the null hypothesis is true. Thus, if the p-value is a small value, then the sample data fail to support H_o, and the decision is to reject H_o (*63*).

The F-test is performed on the ε-N_f and PV-ε curves for both SP-II and SP-III mixtures which are shown in Figures 24 through 29 using Eq. 33.

$$F^* = \left(\frac{SSE(R)-SSE(F)}{df(R)-df(F)} \div \frac{SSE(F)}{df(F)}\right) \quad (33)$$

where SSE_1 is the error sum of squares for Regression Curve 1 (N_{f50}), SSE_2 is the error sum of squares for Regression Curve 2 (*ER*), SSE(R) is the combined regression curve from both mixtures, df(F) is the total degrees of freedom df_1 + df_2, and df(R) is the degree of freedom for the combined regression curve.

The p-value is determined using the Excel function of F probability distribution for the two data sets (FDIST):

$$p - value = FDIST(F^*, df_a, df_b) \quad (34)$$

where $df_a = df(R) - df(F)$, and $df_b = df(F)$.

For ε-N regression curves through power law, the p-values for SP-II and SP-III mixtures are 7.21e-26 and 0.995 respectively. Because the p-value is greater than $\alpha = 0.05$ for the SP-III mixture, the H_o hypothesis is not rejected and it is concluded that the two fatigue curves are statistically the same. However, for the SP-II mixture, the p-value is less than 0.05 which means that the two fatigue curves are different. For PV-ε regression curves through power law, the p-values for SP-II and SP-III mixtures are 0.998 and 0.306 respectively. Because the p-values are greater than $\alpha = 0.05$ for both mixtures, the H_o hypothesis is not rejected and it is concluded that the two fatigue curves are statistically the same.

CONCLUSIONS

The key features of this study found as:

- Majority of fatigue test results show that fatigue failure according to the Energy Ratio criterion occurred after a sample has achieved 50% reduction in stiffness, which is the traditional fatigue criterion. This suggests that the traditional failure approach is slightly conservative.

- Fatigue life extrapolation using the single-stage Weibull function and RDEC approach showed good consistency with fatigue test results of field SP-II and SP-III mixtures, performed at normal strain levels. However, for low strain testing, extremely high fatigue life data is predicted, which suggests that an overestimation of fatigue life.

- Using the traditional ε-N_f relationship, the FEL values of field SP-II and SP-III mixtures are predicted. The FEL of the SP-II mixture is estimated to be 189 με, using traditional failure criterion (Nf_{50}), and 227 με using the Energy Ratio failure criterion (*ER*). For the SP-III mixture, the FEL is estimated to be 180 με (Nf_{50}) and 311 με (*ER*).

- Using the ε-PV approach, the FEL values of field SP-II and SP-III mixtures are predicted. The FEL of the SP-II mixture is estimated to be 252 με (*ER*) and 215 με (Nf_{50}). For the SP-III mixture, the FEL is estimated to be 291 με (*ER*) and 334 με (Nf_{50}).

- PV values predicted using the material property-based PV prediction model showed good consistency with PV values determined from laboratory testing. However, the estimated FEL values using the PV model are much lower than those predicted using the ε-N_f and ε-PV models.

- The effect of polymer modified binder on the FEL of HMA mixtures showed mixed results, with an increase in estimated FEL of SP-III mixture but reducing the estimated FEL of SP-II mixture.

- The estimated FEL of laboratory mixtures is much lower than that of the field mixes. In particular, the fatigue performance of laboratory SP-II mixtures compares well with that of field SP-II mixtures. However, the laboratory SP-III mixture performs poorly when compared with fatigue performance of the field SP-III mixture.

- The F-test is performed on the ε-N_f and PV-ε curves to determine whether the curves developed using the traditional (N_{f50}) and Energy Ratio (*ER*) approaches are statistically the same. For ε-N regression curves through power law, it is determined that the two fatigue curves are statistically the same for the SP-III mixture. However, the opposite is the case for the SP-II fatigue curves. For the PV-ε curves, the F-Test shows that the fatigue curves are statistically the same using the different fatigue failure approaches.

THIS PAGE LEFT BLANK INTENTIONALLY

COMPARISON OF DIFFERENT FAILURE CRITERIA FOR FATIGUE TESTING

INTRODUCTION

Traditionally, third point loaded beam fatigue has been used to characterize fatigue performance under laboratory conditions (*8*). This includes subjecting beams to damage inducing cyclic loading (displacement control) and monitoring its stress history. Using the beam geometry, applied displacement and measured load, strain and stress in beam are calculated. Further, stiffness of material is calculated using stress and strain history. Then, the number of cycles at 50% reduction in stiffness is recorded as failure of the beam. This procedure is repeated at other strain levels to obtain relation between applied strain and number of cycles to failure. The same relation is given in Eq. 35. Sometimes, initial stiffness of material is also incorporated into fatigue model and is given in Eq. 36.

$$N_f = k_1 \left(\frac{1}{\varepsilon}\right)^{k_2} \tag{35}$$

$$N_f = k_1 \left(\frac{1}{\varepsilon}\right)^{k_2} \left(\frac{1}{E}\right)^{k_3} \tag{36}$$

where N_f = number of cycles at failure, ε = maximum tensile strain in beam, E = initial stiffness and k_i = regression coefficients.

Under the controlled displacement mode of loading, the stress in the beam reduces with the increase in number of cycles. Due to testing difficulties, it is difficult to monitor development and propagation of cracks in the beam. Often, it takes a large number of repetitions of load to see a macrocrack in the beam. Due to nature of loading, measured load might not decrease beyond certain value. Also, 50% reduction in stiffness has been arbitrarily defined as failure point. Such an approach might not indicate better utilization of material and time resources available.

Several researchers have proposed energy based approaches to analyze fatigue data. Among them dissipated energy, cumulative dissipated energy and dissipated energy ratio approaches are popular among pavement engineering community due to its simplistic nature. These approaches fail to account for the viscoelastic nature of asphalt concrete. On the other hand, viscoelastic continuum damage approach has shown promising results in terms of robustness and efficient utilization of available resources.

In summary, this study compared fatigue failure criterion developed using the stiffness based approach with viscoelastic continuum damage approach. Such a comparison can aid the phenomenological approach in describing fatigue performance in a rational manner.

Background on Current Fatigue Failure Criteria

As mentioned previously, in the phenomenological approach, failure is defined as the number of cycles at which the stiffness of the material decreases by 50% (*8*). Initial stiffness of the beam is measured at 50^{th} loading cycle. This is to account for the initial setting of the beam. However, one might expect stiffness reduction from the first cycle itself. Thus, in this approach, damage in initial few cycles is ignored. This often leads to unrealistic values especially at higher strain amplitude levels.

Other researchers have used dissipated energy to model fatigue behavior (*64, 65, 66*). Dissipated energy is defined as energy lost during each cycle of loading. This includes energy lost due to damping, viscoelastic effects and damage growth. Dissipated energy can be calculated by calculating the area within the stress-strain curve. Mathematically, dissipated energy in each cycle i is given by Eq. 37. Further, dissipated energy in each cycle is summed to obtain cumulative dissipated energy as shown in Eq. 38.

$$w_i = \pi \sigma_{amp} \varepsilon_{amp} \sin \varphi \tag{37}$$

$$W_i = \sum_1^N w_i \tag{38}$$

where w_i = dissipated energy in cycle i, σ_{amp} = stress amplitude, ε_{amp} = strain amplitude, φ = phase angle between stress and strain and W_i = cumulative dissipated energy up to cycle i.

Van Dijk and Vesser (*64*) found a strong relation between numbers of cycles and cumulative dissipated energy. Pronk and Hopman (*65*) refined the dissipated energy approach by defining energy ratio to check for linearity. ER is defined as ratio of initial dissipated energy to dissipated energy in cycle i multiplied by number of cycles. Deviation from the straight line in the plot of the ER against the number of cycles indicates development of macrocracks in the beam. However, deviation from the straight line is subjected to individual judgment.

Guzlan and Carpenter (*18*) used the Dissipated Energy Ratio (DER) to quantify relative change in dissipated strain energy. DER is defined where Guzlan and Carpenter (*18*) found a strong relationship between DER and number of cycles to failure. A plot of DER vs. number of cycles indicates three distinct regions. Research by Carpenter and Shen (*7*) indicated a linear relationship between the plateau value and number of cycles to 50 percent initial stiffness (semi-log scale). Due to overly sensitive dissipated energy differences, plot of DER vs. number of cycles indicates scatter. Thus, it is difficult to interpret the failure location visually as well as mathematically.

Rowe and Bouldin (*13*) introduced ER for modeling fatigue behavior and it is described in detail in the literature review. The ER is obtained by multiplying stiffness (kPa) by the corresponding number of cycle. The ER is cross plotted against number of cycles to determine the failure location. The peak value in this plot indicates the transition from micro-cracking to macro-cracking.

In all the above cases, material is considered to be elastic. However, asphalt concrete exhibits rate dependent and temperature dependent behavior. Kim (*20*) successfully applied the elastic-viscoelastic correspondence principle for modeling sand-asphalt mixture behavior under multi-level cyclic loading. Kim (*20*) found that the secant pseudostiffness (stress corresponding to maximum pseudostrain divided by maximum pseudostrain in each cycle) value decreases with increasing damage. Daniel (*21*) and Daniel and Kim (*22*) found that the relationship between the normalized pseudostiffness ($C1$) and the damage parameter ($S1$) is unique for a given asphalt concrete mix (hereafter referred to as the damage characteristic curve) under uniaxial mode of loading. Swamy (*23*) extended viscoelastic continuum damage mode to flexure mode of loading and found that damage characteristic curve is unique at given temperatures under flexure mode of loading. Swamy and Daniel (*24*) found a point of inflection in the damage characteristic curve beyond which the material loses its structural integrity at faster rate. Also, it was observed that normalized pseudostiffness at this inflection point is dependent on mixture properties.

In this study, traditional four point bending beam fatigue testing apparatus is used. AASHTO T321 (*8*) standards are used for fatigue testing. For determining viscoelastic properties, displacement controlled cyclic loading mode is used.

Laboratory Testing

Initially, the prepared specimen is tested for its viscoelastic properties and subsequently tested for its fatigue properties. During the determination of viscoelastic properties, the specimen is subjected to low strain amplitude cyclic loading to obtain its dynamic modulus and phase angle fingerprint at different temperatures and frequencies. The maximum strain in the specimen is limited to 75 microstrain. Dynamic modulus and phase angle measurements are obtained at -10 °C to 30 °C in 10 °C increments. Within each temperature, frequencies of 15, 10, 5, 2, 1, 0.5, 0.2, and 0.1 Hz are used. Using the time-temperature superposition principle, dynamic modulus and phase angle mastercurves are constructed. Using dynamic modulus and phase angle mastercurve coefficients, the relaxation modulus mastercurve is obtained using the inter-conversion technique (*67*).

In the second stage, fatigue testing is conducted on specimens to obtain fatigue properties on mixture. All specimens are tested at damage inducing strain level. In this research, the strain amplitudes used are in range of 400-1200 microstrain. Using the deflection history, load response history, and geometry of test specimen, the maximum strain and stress in the specimen are calculated using Eqs 39 and 40 respectively.

$$\varepsilon = \frac{12\, h\, \delta}{3L^2 - 4a^2} \tag{39}$$

$$\sigma = \frac{P\, L}{b\, h^2} \tag{40}$$

Where P = Load applied by actuator at time t, b =average specimen width and h =average specimen height, δ = deflection at center of beam at time t, a = distance between inside clamps and L = distance between outside clamps.

Analysis procedure

The relaxation modulus mastercurve is obtained using dynamic modulus and phase angle mastercurve coefficients through the inter-conversion technique. Using the computed strain history and relaxation modulus mastercurve, pseudostrain is computed using Eq. 41. This pseudostrain accounts for all viscoelastic effects and separates effects of damage and healing within the specimen.

$$\varepsilon^R(t) = \frac{1}{E_R}\int_0^t E\,(t-\tau)\frac{d\varepsilon}{d\tau}\,d\tau \tag{41}$$

where E_R = reference modulus, $E(t)$ = relaxation modulus, ε = computed physical strain, t = elapsed time between the time loading began and the time of interest and τ = time variable.

In a fatigue test, loops are seen in cross plots of measured stress vs. pseudostrain. Further, the slope of these loops decreases as testing progresses. The secant pseudostiffness (S_i^R) in any cycle i is calculated by dividing measured stress by maximum pseudostrain in cycle i. To account for specimen to specimen variation, secant pseudostiffness is divided by secant pseudostiffness in first cycle of loading. From here onwards for simplicity, this value will be referred to as normalized pseudostiffness ($C1$). Due to continuous growth of damage, the numerical value of normalized pseudostiffness continuously decreases (has a value of 1 at the undamaged condition, 0 at complete failure). The variation of normalized pseudostiffness during a fatigue test is shown in Figure 40. Using the histories of normalized pseudostiffness and computed physical strain, the damage parameter is computed. The equation to compute damage parameter is presented in Eq. 42.

$$S1_i \cong \sum_{i=1}^{N}\left[\frac{I}{2}\left(\varepsilon_{max,i}^R\right)^2\left(C1_{i-1}-C1_i\right)\right]^{\frac{\alpha}{1+\alpha}}\left(t_i-t_{i-1}\right)^{\frac{1}{1+\alpha}} \tag{42}$$

Where $\varepsilon_{max,i}^R$ = maximum pseudostrain in cycle i, $C1_i$ = normalized pseudostiffness in cycle i, $S1_i$ = damage parameter in cycle i, α = material constant and t = time to maximum pseudostrain in cycle i.

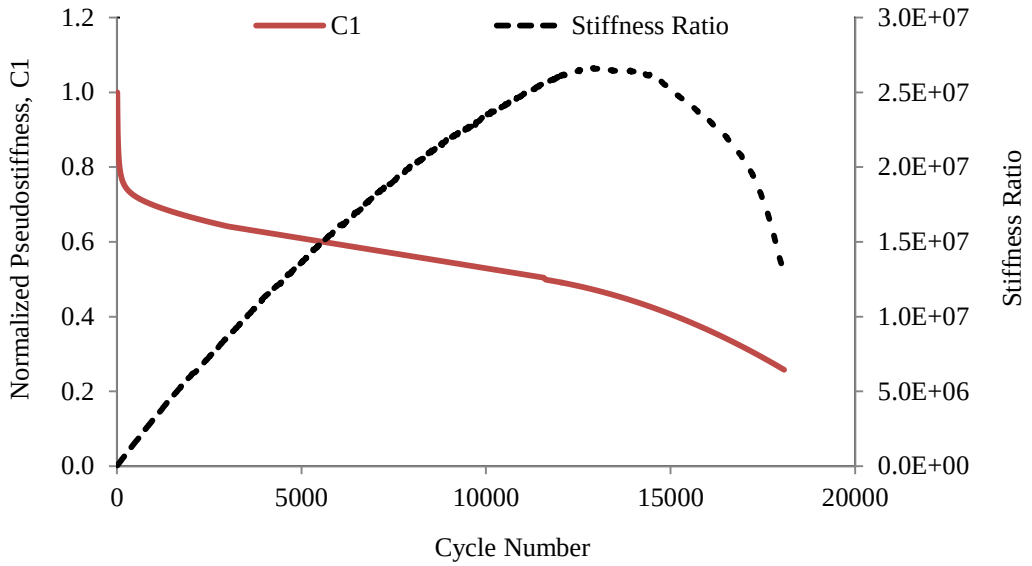

FIGURE 40 Variation of Normalized Pseudostiffness and Stiffness Ratio with Number of Repetitions

Due to continuous growth of damage, the numerical value of the damage parameter continuously increases (with initial value of 0). Further, the normalized pseudostiffness is plotted against the damage parameter to obtain the damage characteristic curve. This curve is fitted with a generalized exponential model presented in Eq. 43.

$$C1 = e^{k_1 \times (S1)^{k_2}} \tag{43}$$

Where $C1$ = normalized pseudostiffness, $S1$ = damage parameter and k_i = regression coefficients.

Visual examination of the actual damage characteristic curve and predicted values from the generalized exponential model indicate that the generalized exponential model over-predictes at the lower normalized pseudostiffness values. Thus, using data points below which deviation is seen is fitted with the second order polynomial. The composite mode consisting of the generalized exponential model and the second order polynomial is used for further analysis. The point of intersection of the generalized exponential model and the second order polynomial is referred to as the point of inflection. The characteristic damage curve obtained for SP-II-5 specimen (SP-II mixture) is shown in Figure 41. The number of cycles corresponding to this inflection point has been documented as failure criterion (*24*). The same figure shows the fitted generalized exponential model and the second order polynomial. More details about the viscoelastic continuum damage approach as applied to flexure mode of loading can be found elsewhere (*23, 24*).

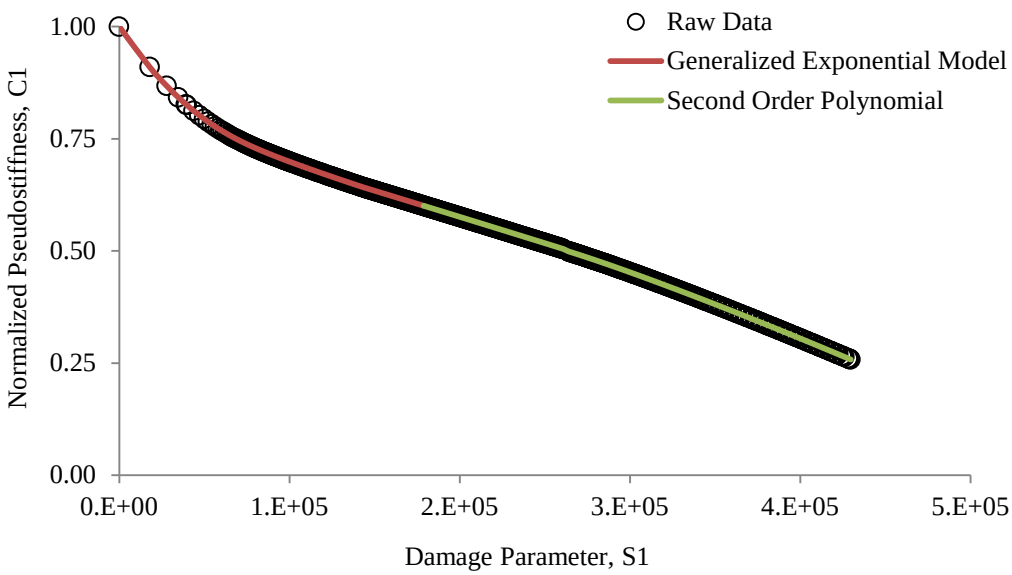

FIGURE 41 Damage Characteristic Curve for SP-II-K1 Specimen

Using the computed strain and stress, stiffness in each cycle of loading is computed. Further the stiffness ratio is computed using initial stiffness and stiffness corresponding to the number of cycles. The formula to compute the stiffness ratio is Eq. 44. The variation of the stiffness ratio with number of cycles is shown in Figure 40. During the course of the fatigue test, the stiffness ratio increases initially and then decreases. The number of cycles corresponding to maximum stiffness ratio has been considered to be failure point (*13*).

$$SR = \left(\frac{S_i}{S_0}\right) N_i \tag{44}$$

Where SR = stiffness ratio, S_i = stiffness in cycle N_i, and S_0 = initial stiffness.

Results

Damage characteristic curves for SP-II and SP-III mixtures using alpha = 1 +1/n are shown in Figures 42 and 43 respectively.

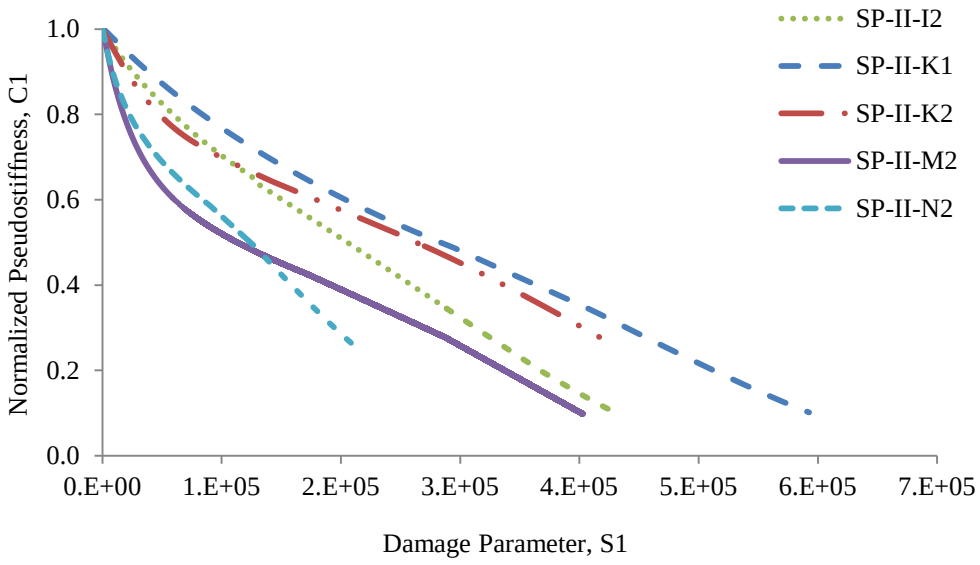

FIGURE 42 Damage Characteristic Curves for SP-II Mixture

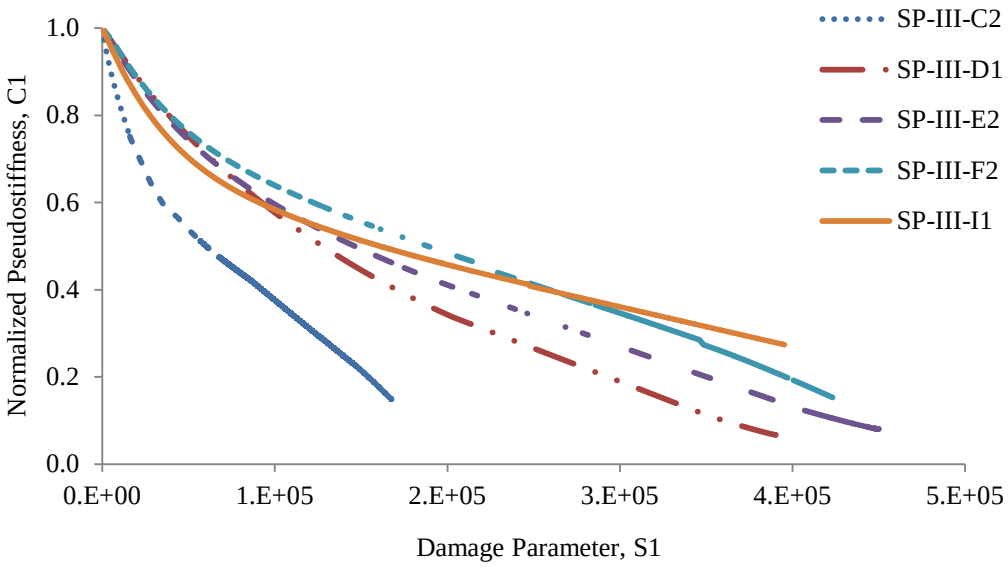

FIGURE 43 Damage Characteristic Curves for SP-III Mixture

Comparison of Parameters at Maximum Stiffness Ratio

The number of cycles to 50% reduction in stiffness is compared with the number of cycles at maximum energy ratio for SP-II and SP-III mixtures in Figures 44 and 45, respectively. In general, the number of cycles at maximum energy ratio is higher than the number of cycles needed to reach 50% reduction in stiffness. This indicates the traditional approach of 50% stiffness is conservative.

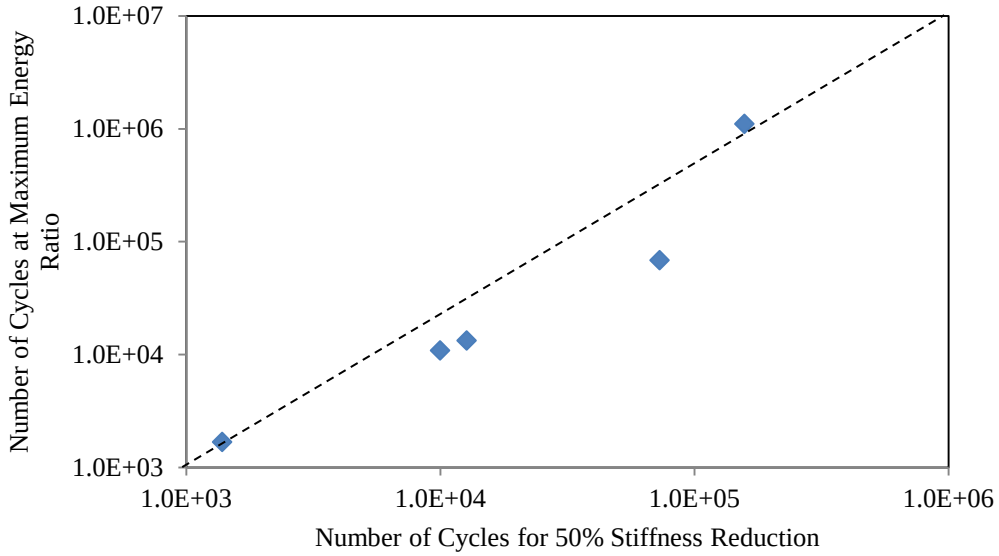

FIGURE 44 Comparison of number of cycles at maximum energy ratio and number of cycles for 50% stiffness reduction for SP II mixture

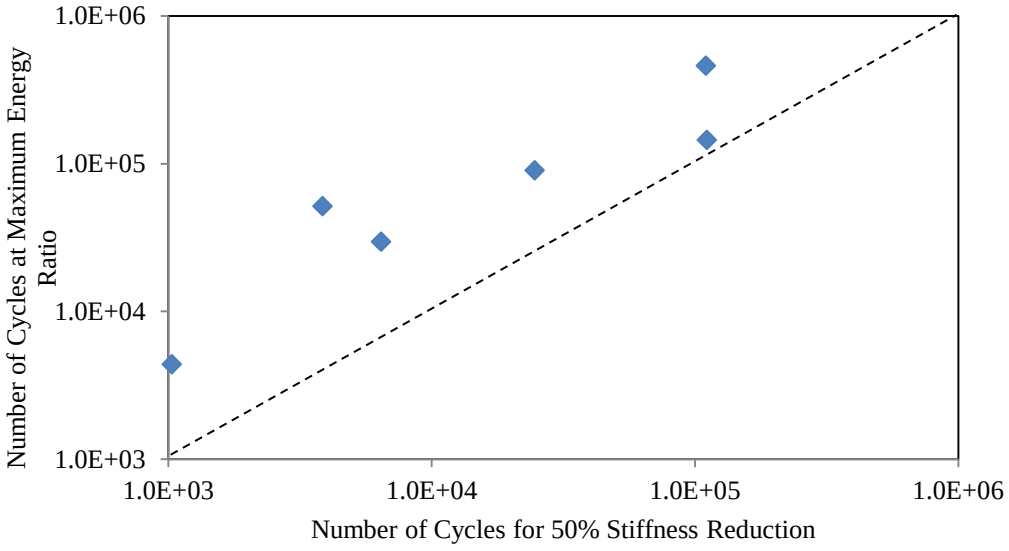

FIGURE 45 Comparison of Number of Cycles at Maximum Energy Ratio and Number of Cycles for 50% Stiffness Reduction for SP-III Mixture

The number of cycles at the inflection point in the damage characteristic curve (using alpha = 1 + 1/n) is compared with the number of cycles at maximum energy ratio for SP-II and SP-III mixtures in Figures 46 and 47 respectively. In general, a strong correlation is found between the number of cycles at the inflection point in the damage characteristic curve and number of cycles at the maximum ER. Further, the number of cycles at the inflection point in the damage characteristic curve is always less than the number of cycles at the maximum ER.

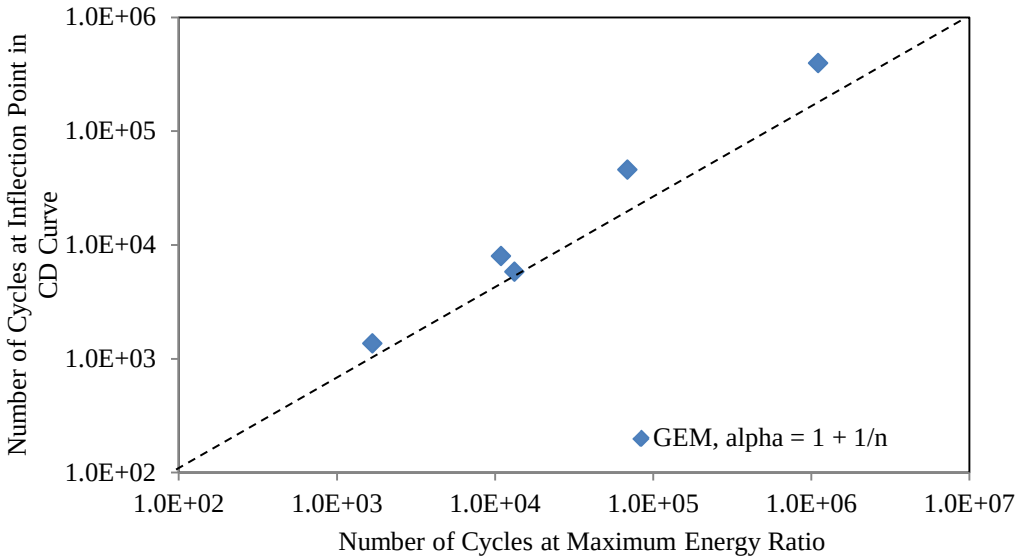

FIGURE 46 Comparison of Number of Cycles at Inflection Point and Number of Cycles at Maximum Energy Ratio for SP-II Mixture

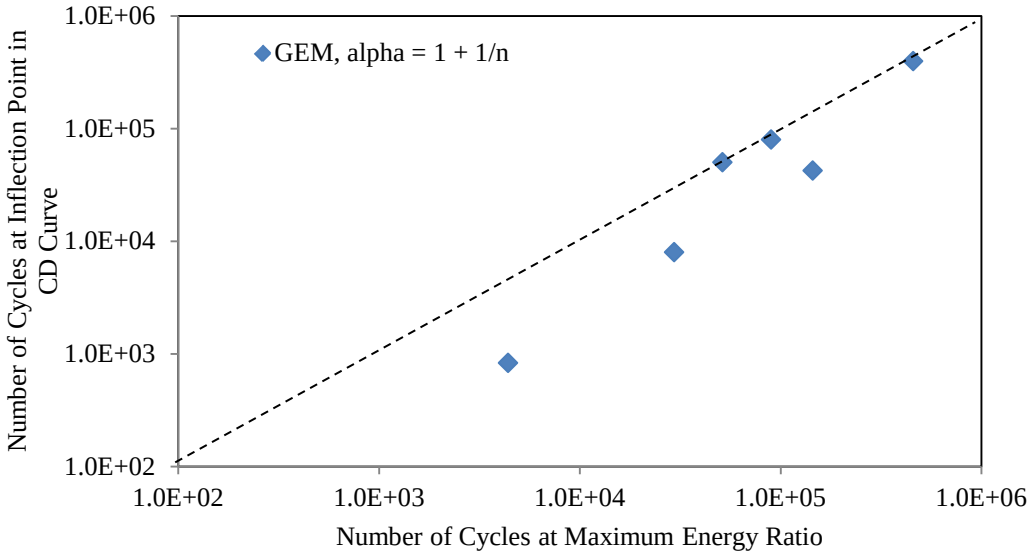

FIGURE 47 Comparison of Number of Cycles at Inflection Point and Number of Cycles at Maximum Energy Ratio for SP-III Mixture

Comparison of CD Method with Traditional Method

A scatter plot of the number of cycles at the inflection point in the damage characteristic curve vs. number of cycles at 50% reduction in stiffness for SP-II and SP-III mixtures are presented in Figures 48 and 49 respectively. The coefficient of correlation (with power fit, both on log scales) is in range of 0.6575 to 0.9245. R^2 values and visual interpretation indicates a strong correlation between these two parameters.

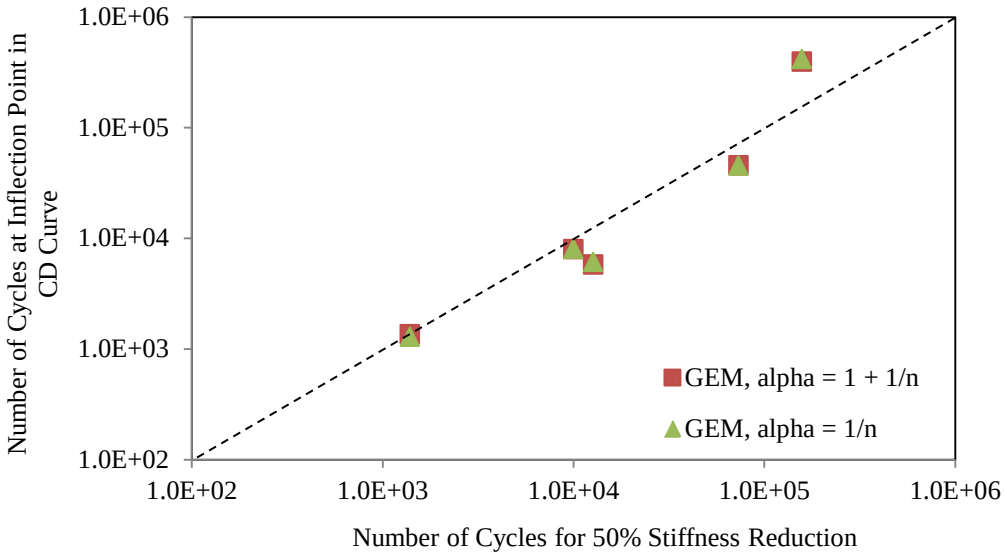

FIGURE 48 Comparison of Number of Cycles at Inflection Point and Number of Cycles for 50% Stiffness Reduction for SP-II Mixture

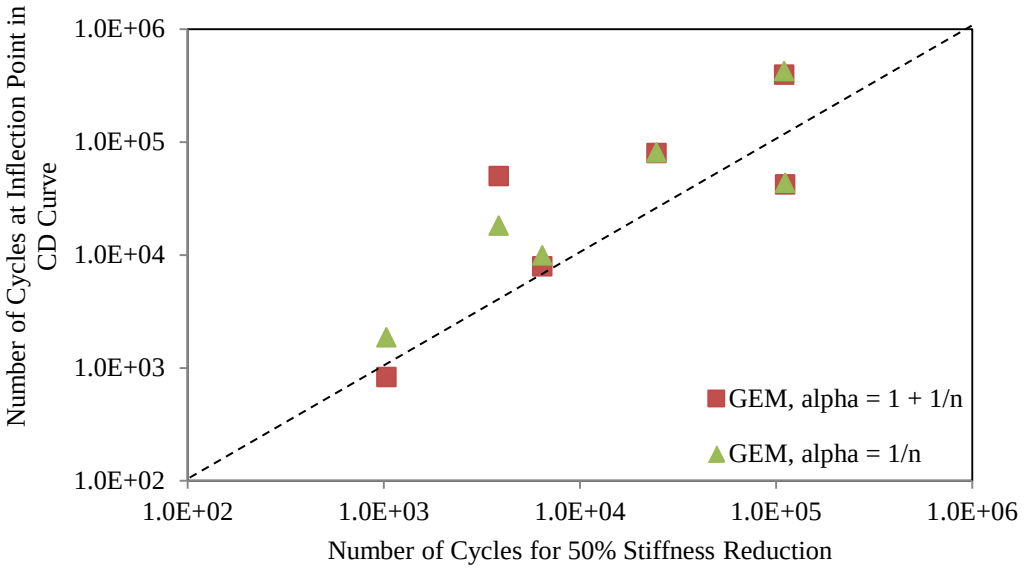

FIGURE 49 Comparison of Number of Cycles at Inflection Point and Number of Cycles for 50% Stiffness Reduction for SP-III Mixture

Effect of Strain Amplitude

The effect on strain amplitude on number of cycles is investigated for both the SP II and SP III mixtures. Criterion like 50% reduction in stiffness, the maximum stiffness ratio and the inflection point in damage characteristic curve are used in evaluation. The plots for SP-II and SP-III mixtures are shown in Figures 50 and 51 respectively.

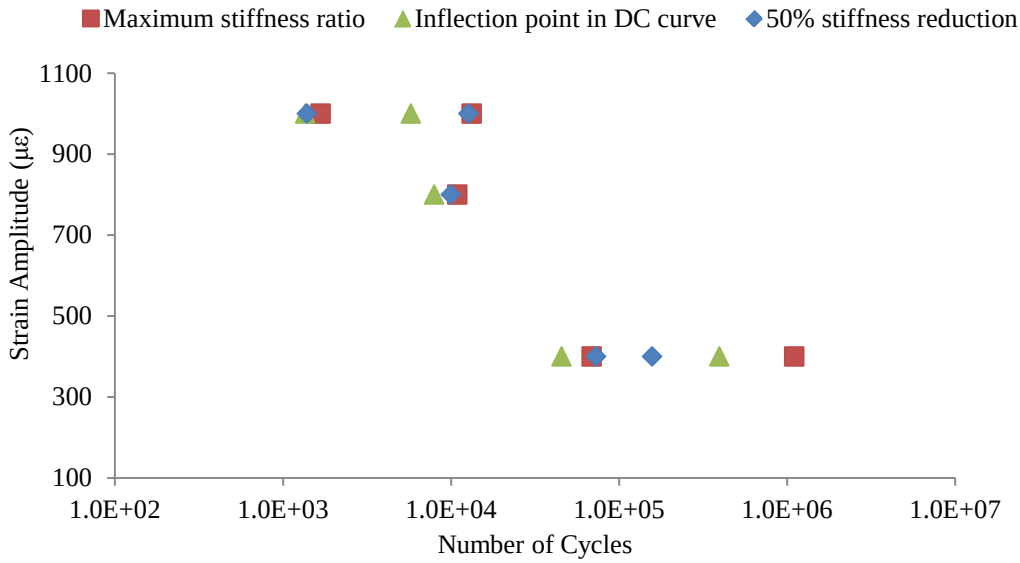

FIGURE 50 Effect of Strain Amplitude on Failure Criteria for SP-II Mixture

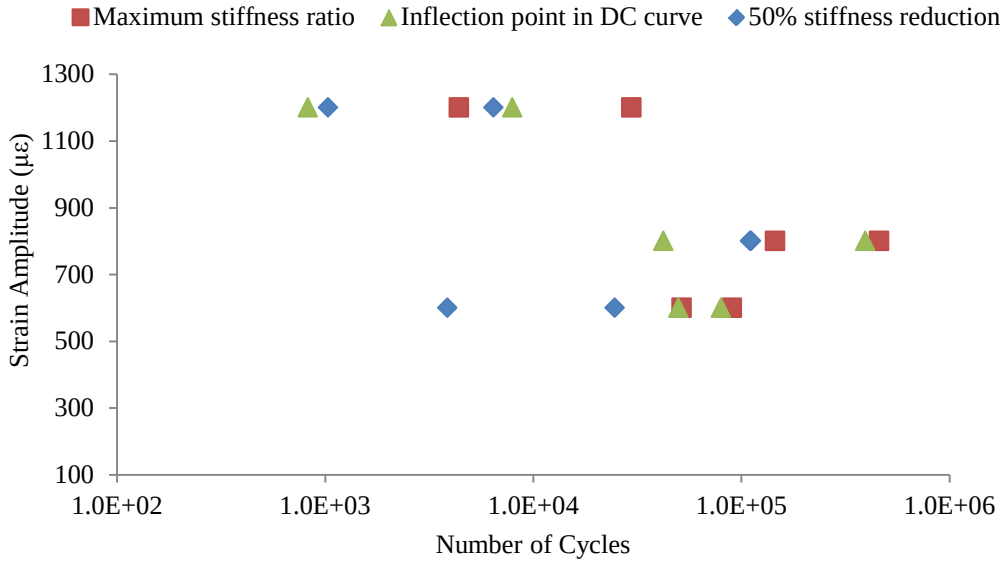

FIGURE 51 Effect of Strain Amplitude on Failure Criteria for SP-III Mixture

In the case of the SP-II mixture, with the decrease in strain amplitude, the number of cycles increased for all three cases. However, this is not the case for the SP-III mixture. In the case of SP-II mixture, the R^2 values are 0.797, 0.738 and 0.8195 for 50% reduction in stiffness, maximum stiffness ratio and inflection point in damage characteristic curve respectively. For the SP-III mixture, R^2 value is 0.219, 0.403 and 0.5904 for 50% reduction in stiffness, maximum stiffness ratio and inflection point in damage characteristic curve respectively. This indicates that there is better correlation between the strain amplitude and the number of cycles at inflection point in the damage characteristic curve.

Summary

This section summarizes the compared fatigue failure criterion developed using the stiffness based approach with viscoelastic continuum damage approach, as performed in this study:

- Dynamic modulus testing is performed on asphalt beam samples to determine the dynamic modulus and phase angle master curves. Using mastercurve coefficients, a relaxation modulus mastercurve is obtained whereby the pseudo-strain is computed for each test.

- The secant pseudostiffness (stress corresponding to maximum pseudostrain divided by maximum pseudostrain in each cycle) value is found to decrease with increasing damage. The damage characteristic curve describes the relationship between the normalized pseudostiffness (C1) and the damage parameter (S1).

- Using the VCDM approach, a point of inflection is identified in the damage characteristic curve beyond which the material loses its structural integrity at faster rate. This point is considered the fatigue failure of the sample.

- A strong correlation is found between the VCDM criterion and the energy ratio criterion. Further, the fatigue life of the VCDM approach is always less than the ER fatigue life.

- A strong correlation is also found between the VCDM criterion and the traditional criterion (N_{f50}).

- In general, the ER fatigue life is higher than traditional fatigue life (N_{f50}). This indicates the traditional approach of 50% stiffness is conservative.

- The effect of strain amplitude on the fatigue life of SP-II and SP-III mixtures is analyzed using the three different failure approaches. In case of the SP-II mixture, with decrease in strain amplitude, the number of cycles increased for all three cases. This is not the case for SP-III mixture. Higher R^2 values for the inflection point in the damage characteristic curve suggest that there is better correlation between strain amplitude and the number of cycles at the inflection point in the damage characteristic curve.

THIS PAGE LEFT BLANK INTENTIONALLY

FATIGUE CRACK PROPAGATION IN HMA MIXTURES

INTRODUCTION

It has been well documented that fatigue cracking has three stages; crack initiation, propagation, and rapid failure (*68*). Under controlled displacement flexural mode of loading, the stress in the beam reduces with an increase in loading cycles. Due to testing difficulties, it is difficult to monitor development and propagation of cracks in the beam. Often, it takes a large number of load repetitions to see a macrocrack in the beam. For this study, traditional four-point bending is performed on HMA beam specimens and the resulting fatigue cracking is analyzed. Fatigue testing is conducted in an environmental chamber where the temperature is kept constant at 20 °C. At the end of each test, each beam is examined and where visible, cracks are highlighted and photographed. In addition, crack lengths are measured using a scale roller pen, and separated into three categories, depending on where the location of the crack existed: within the asphalt mastic, through aggregates, and at the interface between aggregate and asphalt mastic.

The mastic is a the mixture of fine aggregate passing the #200 sieve and asphalt binder, which is a viscoelastic composite that has adhesive and cohesive properties capable of withstanding tensile forces (*69*). The interface is defined as the surface that is the boundary between the binder, or mastic, and the aggregate. The aggregate consists of coarse particulate matter that is coated with binder and forms the load-bearing skeleton of the HMA. Cracks can initiate and propagate through any of these three phases. The objective of this paper is to determine a pattern or trend, if any, of crack initiation and propagation in HMA materials, as well as understand why fatigue results may differ under similar testing conditions.

Background

Traditional mechanistic-empirical approaches for predicting fatigue of HMA mixtures require controlled stress (strain) laboratory testing, usually dictated by a single temperature over a range of applied stress (strain) levels. The number of cycles to failure is then recorded along with the critical stress (strain) level and a plot of this relationship describes the fatigue behavior of a HMA mixture. Usually, replicate samples are required for testing at different stress or strain levels. Results of fatigue testing of replicate samples should in theory be similar. However, this is not always the case as it is virtually impossible to recreate two to three identical samples. Aggregate alignment and distribution vary with each sample prepared, and because of that, crack initiation and propagation rates change with each test. Therefore, it can only be assumed that the fatigue life differs from one sample to another, despite similar testing conditions.

Many test factors can be controlled such as mixture type, sample stiffness, percentage air voids, temperature, frequency, and aggregate gradation. However, due to the limited sample size, factors which are nearly impossible to control are the location and distribution of large size aggregates (greater than ½ inch). The beam sample size for fatigue testing is 15 in. x 2.5 in. x 2.0 in. (*8*). Within these boundaries, larger size aggregates can congregate, which may lead to a poor density gradient, and ultimately premature fatigue failure. As stated earlier, fatigue failure has three stages; crack initiation, propagation, and failure. The presence of larger-size aggregates

within close proximity of each other may induce crack initiation, as well as affect crack propagation rates.

There are numerous studies of crack behavior in metallic materials, yet crack initiation, crack path and propagation are not well understood in asphalt concrete. One particular study characterized crack initiation and propagation through HMA materials. In particular, crack pathways are evaluated by micro-mechanical testing of the phases of asphalt concrete in tension, compression, and shear, Results showed that the interface phase is preferential for crack initiation and propagation (*69*). However, notched samples are tested under monotonic loading only. This study investigates cracking due to fatigue failure on un-notched HMA samples and the effects of the chosen crack path on the associated fatigue life.

Fatigue Test Results

SP-II Mixture

Table 13 presents the fatigue test results of SP-II mixture samples. The applied strain and initial stiffness of the beam (taken at 50 load cycles) are shown, as well as the percent of air voids and fatigue life of each test specimen. The fatigue life is the number of cycles required to achieve failure. AASHTO T321-07 (*8*) standards require that a sample achieve 50% reduction in initial stiffness (N_{f50}) before considered failed. However, this may only lead to minor cracking, even micro-cracking which may not be visible to the naked eye. Therefore, beam samples are tested until they achieved 80-90% reduction in initial stiffness, whereby macro-cracking can be easily identified. Also listed in Table 13 is the failure criterion ($N_{f(ER)}$) defined by the ER method. The ER approach is based on a stress-controlled study by Hopman et al. (*14*) which claims to identify the point at which micro-cracking becomes a macro-crack (defined as fatigue failure). The ER is obtained by multiplying stiffness by corresponding number of cycle. The point at which the maximum value of *ER* occurs is defined as the fatigue failure. The peak in the curve indicates the transition point between micro-crack formation and propagation of a macroscopic crack. The ER is defined in Eq. 45:

$$Energy\ Ratio\ (ER) = Cycle\ Number^{*}\ Stiffness \tag{45}$$

where *E* is the flexural stiffness (kPa).

Table 13 shows that the strain range varied from 200 to 1000 με. Sample SP-II-L2 is tested at 200 microstrain (με) for 10 days, achieving 8.5 million cycles, yet flexural stiffness reduced by only 30%. Therefore, testing is stopped and the applied strain is increased to 400 με for the next test.

TABLE 13 Flexural Fatigue Test Results for SP-II Mixture Samples

Beam ID	Applied ε_t (με)	Initial E_0 (psi)	% Air Voids	Cycles Tested	Failure Criteria		Avg. Cycles to Failure	
					N_{f50}	$N_{f\ (ER)}$	N_{f50}	$N_{f(ER)}$
L2	200	954,638	5.4	8,479,090	NA	NA	NA	NA
N2	400	646,000	5.2	115,101	79,008	69,069	355,377	469,631
A1	400	880,310	5.4	389,811	263,411	239,818		
M2	400	666,158	5.9	1,535,746	723,711	1,100,007		
I2	800	471,000	5.1	23,612	11,700	10,910	11,100	45,661
L1	800	655,716	5.8	156,076	10,500	80,412		
N1	1000	853,302	4.8	2,665	1,085	1249	2,795	5,795
O2	1000	531,200	5.7	17,256	4,504	10,341		

Table 14 presents crack lengths measured for each SP-II sample. Crack lengths are measured as they pass through the asphalt mastic, aggregate, and interface phases. Each sample face is labeled clearly; Faces 1 and 3 are the sides of the beam, while Faces 2 and 4 are the bottom and top sides respectively. Micro and macro-cracking usually occurs at the base of the sample (Face 2) first, due to the presence of the maximum tensile strain, which is induced during flexure. The cracking propagates upward through the beam until it eventually appears on the topside of the beam. This process basically simulates the behavior of fatigue cracking in the field.

Replicate samples which are tested under similar conditions are analyzed. Samples SP-II-A1, SP-II-M2, and SP-II-N2 are tested at 400 με. All tests are conducted at the same frequency (10 Hz) and temperature (20 °C), and contain similar air voids (5-6%). Sample SP-II-A1 failed after 263,111 cycles (N_{f50}). Table 14 shows that sample SP-II-A1 had a total crack length of 3 inches. The majority of the crack length occurred along the interface (93%), whereas the remaining cracks propagated through the asphalt mastic (3%) and aggregates (4%).

Figure 52 illustrates the cracking in the base of sample SP-II-A1 and shows that the crack path propagates at the interface between large size aggregates and asphalt mastic. The crack then propagated towards the topside of the beam, as shown in Figure 53. When compared with replicate test samples, the fatigue life data differs. It can be seen from Table 13 that sample SP-II-M2 is of same mix type, contained similar air voids but had slightly lower flexural stiffness. SP-II-M2 is also tested at 400 με but yielded a far greater fatigue life.

FIGURE 52 Fatigue Cracking in HMA Beam Sample SP-II-A1

FIGURE 53 Fatigue Crack Propagating Upwards in HMA Beam Sample SP-II-A1

Figure 54 shows the crack path in sample SP-II-M2. The data shown in Table 14 shows that only 33% of the crack length occurred at the interface, with the majority, 52%, passing through aggregates. As expected, the crack propagation rate is reduced when cracks pass through aggregates, therefore extending the fatigue life of the material. This scenario may explain the superior fatigue life of sample SP-II-M2 when compared with sample SP-II-A1.

FIGURE 54 Fatigue Cracking in HMA Beam Sample SP-II-M2

The last replicate sample, SP-II-N1, is shown in Figure 55. Little or no cracking is evident in the sample, except for minor cracking which is visible at the interface of a large aggregate in the base of the sample. The reason for low cracking in sample SP-II-N1 is because the test is stopped after achieving only 70% reduction in stiffness, whereas 80-90% usually initiates unstable macro-cracking. However, the sample SP-II-N1 achieved 50% reduction in stiffness (failure) well before samples SP-II-A1 and SP-II-M2. The remaining SP-II samples described in Table 13 all show similar results (N_{f50} data) to their replicate test samples.

FIGURE 55 Fatigue Cracking in HMA Beam Sample SP-II-N2

TABLE 14 Crack Lengths in Failed SP-II Samples

Sample	Sample	Fatigue Cracking (in)				Crack Location (%)		
I2	Side	Mastic	Aggregate	Interface	Total	Mastic	Aggregate	Interface
Side 1	Face 1	0.3	0.77	1.07	2.1	14	36	50
Bottom	Face 2	1.29	1.84	2.01	5.1	25.1	35.8	39.1
Side 2	Face 3	0	0	0.55	0.6	0	0	100
Top	Face 4	0	0	0	0	NA	NA	NA
M2	Face 1	0.52	0.45	1.89	2.9	18.2	15.7	66.1
	Face 2	0.55	1.84	1.17	3.6	15.4	51.7	32.9
	Face 3	0.45	0	1.74	2.2	20.5	0	79.5
	Face 4	1.86	0	0.42	2.3	81.6	0	18.4
L1	Face 1	0.25	0	0.6	0.9	29.4	0	70.6
	Face 2	0.89	0	1.61	2.5	35.6	0	64.4
	Face 3	0	0	0.79	0.8	0	0	100
	Face 4	0	0	0	0	NA	NA	NA
N2	Face 1	0	0	0	0	NA	NA	NA
	Face 2	0	0	1.17	1.2	0	0	100
	Face 3	0	0	0	0	NA	NA	NA
	Face 4	0	0	0	0	NA	NA	NA
N1	Face 1	0.4	0	0.17	0.6	70.2	0	29.8
	Face 2	0.22	1.19	1.6	3	7.3	39.5	53.2
	Face 3	0.72	0	1.32	2	35.3	0	64.7
	Face 4	0	0	0	0	NA	NA	NA
A1	Face 1	0.25	0.22	0.12	0.6	42.4	37.3	20.3
	Face 2	0.1	0.12	2.8	3	3.3	4	92.7
	Face 3	1.14	0	0	1.1	100	0	0
	Face 4	0	0.15	0.79	0.9	0	16	84
O2	Face 1	0.45	0	0.77	1.2	36.9	0	63.1
	Face 2	0.92	0.37	1.07	2.4	39	15.7	45.3
	Face 3	1.07	0	0	1.1	100	0	0
	Face 4	0	0	0	0	NA	NA	NA
TOTAL		11.38	6.95	21.66	40	28.5	17.4	54.2

SP-III Mixture

Table 15 presents fatigue test results of the SP-III mixture samples. Once again, sample name, applied strain, sample stiffness, percent air voids, and fatigue life of each test specimen is shown. The applied strain varied from 70 to 1200 με. Initial test samples, SP-III-A1 and SP-III-B1, experienced 20.7 and 3.5 million cycles, respectively, without achieving failure. Therefore, testing is continued at higher strains and the results are analyzed. In general, with increasing strain, fatigue life reduces. This trend is shown in Table 15, when looking at the average number of cycles to failure for each strain level.

As with the SP-II mixtures, fatigue results from replicate samples tested at the same applied strain are analyzed and discussed. Samples SP-III-F2, SP-III-J1, and SP-III-M2 are tested at 800 με, under identical conditions. Table 16 presents crack lengths measured for each SP-III sample. Crack lengths are measured as they pass through the asphalt mastic, aggregate, and interface phases. Each sample face is labeled clearly; Faces 1 and 3 are the sides of the beam, while Faces 2 and 4 are the bottom and top sides respectively.

TABLE 15 Flexural Fatigue Test Results for SP-III Mixture Samples

Beam ID	Applied ε_t (με)	Initial E_0 (psi)	% Air Voids	Cycles Tested	Failure Criteria		Avg. Cycles to Failure	
					N_{f50}	$N_{f(ER)}$	N_{f50}	$N_{f(ER)}$
A1	70	437,320	9.9	20,741,011	NA	NA	NA	NA
B1	400	537,945	4.9	3,539,851	NA	NA	NA	NA
C1	600	557,499	4.9	833,560	770,008	748,820	770,008	748,820
J1	800	455,466	4.8	106,276	38,001	52,926	64,668	82,776
M2	800	415,678	5.9	79,176	42,001	46,826		
F2	800	402,190	5	150,000	114,001	148,576		
B2	1000	433,644	4.8	50,701	29,801	35,276	25,201	30,276
P1	1000	582,762	4.8	40,901	20,601	25,276		
P2	1200	485,731	5	12,326	6,476	7,551	8,026	22,149
Q2	1200	451,938	5.8	52,526	9,576	36,746		

Figure 56 shows multiple cracking primarily located at the interface of aggregates and asphalt mastic of sample SP-III-F2. Table 15 confirms this observation with 80% of total cracking occurring at the interface. From Figure 57, cracks are highlighted propagating upward through sample SP-III-F2 from the bottom side. The crack follows a path along the interface of a large aggregate whereupon it stops about halfway through the beam. The fatigue life of sample SP-III-F2 is 114,000 cycles. When compared with the replicate sample SP-III-J1, which has a much shorter fatigue life, it can be seen that almost 90% of the cracking occurred at the interface also. Figure 58 shows the crack path in the base of sample SP-III-J1. Large air voids are visible which may have initiated cracking, and almost certainly increased the crack propagation rate. Therefore, the fatigue life of sample SP-III-J1 with 38,000 cycles, is much shorter than that of sample SP-III-F2.

FIGURE 56 Fatigue Cracking in HMA Beam Sample SP-III-F2

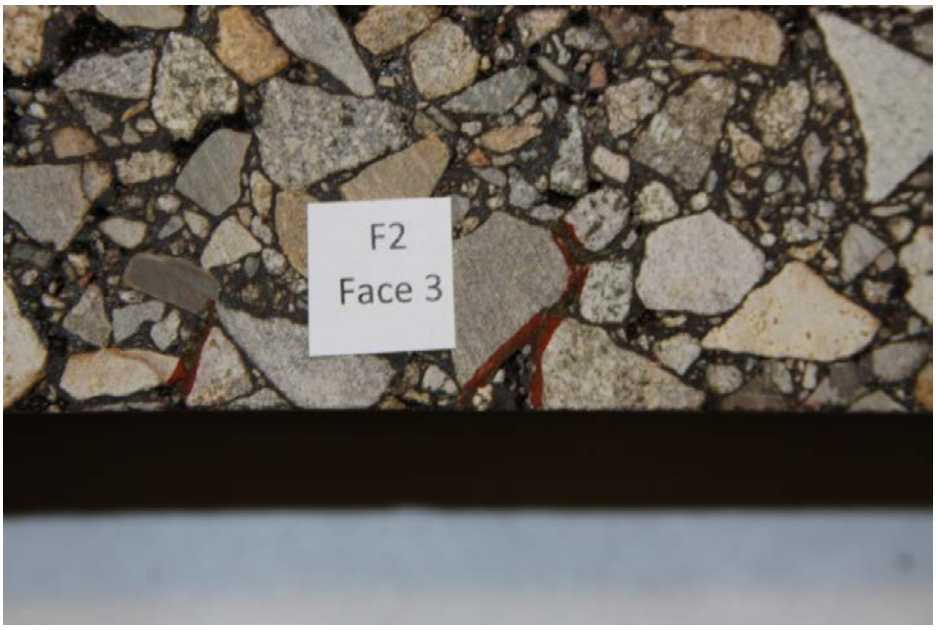

FIGURE 57 Fatigue Crack Propagating Upwards in HMA Beam Sample SP-III-F2

FIGURE 58 Fatigue Cracking in HMA Beam Sample SP-III-J1

Finally, sample SP-III-M2 showed a fatigue life similar to that of sample SP-III-J1, with 42,000 cycles. Once again, Table 16 shows that 60% of the crack path is located at the interface. Figure 59 shows some air voids present between large size aggregates, but surprisingly, the crack path did not pass through the air voids. Instead, the crack followed a path along the interface between two large aggregates. This suggests that the effect of air voids is minimal on cracking in this sample. When comparing all three samples, each show similar values in terms of flexural stiffness, ranging between 400-450 ksi, and percentage air voids varying from 5 to 6%. Therefore, judging by the photographic evidence of cracking highlighted in each sample, the distribution of large-size aggregates seems to play a vital role. Sample SP-III-F2 has a much better distribution of large size aggregates within the asphalt mastic than that shown in samples SP-III-J1 and SP-III-M2. In addition, the presence of voids does not necessarily cause crack initiation or even propagation. Rather, the presence of larger size aggregates close to one another, and crack propagation along the interface of these aggregates may reduce the fatigue life in the HMA materials.

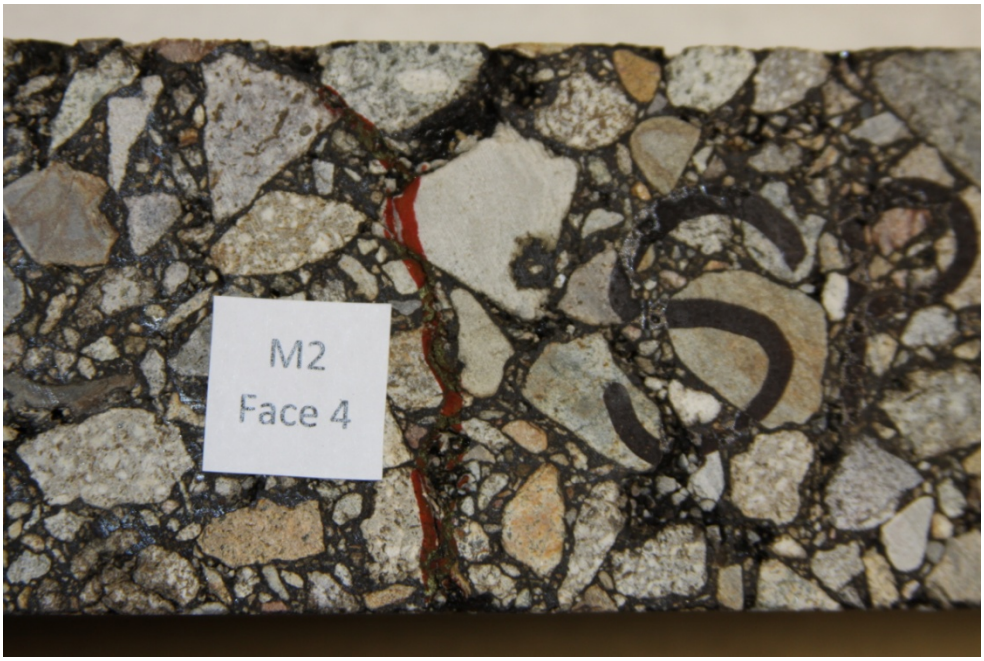

FIGURE 59 Fatigue Cracking in HMA Beam Sample SP-III-M2

From this study, the measured crack lengths from fatigue test results of SP-II and SP-III mixtures show that the majority of the cracking occurred at the interface. 54% and 70% of the total fatigue crack lengths in SP-II and SP-III samples are measured at the interface phase. This finding concurs with other studies which showed that the interface phase is preferential for crack initiation and propagation (*69*).

TABLE 16 Crack Lengths in Failed SP-III Samples

Sample	Sample	Fatigue Cracking (in)				Crack Location (%)		
P1	Side	Mastic	Aggregate	Interface	Total	Mastic	Aggregate	Interface
Side 1	Face 1	0.32	0	1.29	1.61	19.9	0	80.1
Bottom	Face 2	0.87	0.94	1.53	3.34	26	28.1	45.8
Side 2	Face 3	0.27	0.22	0.57	1.06	25.5	20.8	53.8
Top	Face 4	0	0	0	0	NA	NA	NA
M2	Face 1	0	0.34	0.57	0.91	0	37.4	62.6
	Face 2	0.72	0.17	1.32	2.21	32.6	7.7	59.7
	Face 3	0.25	0	0.65	0.9	27.8	0	72.2
	Face 4	0	0	0	0	NA	NA	NA
B1	Face 1	0	0	0	0	NA	NA	NA
	Face 2	0.25	0.47	0.92	1.64	15.2	28.7	56.1
	Face 3	0	0	0.27	0.27	0	0	100
	Face 4	0	0	0	0	NA	NA	NA
F2	Face 1	0	0	0.52	0.52	0	0	100
	Face 2	0.35	0.42	3.13	3.9	9	10.8	80.3
	Face 3	0	0	1.59	1.59	0	0	100
	Face 4	0	0	0	0	NA	NA	NA
Q2	Face 1	0.65	0.2	0.97	1.82	35.7	11	53.3
	Face 2	0.46	0.63	1.29	2.38	19.3	26.5	54.2
	Face 3	0	0	0.49	0.49	0	0	100
	Face 4	1.41	0	0.94	2.35	60	0	40
J1	Face 1	0	0	1.12	1.12	0	0	100
	Face 2	0.42	0	2.97	3.39	12.4	0	87.6
	Face 3	0.41	0	0.55	0.96	42.7	0	57.3
	Face 4	0	0	0	0	NA	NA	NA
B2	Face 1	0	0	0.62	0.62	0	0	100
	Face 2	0.46	0	0.2	0.66	69.7	0	30.3
	Face 3	0	0	0	0	NA	NA	NA
	Face 4	0	0	0	0	NA	NA	NA
P2	Face 1	0.27	0.12	0.5	0.89	30.3	13.5	56.2
	Face 2	0.19	0.22	2.26	2.67	7.1	8.2	84.6
	Face 3	0	0	0.65	0.65	0	0	100
	Face 4	0	0	0	0	NA	NA	NA
TOTAL		7.3	3.73	24.92	36	20.3	10.4	69.3

CONCLUSIONS

The conclusions being made here are:

- HMA mixture samples of similar mix design which are tested under similar conditions did not necessarily show similar fatigue lives. HMA fatigue life depends greatly on the ability of the material to withstand crack propagation. This study shows that the location and distribution of large size aggregates within the asphalt matrix affects crack propagation, whereby crack paths often propagate at the interface of the large aggregates and asphalt mastic.

- Failure due to fatigue cracking most often occurred at the interface of HMA samples where 54% and 70% of the total fatigue crack lengths in SP-II and SP-III samples are measured at the interface phase.

- Approximately 30% and 20% of the total fatigue crack lengths are measured in the mastic phase, and 17% and 10% are measured in the aggregate phase, of SP-II and SP-III samples.

CONCLUSIONS AND RECOMMENDATIONS

General

This study documents an extensive laboratory investigation of fatigue endurance limits in asphalt concrete. In addition, alternative fatigue failure criteria are compared, as well as the effect of crack propagation paths, and polymer-modified binder, on the fatigue life of asphalt concrete. The fatigue endurance limit is defined as the strain level below which a material sustains an infinite fatigue life without accumulating damage. Although, an infinite fatigue life for an asphalt pavement is not practical for design, a design life of 50 years or more is considered extraordinary long. Such a structure is termed as perpetual pavement, and is considered the future of pavement design. Although most of study focuses on laboratory fatigue failure of asphalt concrete, attempts are made to relate the findings with the field asphalt concrete fatigue, which can be incorporated in current pavement design methods.

Fatigue failure, especially in asphalt concrete, is a poorly understood problem. The main problem with the past studies on identifying fatigue endurance limits is that those studies are mostly based on the phenomenological approach which relates the number of loading cycles to fatigue failure with applied tensile strain and the initial stiffness of material. However, asphalt concrete is a viscoelastic material, which means that fatigue failure is temperature dependent.

In the literature review section, previous studies done to investigate the fatigue endurance limit as well as their limitations are covered. A number of laboratory test methods developed in the past to determine fatigue failure are described. Very few studies, if any, address the fatigue failure of asphalt concrete from the viscoelastic point of view. Hence, the use of viscoelastic damage mechanics is recommended in addressing the current problem in asphalt concrete for fatigue failure.

Next, the experimental work performed in this study is presented. In order to facilitate current standards, fatigue testing is performed using AASHTO T321-07. Four point bending is applied to beams using controlled strain loading for a range of strain amplitudes. In addition, dynamic modulus testing is conducted to determine the linear viscoelastic range of asphalt concrete which is represented by dynamic modulus and phase angle mastercurves as well as the relaxation modulus. Dynamic modulus testing is usually performed on cylindrical samples (6 in. tall) under compression. On the contrary, dynamic modulus testing of beam samples under flexural loading may be more useful as sample slabs (2-3 in. tall) that can be extracted from the field and then directly tested, once they are cut to size. Laboratory sample preparation also included compaction using a linear kneading compactor, sample sizing using a stone-cutting saw, and finally sample conditioning using an environmental chamber. Each fatigue test at a certain strain level required additional replicate samples (2-3) to be tested.

The results of laboratory fatigue testing at normal and low strain levels are presented. Failure is defined as 50% reduction in stiffness and the majority of tests are conducted until sample stiffness has reduced by 80-90% in order to identify fatigue cracking. Beam samples which did not fail, had their fatigue life determined using extrapolation techniques. In this way, a more complete picture of the fatigue behavior of asphalt concrete is described. Although previous studies have shown that an endurance limit does exist for HMA mixtures, an established value is

yet to be determined, with values varying from 70-300 microstrain (με) based on mixture variability. The concluding section determines the FEL of HMA mixtures using the phenomenological approach as well as a fundamental energy based approach, the dissipated energy concept. Furthermore, two different stiffness-based fatigue failure criteria are compared, as well as their effect of the estimated FEL of HMA materials. In addition, the effect of certain mixture variables on the FEL is investigated. Starting from last one and half decades, polymer has been a part of asphalt binder. Therefore this study includes fatigue behavior of a polymer modified binder as well as that of base asphalt binder which is described in the concluding section. Polymer-modified PG 70-22 and unmodified PG 64-22 binders are investigated for their effect on FEL of asphalt concrete.

Flexural fatigue testing has been used by the asphalt pavement industry for several decades. Various approaches have been used to relate fatigue performance with parameters such as stiffness, dissipated energy, cumulative dissipated energy, pseudostiffness and so on. Traditional fatigue relation testing relates the number of loading cycles to failure with the applied tensile strain and the initial stiffness of material. Furthermore, the number of loading cycles to failure is defined as that number of cycles at which the stiffness of a material reduces by 50%. Also, approaches based on cumulative dissipated energy require visual interpretation of plots and often ignore viscoelastic effects. On the other hand, approaches based on viscoelastic continuum damage have shown promising results. This approach has considerable advantages such as reduction in testing time and resources, and is based on the fundamental energy based approach. Therefore, a viscoelastic damage mechanics model is very appropriate to examine fatigue failure in asphalt concrete. Stiffness based failure criteria with failure criteria based on viscoelastic continuum damage approach is looked at in the Comparison of Different Failure Criteria for Fatigue Testing section.

For this study, fatigue testing of HMA mixtures required controlled strain laboratory testing of replicate samples at various strain amplitudes. The number of cycles to failure is recorded along with the critical strain level and this relationship is used to describe the fatigue behavior of asphalt concrete. Replicate samples are tested at each strain level. However, fatigue test results of replicate samples did not always provide similar results. It is impossible to recreate two to three identical samples, hence crack paths in failed samples vary considerably. A study on the effect of the crack path on the fatigue life of asphalt concrete is looked at. Fatigue cracks are highlighted and photographed in each failed specimen. Crack lengths are separated into three categories, depending on where the crack existed; (1) within the asphalt mastic, (2) through the aggregates, and (3) at the interface between aggregate and asphalt mastic. Fatigue life data of replicate samples are analyzed using the crack path data as a means to understand inconsistent results.

Conclusions

A summary of mixture fatigue results, comparison of selected fatigue analysis approaches, and the effects of polymer-modified binder on HMA mixture fatigue resistance are summarized in this section.

- The following table summarizes the findings of the fatigue endurance limits for SP-II (field and lab mixes) and SP-III (field and lab mixes) based on this study:

HMA Mix Type	Strain-Nf
SP-II (field)	195
SP-II (lab)	125
SP-III (lab)	185
SP-III (field)	180

- Fatigue test results show that fatigue failure according to the ER criterion occurred after a sample has achieved 50% reduction in stiffness, which is the traditional fatigue criterion. This suggests that the traditional failure approach is slightly conservative.

- Fatigue life extrapolation using the single-stage Weibull function and RDEC approach showed good consistency with fatigue test results of SP-II and SP-III mixtures, performed at normal strain levels. However, for low strain testing, extremely high fatigue life data is predicted, which suggests an overestimation of fatigue life.

- The FEL values of SP-II and SP-III mixtures are predicted using the traditional ε-N relationship. The FEL of the SP-II mixture is estimated to be 195 με, using traditional failure criterion (Nf_{50}). For the SP-III mixture, the FEL is estimated to be 180 με (Nf_{50}).

- The FEL values of the SP-II mixture using the ε-PV approach are estimated to be 252 με (*ER*) and 215 με (Nf_{50}), and for the SP-III mixture, the FEL is estimated to be 291 με (*ER*) and 334 με (Nf_{50}).

- PV values predicted using the material property-based PV prediction model showed good consistency with PV values determined from laboratory testing. However, the estimated FEL values using the PV model are much lower than those predicted using the ε-N_f and ε-PV models.

- The effect of polymer modified binder on the FEL of HMA mixtures showed mixed results, with an increase in estimated FEL of the SP-III mixture but reduced the estimated FEL of the SP-II mixture.

- The FEL of laboratory mixtures is much lower than that of the field mixes. In particular, the fatigue performance of laboratory SP-II mixtures compares well with that of field SP-II mixtures. However, the laboratory SP-III mixture performs poorly when compared with the fatigue performance of the field SP-III mixture.

- The F-test is performed on the ε-N_f and PV-ε curves to determine whether the curves developed using the traditional (N_{f50}) and Energy Ratio (ER) approaches are statistically the same. For ε-N regression curves through the power law, it is determined that the two fatigue curves are statistically the same for the SP-III mixture. However, the opposite is the case for the SP-II fatigue curves. For the PV-ε curves, the F-Test shows that the fatigue curves are statistically the same using the different fatigue failure approaches.

- Using the VCDM approach, a point of inflection is identified in the damage characteristic curve beyond which the material loses its structural integrity at faster rate. This point is considered the fatigue failure of the sample.

- A strong correlation is found between the VCDM criterion and the stiffness-based failure criteria.

- Asphalt concrete beam samples of similar mix type which are tested under similar conditions did not necessarily show similar fatigue lives. The fatigue life depends greatly on the chosen crack path. This study showed that the path of least resistance i.e. the interface of the aggregates and asphalt mastic, greatly affected the associated fatigue life.

- Failure due to fatigue cracking most often occurred at the interface of HMA samples where 54% and 70% of the total fatigue crack lengths in SP-II and SP-III samples are measured at the interface phase.

- Approximately 30% and 20% of the total fatigue crack lengths are measured in the mastic phase, and 17% and 10% are measured in the aggregate phase, of SP-II and SP-III samples.

Recommendations

- In this study, only PG 64-22 and 70-22 were used to determine the fatigue endurance limits of SP-II and SP-III mixes. To expand the data base and get values for different binder grades, SP-III should be test for these PG grades below:

    - PG 58-22
    - PG 58-28
    - PG 64-28
    - PG 70-28
    - PG 70-16
    - PG 76-16
    - PG 76-22
    - PG76-28
    - PG82-16
    - PG82-22

- In addition, FEL of high Reclaimed Asphalt Pavement (RAP) mixes should be tested in the laboratory and be compared to the fatigue endurance limits values of lower RAP content HMA.

- Fatigue endurance limits of warm-mix asphalt should be tested and compared to the fatigue endurance limits values of HMA.

- This study considered short term aging when testing the asphalt concrete samples, the get a better representation of field conditions, long term aging should be considered.

REFERENCES

1. Romanoschi, S. A., Gisi, A. J., Portillo, M. Dumitru, C. "First Findings from the Kansas Perpetual Pavements Experiments." *Transportation Research Record*, No. 2068, 2008, pp. 41-48.

2. Tarefder, R. A. and Bateman, D. "Future Design of Perpetual Pavements for New Mexico," *Final Report*, Submitted to Research Bureau, New Mexico Department of Transportation, 2010.

3. Monismith, C. L., and Epps, J. A. "Asphalt Mixture Behavior in Repeated Flexure." *Report No. TE 70-5*, Institute of Transportation and Traffic Engineering, University of California, Berkley, 1970.

4. Tayebali, A. A., Deacon, J. A., Coplantz, J. S., Harvey, J. T., and Monismith, C. L. "Fatigue Response of Asphalt-Aggregate Mixes." *Report No. SHRP A-404*, Strategic Highway Research Program, National Research Council, Washington, D.C., 1992.

5. Hibbeler, R.C. *Mechanics of Materials*. Prentice-Hall, Inc., Upper Saddle River, NJ, 2005.

6. Carpenter, S. H., Ghuzlan, K. A., and Shen, S. "Fatigue Endurance Limit for Highway and Airport Pavement." *Transportation Research Record*, No. 1832, 2003, pp. 131-138.

7. Carpenter, S. H., and Shen, S. "Application of the Dissipated Energy Concept in Fatigue Endurance Limit Testing." *Transportation Research Record*, No. 1929, 2005, pp. 165-173.

8. AASHTO T321-07. "Standard Test Method for Determining the Fatigue Life of Compacted Hot-Mix Asphalt (HMA) Subjected to Repeated Flexural Bending." *American Association of State Highway and Transportation Officials* (AASHTO), Washington D.C., 2007.

9. ASTM D7460-10. "Standard Test Method for Determining Fatigue Failure of Compacted Asphalt Concrete Subjected to Repeated Flexural Bending." *ASTM International*, West Conshohocken, PA, 2010.

10. Prowell, B., Brown, E. R., Daniel, J., Bhattacharjee, S., Von Quintus, H., Carpenter, S. H., Shen, S., Anderson, M., Swamy, A. K., and Maghsoodloo, S. "Endurance Limit of Hot Mix Asphalt Mixtures to Prevent Fatigue Cracking in Flexible Pavements." *Updated Draft Final Report, NCHRP 9-38*, National Cooperative Highway Research Program, Washington, D.C, 2008.

11. Di Benedetto, H., Ashayer Soltani, M. A. and Chaverot, P., "Fatigue Damage for Bituminous Mixtures." *Proceedings of the 5th Int. RILEM Symposium MTBM*, Lyon, 1997, pp. 263-270.

12. Pronk, A.C., "Analytical Investigation of the Corrections of Formulas Used in Bending Beam Tests." *Efficient Transportation and Pavement Systems: Characterization, Mechanisms, Simulation, and Modeling*. Taylor and Francis Group, London, UK, 2008.

13. Rowe, G.M. and Bouldin, M.G. "Improved Techniques to Evaluate the Fatigue Resistance of Asphaltic Mixtures." *Proceedings of 2nd Eurasphalt & Eurobitumen Congress*, Barcelona, Spain, 2000.

14. Hopman, P.C., Kunst, P.A.J.C. and Pronk, A.C. "A renewed Interpretation Method for Fatigue Measurements, Verification of Miner's Rule." *4th Eurobitumen Symposium,* Madrid, Spain, Vol. 1, 1989, pp. 697-707.

15. Carpenter, S. H., and Shen, S. "Dissipated Energy Approach to Study Hot-Mix Asphalt Healing in Fatigue." *Transportation Research Record*, No. 1970, 2006, pp. 178-185.

16. Carpenter, S.H., Ghuzlan, K. A., and Shen, S. "Fatigue Endurance Limit for Highway and Airport Pavement." Transportation Research Record, No. 1832, 2003, pp. 131-138.

17. Ghuzlan, K. "Fatigue damage analysis in asphalt concrete mixtures based upon dissipated energy concepts," thesis, presented to University of Illinois at Urbana-Champaign, IL, in partial fulfillment of the requirements for the degree of Doctor of Philosophy, 2001.

18. Ghuzlan, K., and Carpenter, S. H. "Energy-Derived, Damage-Based Failure Criterion for Fatigue Testing." *Transportation Research Record*, No. 1723, 2000, pp. 141–149.

19. Underwood, B.S. and Kim, Y.R. "Analytical Techniques for Determining the Endurance Limit of Hot Mix Asphalt Concrete," *Proceedings of the 2009 International Conference on Perpetual Pavement*, Columbus, OH, 2009.

20. Kim, Y.R. "Evaluation of Healing and Constitutive Modeling of Asphalt Concrete by Means of Theory of Nonlinear Viscoelasticity and Damage Mechanics." *Doctoral dissertation*, Texas A & M University, College Station, TX, 1988.

21. Daniel, J.S. "Development of a Simplified Fatigue Test and Analysis Procedure Using a Viscoelastic, Continuum Damage Model and its Implementation to WesTrack Mixtures." *Doctoral dissertation*, North Carolina State University, Raleigh, NC, 2001.

22. Daniel J.S. and Kim, Y.R. "Development of a Simplified Fatigue Test and Analysis Procedure Using a Visco-Elastic Continuum Damage Model." *Journal of the Association of Asphalt Paving Technologists,* Vol. 71, 2002, pp. 619-650.

23. Swamy, A. K. "Evaluating Mode of Loading Effect and Laboratory Fatigue Performance of Asphalt Concrete using Viscoelastic Continuum Damage Mechanics." *Doctoral dissertation*, University of New Hampshire, Durham, NH, 2011.

24. Swamy, A. K. and J. S. Daniel. "Modeling Flexural Fatigue Behavior using Viscoelastic 19 Continuum Damage Mechanics Principles." *Proceedings of Engineering Mechanics Institute*, Boston, USA, 2011.

25. Prowell, B., Brown, E. R., Anderson, M., Daniel, J., Swamy, A. K., Von Quintus, H., Shen, S., Carpenter, S. H., Bhattacharjee, S., and Maghsoodloo, S. "Validating the Fatigue Endurance Limit for Hot Mix Asphalt." *NCHRP Report 6-46*, National Cooperative Highway Research Program, Washington, D.C, 2010.

26. Tsai, B. W., Harvey, J.T., and Monismith, C.L. "Application of Weibull Theory in Prediction of Asphalt Concrete Fatigue Performance." *Transportation Research Record*, No. 1832, 2003, pp. 121-130.

27. Tsai, B. W., Harvey, J.T., and Monismith, C.L. "High Temperature Fatigue and Fatigue Damage Process of Aggregate-Asphalt Mixes." *Journal of the Association of Asphalt Paving Technologist*, Vol. 71, 2002, pp. 345-385.

28. Advanced Asphalt Technologies, LLC. "Developing a Plan for Validating an Endurance Limit for HMA Pavements: HMA Endurance Limit Validation Study," National Cooperative Highway Research Program Project, 2008, 9-44.

29. Jud, K., and Kausch, H. H. "Load Transfer Through Chain Molecules After Interpenetration at Interfaces." *Polymer Bulletin*, Vol. 1, 1979, pp. 697–707.

30. Stavrinidis, B., and Holloway, D. G. "Crack Healing in Glass." *Physics and Chemistry of Glasses*, Vol. 24(1), 1983, pp. 19–25.

31. Sukhotskaya, S. S., Mazhorava, V. P., and Terekhin, Y. N. "Effect of Autogenous Healing of Concrete Subjected to Periodic Freeze–Thaw Cycles." *Journal of Hydrotechnical Construction*, Vol. 17(6), 1983, pp. 295–296.

32. Clear, C. A. "The Effect of Autogenous Healing upon Leakage of Water Through Crack Initiation and Arresting in Epoxy." *International Journal of Fracture*, Vol. 55(3), 1985, pp. 209-222.

33. Edvardsen, C. "Water Permeability and Autogenous Healing of Cracks in Concrete." *ACI Materials Journal*, Vol. 96(4), 1999, pp. 448–454.

34. Freund, L. B., and Suresh, S. "*Thin Film Materials: Stress, Defect Formation and Surface Evolution."* Cambridge University Press, Cambridge, United Kingdom, 2003.

35. Little, D. N., Lytton, R. L., Williams, D., and Kim, Y. R. "An Analysis of the Mechanism of Microdamage Healing Based on the Applications of Micromechanics First Principles of Fracture and Healing." *Journal of the Association of Asphalt Paving Technologists*, Vol. 68, 1999, pp. 501–542.

36. Petersen, J. C. "Chemical Composition of Asphalts Related to Asphalt Durability: State of the Art." *Transportation Research Record*, No. 999, 1984, pp. 13–30.

37. Lytton, R.L. "Characterizing Asphalt Pavements for Performance." *Transportation Research Record*, No. 1723, 2000, pp. 5–16.

38. Thompson, M.R., ad Carpenter, S.H. “Design Principles for Long Lasting Pavement,” *Proceedings, International Symposium of Design and Construction of Long Lasting Asphalt Pavements*, National Center for Asphalt Technology, Auburn, AL, 2004.

39. Brown, S. F., Hakim, B. and Thom, N. H., “Performance and Rehabilitation of Heavy-Duty Pavements in the UK: Some Case Studies.” *Proceedings of the International Symposium on design & construction of long lasting asphalt pavement*. Auburn, Alabama, 2004, pp. 811-829.

40. Bonnaure, F.P., Huibers, A.H.J.J., Boonders, A. “A Laboratory Investigation of the Influence of Rest Periods on the Fatigue Response of Bituminous Mixes,” *Proceedings, Association of Asphalt Paving Technologists*, Vol. 51, Kansas City, Missouri, 1982.

41. Chehab, G. R., Kim, Y. R., Schapery, R. A., Witczak, M. W., and Bonaquist, R. “Characterization of Asphalt Concrete in Uniaxial Tension Using a Viscoelastoplastic Continuum Damage Model.” *Journal of the Association of Asphalt Paving Technologists,* Vol. 72, 2003, pp. 315-355.

42. Walubita, L. “Comparison of Fatigue Analysis Approaches for Predicting Fatigue Lives of Hot-Mix Asphalt Concrete (HMAC) Mixtures.” Thesis, presented to University of Texas A&M, TX, in partial fulfillment of the requirements for the degree of Doctor of Philosophy, 2006.

43. Von Quintus, H.L., Mallela, J., and Jiang, J. “Quantifications of the Effects of Polymer-Modified Asphalt for Reducing Pavement Distress.” *ER-215*, Asphalt Institute, Lexington, KY, 2004.

44. Goodrich, J.L. “Asphalt and Polymer Modified Asphalt Properties Related to the Performance of Asphalt Concrete Mixes.” *Proceedings of Association of Asphalt Paving Technologists Technical Sessions*, Williamsburg, VA, Vol. 57, 1988, pp. 116–175.

45. Lee, H. J., J. Y. Choi, Y. Zhao, and Y. R. Kim. “Laboratory Evaluation of the Effects of Aggregate Gradation and Binder Type on Performance of Asphalt Mixtures.” *In Proceedings of the Ninth International Conference on Asphalt Pavements*, Copenhagen, Denmark. 2002.

46. Leahy, R.B., Hicks, R.G., Monismith, C.L., and Finn, F.N. “Framework for Performance-Based Approach to Mix Design and Analysis.” *Proceedings of the Association of Asphalt Paving Technologists*, Vol. 64, 1995, pp. 431-473.

47. Pierce, L. M. and Mahoney, J.P. “Asphalt Concrete Overlay Design Case Studies.” *Transportation Research Record,* No. 1543, 1996, pp. 3-9.

48. Harvey, J. T., Deacon, J.A., Taybali, A.A., and Leahy, R.B. (1997). “A Reliability-Based Mix Design and Analysis System for Mitigating Fatigues Distress.” *Proceedings of the 8th International Conference on Asphalt Pavements*, University of Washington, Seattle, WA, Vol. 1, 1997, pp. 301-323.

49. Romero, P., Stuart, K.D., and Mogawer, W. "Fatigue Response of Asphalt Mixtures Tested by the Federal Highway Administration's Accelerated Loading Facility." *Journal of the Association of Asphalt Paving Technologists*, Vol. 69, 2000, pp. 212-235.

50. Zhou, F., Hu, S., Chen, D., and Scullion, T. "Overlay Tester: Simple Performance Test for Fatigue Cracking." *Transportation Research Record*, No. 2001, 2007, pp. 1-8.

51. Willis, J.R. and Timm, D.H. "A Comparison of Laboratory Fatigue Thresholds to Measured Strains in Full-Scale Pavements." *Proceedings, International Conference on Perpetual Pavements*, Columbus, Ohio, 2009.

52. Priest, A.L. "Methodology and Calibration of Fatigue Transfer Functions for Mechanistic-Empirical Flexible Pavement Design." *NCAT Report 06-03*, National Center for Asphalt Technology, Auburn University, Alabama, 2006.

53. Tangella, R., Craus, J., Deacon, J.A., and Monismith, C.L. "Summary Report of Fatigue Response of Asphalt Mixtures." *SHRP-A/IR-90-011*, Institute of Transportation Studies, University of California, Berkley, 1990.

54. Thompson, M. and Carpenter, S.H. "Perpetual Pavement Design: An Overview." *Proceedings of the 2009 International Conference on Perpetual Pavement*, Columbus, OH, 2009.

55. Thompson, M. and Carpenter, S.H. "Considering Hot-Mix-Asphalt Fatigue Endurance Limit in Full-Depth Mechanistic-Empirical Pavement Design." *Proceedings International Conference on Perpetual Pavement Design* (CD-ROM), Columbus, OH, 2006.

56. Timm, D., H., and Young, J., B. "Effects of Load Spectra and Variability on Perpetual Pavement Design." *Proceedings, International Symposium of Design and Construction of Long Lasting Asphalt Pavements*, National Center for Asphalt Technology, Auburn, AL, 2004.

57. AASHTO T 168-07. Standard Test Method for Sampling Bituminous Paving Mixtures, *American Association of State Highway and Transportation Officials* (AASHTO), Washington D.C., 2007.

58. AASHTO T 30-08. Standard Method of Test for Mechanical Analysis of Extracted Aggregate, *American Association of State Highway and Transportation Officials* (AASHTO), Washington D.C., 2008.

59. AASHTO T 308-08. Standard Method of Test for Determining the Asphalt Content of Hot-Mix Asphalt (HMA) by the Ignition Method, *American Association of State Highway and Transportation Officials* (AASHTO), Washington D.C., 2008.

60. AASHTO T 312-07. Standard Method of Test for Preparing and Determining the Density of Hot Mix Asphalt (HMA) Specimens by Means of the Superpave Gyratory Compactor, *American Association of State Highway and Transportation Officials* (AASHTO), Washington D.C., 2007.

61. AASHTO T 269-07. “Standard Method of Test for Percent Air Voids in Compacted Dense and Open Asphalt Mixtures.” *American Association of State Highway and Transportation Officials* (AASHTO), Washington D.C., 2007.

62. AASHTO T 209-07. Standard Method of Test for Theoretical Maximum Specific Gravity and Density of Hot Mix Asphalt (HMA), *American Association of State Highway and Transportation Officials* (AASHTO), Washington D.C., 2007.

63. Ott, R.L. “An Introduction to Statistical Methods and Data Analysis.” 5th Ed. Michael Longnecker, Texas A&M University, Texas, 2001.

64. Van Dijk, W., and Vesser, W. “The Energy Approach to Fatigue for Pavement Design.” *Journal of Association of Asphalt Paving Technologists*, Vol. 46, 1977, pp. 1–40.

65. Pronk, A.C. and Hopman, P.C. “Energy Dissipation: The Leading Factor of Fatigue. Highway Research: Sharing the Benefits.” *Proceedings of the Conference, the United States Strategic Highway Research Program*, London, UK, 1990.

66. Pronk, A.C., “Comparison of 2 and 4-Point Bending Tests and Healing in 4-Point Dynamic Bending Test based on the Dissipated Energy Concept.” *Proceedings of the 8th International Conference on Asphalt Pavements*, Seattle, Washington, USA, 1997.

67. Park, S.W., Kim, Y. R., and Schapery, R.A. ‘‘A Viscoelastic Continuum Damage Model and its Application to Uniaxial Behavior of Asphalt Concrete.’’ *Mechanics of Materials*, Vol. 24(4), 1999, pp. 241–255.

68. Kravchenko, P.E. *Fatigue Resistance.* Oxford; Pergamon Press, New York, 1964.

69. Kias, E.M.C. “Laboratory Evaluation of Cracking in Asphalt Concrete.” Master’s Thesis, University of New Mexico, Albuquerque, NM, 2008.

New Mexico Department of Transportation
RESEARCH BUREAU
7500B Pan American Freeway NE
PO Box 94690
Albuquerque, NM 87199-4690
Tel: (505) 841-9145